UNIVERSITY OF ALBERTA

A Laboratory Study of the Stability and Flow of Nanoparticle Suspensions through Porous Media using Magnetic Techniques

by

Shahjahan Khan

A thesis submitted to the Faculty of Graduate Studies and Research
in partial fulfillment of the requirements for the degree of

Master of Science

in

Petroleum Engineering

Department of Civil and Environmental Engineering

Spring, 2012

Edmonton, Alberta

DEDICATION

This work is dedicated to my loving parents, Akhtar Z. Khan and Raheela Z. Khan. Prayers of my parents, their love and encouragement have a key role in every success of my life and I am thankful to God Almighty for this great blessing.

ABSTRACT

A magnetic susceptibility technique is applied to find the effects of a wide range of parameters on the stability and transport of the nanoparticle suspensions. First section of the study is related to stability of nanoparticle suspensions with particular emphasis on determining an optimum nanoparticle suspension recipe. The parameters considered included sonication time, sonication power, type of dispersants, dispersant concentration, nanoparticle concentration and applied magnetic field.

In the second part of the study, the transport and retention of the nanoparticles in non-metallic horizontal flow cell containing porous medium were examined while using various nanoparticle suspension recipes. Furthermore, effects of a number of parameters such as permeability, matrix type, flow rate, suspension recipe type etc. were also observed. Based on the findings of the study, an empirical method of finding optimum suspension recipe has been proposed/ suggested, which could be further improved by incorporating more factors affecting stability of nanoparticle suspensions.

ACKNOWLEDGEMENTS

I would like to express my sincere gratitude and deepest thanks to my supervisors Dr. David K. Potter and Dr. Ergun Kuru for their trust in me and offering me the opportunity to benefit from their valuable knowledge. Their encouragement, support and guidance throughout the course of my research work are much appreciated.

Thanks are also due to Stephen Gamble, the laboratory coordinator for his assistance in designing and construction of flow cell apparatus and to Dr. Tayfun Babadagli for lending some apparatus in carrying out this research work.

Last but not the least; I would like to express my utmost thanks to my spouse, children and parents for their patience and support throughout my MSc degree.

TABLE OF CONTENTS

LIST OF TABLES

LIST OF FIGURES

LIST OF NOMENCLATURE AND SYMBOLS

AFM	Atomic Force Microscope
Ca-DTPMP	Calcium Diethylenetriaminepenta
$C_{i(in)}$	Injected particle concentration, % (vol/vol)
C_i (x, t)	Particle concentration in fluid, % (vol/vol)
C_o	Concentration of particles at the injection point, % (vol/vol)
CTAB	Cetyltrimethyl Ammonium Bromide (cationic surfactant)
C_x	Concentration of solid particles at any point before the drainage front, % (vol/vol)
d	Diameter of the tube
d_p	Size of the particle
D	Sensor Aperture + 8 mm
D_B	Brownian diffusion coefficient
DDBS	Sodium Dodecylbenzeno Sulfonate (anionic surfactant)
D_i m/m	L_x/L_{core} (L_x is length from injection point to point of interest),
DLVO	Derjaguin-Landau-Verwey- Overbeek
f_i	Volume fraction of i component
g	Gravitational acceleration (m/s^2)
H	Magnetizing field (A/m)
k	Boltzmann constant

LSRV	Low Shear Rate Viscosity
M	Magnetization (A/m)
nm	Nano meter
NP(s)	Nanoparticle(s)
P	Particles distribution factor, dimensionless (Empirically determined)
pHzpc	pH of zero potential charge
PPCA	Phosphino Polycarboxylic Acid
PV(s)	Pore Volume(s)
R	Length/ radius of investigation, normalized length
r	Radius of spherical solid particles (m)
t	Time, min or hours
Δt	Time change
T	Absolute temperature
TGT	Tergitol (non-ionic surfactant)
x	Length, one dimensional coordinate, m
X or X_v	True volume magnetic susceptibility, (-)
XG	Xanthan Gum (polymer)
X_{mv}	Measured Volume Susceptibility
X_{vi}	Volume susceptibility of i component

X_{VT}	Total volume susceptibility within volume of investigation of tool
Δx	Three dimensional mean transfer distance
$\square$	Porosity % (vol/vol)
λ	Filtration coefficient, 1/m
v_s	Terminal velocity of solid particles (m/s)
ρ_s	Density of solid particles (Kg/m^3)
ρ_f	Density of fluid (Kg/m^3)
μ	Dynamic viscosity ($N\text{-}s/m^2$)

1 INTRODUCTION

1.1 Overview

Nanoparticles are very fine particles with size in the range of 1 nm to 100 nm or up to few hundred nano meters (nm), where nano meter is defined as the billionth part of a meter. Nanoparticles have high specific surface area and unique electrical (Alivisatos, 1996), chemical (Ozin, 1992) and magnetic (Jun et al., 2005) properties those are quite different from bulk material. Many researchers (Lee et al., 1999; Eastman et al., 2001; Chopkar et al., 2006) have shown a significant increase in thermal conductivity properties of base fluid with the introduction of small amounts of nanoparticles. The conductivity response with the addition of these nanoparticle suspensions has been reported to be significantly higher than predicted by macroscopic theory (Ding and Wen, 2004). This heat transfer intensification characteristic is providing useful industry application in fluid transportation, heating, cooling, metallurgical industry etc.

Nano sized particles are suited for flow through porous media since most of the pores and pore throats are of micron scale or larger and are therefore likely not to pose any restrictions in the flow of nanoparticles. Secondly, due to smaller size they can exhibit better particle suspension, as the particle settlement velocity under the effect of gravity reduces with decrease in size of the particles.

The agglomeration and transport behaviour of nanoparticles have been studied by many researchers for various purposes. The knowledge of agglomeration and transport behaviour of nanoparticle suspensions, obtained from different theoretical models and experimental findings has been used in different industrial applications (pipe flow) as well as in soil decontamination (porous media flow). A review about the agglomeration and transport behaviour of the nanoparticle suspensions is presented in chapter 2 of this report.

Nano technology has received a considerable attention in last one decade especially in the fields of electronics and medical. However, in petroleum industry only limited use of this technology has been seen so far. At present, numerous research efforts are underway to get benefit from this technology particularly in the fields of formation evaluation and improved oil recovery. Some of the potential future applications and active research areas of nanotechnology in petroleum industry are enumerated below.

- Use of nanoparticles in preparing stabilized emulsions or foams for application in improved oil recovery (IOR). Uniform size of droplets and shear thinning behaviour makes nanoparticle emulsions as appropriate mobility and conformance control agent in IOR (Zhang et al., 2011).

- Injection of nanoparticle suspensions in reservoir for slow release of corrosion inhibitors (Zhang et al., 2011) or other chemicals such as scale inhibitors. Earlier, Shen et al. (2008) performed experiments on the transport of sub-micron sized Ca-DTPMP nanoparticle suspensions for scale inhibition and highlighted the advantages of this method over conventional “squeeze treatment”.

- High magnetic susceptibility nanoparticles may be coated on proppants which can then be used in near well bore fracture diagnostics (Barron et al., 2010).

- Delivery of nano metal particles to high viscosity heavy oil/ bitumen reservoirs and their controlled adhesion to rock matrix can give increased heat conduction and viscosity reduction which would ultimately result in improved recovery and lower steam oil ratio (Shokrlu and Babadagli, 2010).

- Agglomerate of nano sized particles in drilling fluids can help in forming low leak off mud cakes and the magnetic susceptibility characteristics of

nanoparticles may be used in determining the thickness of mud cake and there from efficiency of drilling fluid.

- Collection of information about the reservoir's static/ dynamic properties from the changed state of injected nanoparticles, also termed as "nano-reporters" (Zhang et al., 2011).

- Saturation estimation from acoustic response generated by the delivery of para-magnetic nanoparticles in formation and applying magnetic field. (Ryoo et al., 2010)

Long term stability and improved transport efficiency are the key parameters needed for application of majority of these techniques. Therefore a comprehensive understanding of the parameters affecting stability and transport of nanoparticle suspensions is essentially needed.

1.2 Statement of the Problem

Nanoparticle suspensions are mixture of the nanoparticles in the base fluid those can be prepared using different methods including high shear rate mixing, sonication and addition of dispersants. Use of these techniques is essentially needed in order to keep the nanoparticles or their agglomerates in dispersed form. The nanoparticles have strong tendency to form agglomerates due to their unstable nature. The unstable characteristics of these nanoparticles are mainly due to dominance of attractive van der waals forces over electrostatic repulsive forces at small size range. When attractive forces are dominant, agglomerates or clusters of nanoparticles are formed which not only facilitates non-uniform distribution of nanoparticles in suspensions but also increases the particle settlement rate.

The interplay of forces in nanosized particles is very complex as compared to micron sized particles and perhaps is not fully understood yet. Nanoparticle agglomeration, adhesion and stability of nanoparticle suspension have been an

area of interest for the use of nanoparticles in various industrial applications. Various models relating to stability and transport of nanoparticle suspensions through porous media have failed to fully replicate the measured results. Some of the discrepancies reported between measured and predicted response are discussed in chapter 2. Such differences could be due to number of simplifications or assumptions made in modelling and simulation studies. Zhang et al. (2011) have also stated the inability of available models to completely predict the transport of nanoparticles.

To our knowledge, no empirical method has been established so far, for preparation of optimum nanoparticle suspension recipe that offers stable response and minimum particle adhesion when flowed through porous media. This demanded the need for finding experimentally the factors affecting the stability of nanoparticle suspensions and finally coming up with optimum suspension recipe exhibiting better transport characteristics through porous media.

Various researchers have studied the effects of different parameters (e.g. permeability, lithology, flow rate etc.) on stability and transport of nanoparticle suspension. The suspension preparation methods, type of dispersants, amount of dispersants, sonication time and type of particles used in these studies were different from each other, which raises the question that whether optimum concentration of dispersant or sonication was applied or not. Optimum values of sonication and dispersants could have increased the stability and transport of nanoparticle suspensions.

Shen et al. (2008) sonicated their suspensions after adding dispersants whereas others (Shah, 2009; Shokrlu and Babadagli, 2010) sonicated first and then added dispersants in preparation of nanoparticle suspensions. Shah (2009) and Shokrlu and Babadagli (2010) used 30 minutes sonication to disperse the nanoparticles whereas Shen et al. (2008) performed sonication of 25 minutes and more. Although, Shen et al. (2008) have demonstrated that at higher ionic concentration, higher sonication energy and higher concentration of dispersant improves the

stability and transport of Ca-DTPMP suspensions, question stays about the optimum amount of sonication needed.

Similarly, some researchers maintained only one concentration of dispersant (e.g shah, 2009) whereas others changed it proportional to the weight percentage of nanoparticles used (e.g. Darko-Kagya and Reddy, 2010). The criteria for finding optimum concentration with change in ingredients of suspension recipe also need to be established.

Sometimes the conclusion drawn from these experiments were contradictory. The reason for these contradictions could possibly be different set of conditions used in the experiments. Li et al. (2008) demonstrated that nanoparticle attachment in coarser sand packs is lesser than in finer sands, whereas Rodriguez et al. (2009) demonstrated that the particle retention was independent of the permeability. Reason for these contradictory conclusions need to be found out.

In view of the above discussion, performing an extensive study on the stability and transport of nanoparticle suspensions was deemed necessary wherein majority of the parameters investigated separately by many researchers could be performed with an optimum suspension recipe. Furthermore, guidelines could also be established for obtaining an optimum suspension recipe. In order to obtain the optimum suspension recipe, questions like those listed below would need to be addressed.

- What would be an optimum concentration of any dispersant to achieve stable nanoparticle suspension?

- Which dispersant (in a group of dispersants) provide better suspension stability and offer better transport of nanoparticle suspensions?

- Does an optimum concentration of dispersant depend on concentration of nanoparticles in suspensions?

- What effect does change in sonication time bring toward stability of nanoparticle suspensions?

- What is optimum sonication requirement and does it depend on sonication power too?

- Is optimum sonication power requirement, dependent on concentration of nanoparticles in suspensions?

- Sonication after dispersion (i.e. addition of dispersants) is better or otherwise?

Furthermore, almost all the studies on the transport of micron, sub-micron or nano-sized particle suspensions through porous media or open conduit are performed by monitoring the ratio of concentration of effluent to influent (C/C_o) with pore volume injections. Particle retention and transport is expressed by break through plots such as seen in figure 1-1.

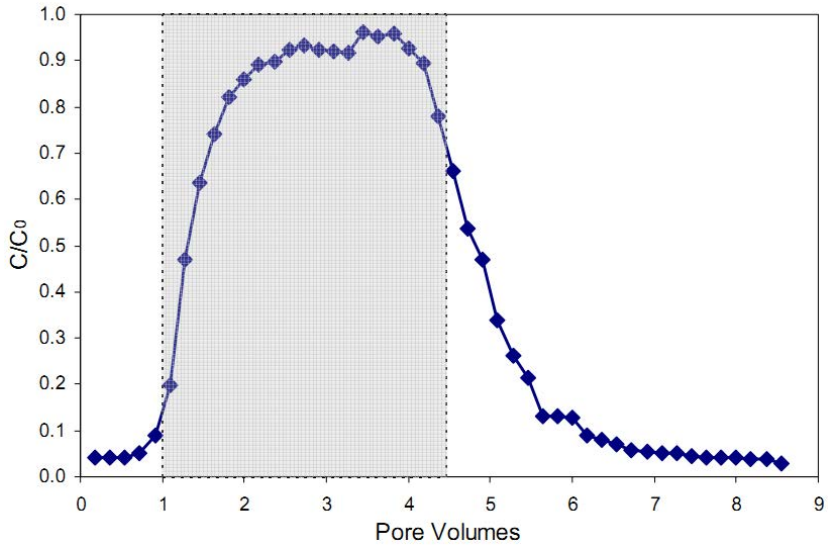

Figure 1-1: Typical nanoparticle breakthrough curve (Rodriguez et al., 2009)

With this kind of plots, it is not quite possible to tell whether or not particle retention is uniform throughout the entire length of the porous media and what could possibly be the governing mechanism/ parameters affecting the retention pattern of these particles. In order to better understand the effects of various parameters such as flow rate, permeability, matrix composition etc. on particle retention and particle distribution, a technique is needed that could provide the particle concentration information along the entire length of core plug. Variations in particle distribution trends at different times during suspension injection and post flush with water would aid in understanding the mechanisms or possible reasons behind such response.

1.3 Objectives and the Scope of the Study

1.3.1 Objectives

- Design and develop optimum fluid formulation for effective suspension of nanoparticles.

- Investigate the factors contributing the transport of nanoparticle suspensions through porous media.

1.3.2 Scope of the Study

1. Carry out an extensive investigation of the effects of following factors on the stability of nanoparticle suspensions by using magnetic susceptibility characteristics of nanoparticles.

    a) Concentration of nanoparticles
    b) Type and concentration of dispersants
    c) Sonication
    d) Method of sample preparation
    e) Applied magnetic field duration

2. Find out a method for preparation of optimum suspension recipe.

3. Investigate the use of magnetic susceptibility characteristics of nanoparticles in estimating the nanoparticle retention and transport through horizontal porous media.

4. Find out the effects of a variety of parameters such as flow rate, lithology, permeability, type of nanoparticles and their concentration, type of suspension recipe etc. on the transport behaviour/ adhesion of nanoparticles.

5. Theoretical discussion on the possible application of nanoparticles in hydraulic fracture diagnostics.

1.4 Structure of the Thesis

Chapter 1 gives a brief overview of nano technology with potential future applications of nanoparticles in reservoir engineering and improved oil recovery. The need for carrying out an empirical method of determining optimum nanoparticle suspensions and their transport through porous media along with objectives and the scope of the study are also presented herein.

Chapter 2 gives a literature review about some potential applications of nanoparticles in reservoir engineering and improved oil recovery and studies performed on the stability of nanoparticle suspensions and their transport through porous media. Various methods applied to achieve the stable nano dispersions are presented in some detail. Earlier application of magnetic susceptibility sensor in monitoring the transport of nano iron particles along with some deficiencies in that study is also discussed.

Chapter 3 includes the material and equipment specifications used in carrying out the experiment work for this study. It also details the experimental procedures

used for static, suspension stability experiments and dynamic, nanoparticle flow experiments through porous media.

Chapter 4 covers the results and discussion about the nanoparticle suspensions stability experiments. The effects of various parameters on the stability of nanoparticle suspensions have been investigated in detail.

Chapter 5 contains the results and discussion about the dynamic, fluid flow experiments through porous media. The effects of various parameters on the transport or adhesion of nanoparticle suspensions are detailed here.

Chapter 6 is on theoretical discussion and expected response from magnetic sensing of nanoparticle coated proppants for hydraulic fracture diagnostics. Also, the effects of different parameters on magnetic susceptibility trends during injection of nanoparticle suspensions are presented.

Chapter 7 presents the conclusions about this study and the recommendations about how to sequentially perform the static and dynamic experiments to find out an optimum recipe for different types of nanoparticles and porous medium used. Few suggestions for further research work are also given.

Chapter 8 contains the references.

2 LITERATURE REVIEW

This chapter presents literature review about some of the nanoparticles applications in petroleum engineering, magnetic susceptibility, different forces those play important role in agglomeration and adhesion of nano sized particles and different studies performed on nanoparticles with an attempt to understand the role of various factors on the stability, dispersion and adhesion of nanoparticle suspensions. In the end, discussion on the improvements in magnetic susceptibility technique (employed earlier in year 2010) on the study of transport of nanoparticle suspensions are presented.

2.1 Application of Nano Technology in Petroleum Engineering

Zhang et al. (2011) have described some of the potential uses of nanoparticles in detection of rock and fluid properties of the formation. They (Zhang et al., 2011) have mentioned that fluid saturations in the formation away from the borehole could be determined by delivering the paramagnetic nanoparticles in the formation, applying magnetic field and measuring the response. The response measured in terms of sound waves is found out to be a function of fluctuation of fluid/ fluid interfacial layer and nanoparticle oscillation. Further research work is needed to interpret the measured response for determining fluid distribution and saturation away from the borehole.

Addition of small fractions of nanoparticles in base fluid has shown significant increase in the thermal conductivity of the base fluid. Research work performed by Masuda et al., (1993), Lee et al., (1999), Eastman et al., (2001) and Chopkar et al., 2006 have highlighted this unique aspect of nano sized particles. This useful feature of nanoparticles needs to be explored for use in heavy oil and bitumen recovery processes, to increase the rate of heat transfer and affect more reservoir area away from the steam injection zone.

Nano sized drilling fluid additives have shown to improve the drilling fluid characteristics thereby addressing various challenging downhole drilling problems particularly in hostile high temperature high pressure (HTHP) environment. Singh and Ahmed (2010) have presented a detailed review of prospective applications of nanotechnology in drilling and completion technology. Research work on the use of nanoparticles has demonstrated applicability of nanoparticles towards wellbore stability, foam emulsions and polymer stability and removal of toxic gasses.

Shen et al. (2008) studied the injection of sub-micron sized Ca-DTPMP particles into porous media for effective scale inhibition purpose. (DTPMP stands for Diethylenetriaminepenta, also known as methylene phosphonic acid which is used for scale inhibition). Injection of Ca-DTPMP particles into the formation is described advantageous over conventional “squeeze treatment”, owing to smooth and controlled release of scale inhibitors. In squeeze treatment, methylene phosphonic acid is injected into the borehole forming precipitates of cationic salts of methylene phosphonic acid only in the near wellbore region. This results in a very high release of scale inhibitor early in the life of well and vice versa. Also noticeable fraction of scale inhibitor (e.g. Ca-DTPMP) is reported to be left in the well. Injection of Ca-DTPMP particles into the formation would enable better distribution of the scale inhibitor (Ca-DTPMP) deeper into the formation and over a bigger area. These particles will settle down and dissolve over a period of time to provide a better inhibition control.

Shokrlu and Babadagli (2010) have discussed the contribution of various phenomena in viscosity reduction of heavy oil/ bitumen with of different nanoparticles. The viscosity reduction characteristic of nanoparticles could be exploited with nanoparticle delivery to the bitumen deposit/ reservoir which would enable higher recovery rates with lower steam oil ratios (SORs).

2.2 Interplay of Forces in Nanoparticles

Interplay of attractive and repulsive forces in nanoparticles has been exploited in various industries, either by facilitating the formation of agglomerates or else by increasing the repulsive forces to attain dispersed aqueous solid suspensions. Stable suspensions are difficult to achieve for nano sized particles as compared to micron sized particle due to increased specific surface area and surface characteristics. Surface adsorption phenomena become dominant with sizes in nano meter range, as surface interaction forces become to dominate over electrostatic repulsive forces.

Nano sized particles, unlike micron sized particles are highly unstable and have a very strong tendency to form agglomerates under the effect of short range attractive van der Waals forces. Brownian motion is also a key factor which is very significant in nano sized particles, as Brownian motion is inversely related to the particle size. High Brownian motion increases the chances of particle collision and raises the aggregation rate.

The electrostatic forces (due to surface potential) and steric forces (due to thin layer of dispersant around particle, preventing particle surfaces coming too close) repel the particles and offer a barrier to coalescence as long as the repulsive forces are dominant. For nano sized particles the normalized surface potential is low (Iijima, M. and Kamiya, H., 2009) that leads to small potential barrier of electric double layer (EDL) which may facilitate the accelerated agglomeration of nanoparticles. The surfaces of nanoparticles can be modified to generate high surface potential and hence high repulsive forces which can prevent particle agglomeration.

It is often seen that the solid particles those are stable in suspensions, get adsorbed to the surface of the porous media through which it is passed. It happens mainly due to difference in the surface charge between nanoparticles and porous media surface.

2.3 Stability and Transport of Nanoparticle Suspensions

Interaction between particles and particle and porous media surface can be altered to accelerate or decelerate agglomeration (suspension stability) and deposition by changing the electric repulsive charge between the nanoparticles or nanoparticle and porous medium surfaces by different methods. Espinasse et al. (2007) said that the methods used to prepare suspensions can have significant affect on transportation and retention of nanoparticles. Stable colloidal suspensions may be formed by long term stirring of nanoparticles and/ or their sonication in water (Bensasson et al., 1994). Another method could be to dissolution of material (e.g. C60) in solvent, their mixing with water followed by evaporation to get aqueous suspensions (Deguchi, 2001). Many researchers have also shown improved stability results of nanoparticle suspensions with the use of dispersants (surfactants/ polymer). Also number of studies on nanoparticle suspensions has shown strong influence of pH and ionic strength on stability, agglomeration and adsorption of nanoparticles. Some of the studies describing these key factors influencing stability of nanoparticle suspensions and their transport through porous media are presented below.

2.3.1 **Ultrasonication**

Shokrlu and Babadagli (2010) used 30 minutes of ultrasonication to achieve the original size of nanoparticles. Earlier, Shah (2009) also used 30 minutes sonication on CuO nanoparticles prior adding dispersant. Ultrasonication for particulate dispersion (disintegration of nanoparticles agglomerates) require presence of some liquid phase where small bubbles are generated and shock waves are produced as they implode (Sonicator 3000 manual), which helps in dissociation of nanoparticles agglomerates. There exists a question that how much sonication is sufficient to effectively disperse the nanoparticles? Furthermore, Shah (2009) introduced dispersant after sonication. There is a likelihood that nanoparticles, agglomerate during time interval between sonication and addition of dispersant. Therefore, the effect of dispersion followed by sonication shall also

be examined in our study for stability of nanoparticles suspensions. Determination of the effectiveness of nanoparticles dispersion method is important since presence of nanoparticles in the form of agglomerates can affect on physio-thermal and viscosity reduction behaviour of nanoparticles suspensions.

Wang et al. (2008) studied the transport and retention of nC60 agglomerates through vertical porous medium of glass beads and Ottawa sand and found that considerable concentration of injected nanosized C60 agglomorates was retained in water saturated porous medium. They used sonication and stirring to create stable suspensions of nC60 aggregates. The retention concentration of C60 ranged from 8% to 49% in glass beads and up to 77% in Ottawa sand column. They showed that the retention of C60 in porous medium was consistent with the mathematical calculations based on interaction between C60 and porous medium surfaces. The retained concentration of C60 aggregates was measured by dissecting the flow column in number of lengths, adding de-ionized water, stirring and ultrasonication. There still exists a possibility that fraction of retained nanoparticles or their aggregates might not have separated from glass beads/ sand. This possibility is seconded by the low overall recovery of injected C60 particulates/ agglomerates in some instances (i.e. 95%).

Aggregate size was determined from dynamic light scattering (DLS) technique and concentration in influent and effluent from UV-vis spectroscopy. Derjaguin-Landau-Verwey- Overbeek (DLVO) theory (Derjaguin and Landau, 1941; Verwey and Overbeek, 1948) was used to calculate the interactions between C60 aggregates and porous medium surface. One of the reasons for consistent experimental results with numerical model used for transport of C60 agglomerates even with the limitations of DLVO theory for small sized particles could be the high average agglomerate size (95 nm). Though the measured and predicted results were generally in agreement, numerical model could not explain the increased retention of C60 agglomerates near the inlet of glass beads column.

With the current experimental setup used in our study one can avoid the above described tedious process of determining the retention concentrations of nanoparticles. However, the magnetic susceptibility technique of determining particulate concentration in porous medium is semi quantitative and also the precision of this method needs to be investigated by counter checking with some other quantitative measurement method such as UV-vis spectroscopy. In most of the transport experiments either UV-vis spectroscopy or mass balance is performed on effluent volumes after different volume injection of nanoparticle suspensions and water flooding and results are presented in the form of influent to effluent concentration ratios. The particulate deposition behaviour along the porous medium length cannot be observed with such a technique until the whole flow experiment is completed.

2.3.2 **Surface Modification with Dispersants**

Surface modification of nanoparticles by using polymers or polymeric surfactants is a technique that could be used to keep the particles dispersed. Dispersants form a thin layer around the nanoparticles which changes the hydrodynamic radius of nanoparticles. Addition of dispersant alters the surface charge of nanoparticles and provides steric repulsive force when particles come close and prevent them from agglomeration.

Anionic and cationic type of polymeric surfactants have been tried in past to increase the electric potential of nanoparticles which further aid in prevention of agglomeration of metal oxides (Nsib et al., 2006). The dispersants form a thin layer around the nanoparticles and/or their aggregates preventing them to further agglomerate and reduce adsorption/ sticking to the surfaces of medium where these are contained in.

Cameselle et al. (2008) used different polymers and surfactants in various concentrations to investigate the stability and effective dispersion of nanoparticle suspensions. Zeta potential was used to observe the stability and effective

dispersion of suspensions. They (Cameselle et al., 2008) found out that aluminum lactate increases the stability of suspensions and due to the benefit that it is environmental friendly it can be used in transport of nanoparticle suspensions for decontamination of soils and ground water.

Rodriguez et al. (2009) performed flow experiments with surface-treated silica nanoparticle suspensions through sedimentary rocks of different lithologies and permeabilities. The silica particles were of two different sizes (i.e. 5nm and 20 nm) and coated with polyethylene glycol, which acted as a dispersant. The thin layer of polyethylene glycol prevents particle from agglomeration by suppressing ionic charges on silica surfaces and allowing stable nanoparticle suspensions. They took refractive index measurements to determine the nanoparticle concentration in effluent. Small ultimate retention (<10%) was seen after the post flush with de-ionized water even in very low permeability rock samples (15 md), but the ultimate retention varied with different rock lithologies. They said that particle retention was independent of permeability. Both Wang et al. (2008) and Rodriguez et al. (2009) described that nanoparticle retention was dependent on lithology of the porous media through which transport of nanoparticles is flowing through.

Shah (2009) used a fixed concentration of Poly DiMethyl Siloxane (PDMS) polymer as dispersant in his study. The fixed concentration of dispersant used in the experiments may or may not be sufficient for effective dispersion of nanoparticles. It would therefore be of interest to find the effect of type and concentration of dispersants.

Shen et al. (2008) prepared Ca-DTPMP sub-micron particle suspensions by using 0.2 wt. % concentration of phosphino-polycarboxylic acid (PPCA) as dispersant in majority of their experiments. Dynamic Light Scattering technique, zeta potential measurements and Transmission Electron Microscopy (TEM) were used in their study of suspension stability and transport. They used a fixed concentration of dispersants and same sonication time in majority of stability and

transport experiments. Sonication power values are not specified those would actually determine the sonication energy applied to suspensions. They (Shen et al., 2008) conducted some experiments wherein sonication energy and dispersant (PPCA) concentration was varied and showed that at higher ionic concentration, higher sonication energy and higher concentration of dispersant improves the stability and transport of Ca-DTPMP suspensions. Shen et al. (2008) prepared suspensions by sonication after addition of dispersant.

Darko-Kagya and Reddy (2010) prepared nano iron suspensions with 10% w/w concentration (w.r.t nano iron particle concentration) of aluminum lactate dispersant and checked the effects of flow rate, concentration of nanoparticles and effect of dispersant on transport of nanoparticles. They reported that difference in mobility of nanoparticle suspensions, with and without the addition of dispersant is higher when concentrated nanoparticle suspensions are used. They explained it as a result of higher tendency of nanoparticles to agglomerate in concentrated nanoparticle suspensions. Another possible reason could be that dispersant concentration was proportionally increased in high concentration suspension that might have increased the dispersion of nanoparticle suspension.

2.3.3 **pH and Ionic Strength**

Effect of ionic strengths and pH of suspensions have been studied by number of researchers. Increase in ionic strength reduces the electric double layer thus allowing van der Waals attractive forces to dominate. On the other hand, pH value of suspensions close to pH value of zero potential charge, pHzpc (value of suspension when electrostatic charge on particles becomes zero) facilitate agglomeration and adhesion.

Kobayashi et al. (2005) studied the effect of pH and ionic concentration on charging behaviour and aggregation rate of different sizes of silica nanoparticles and found out that the magnitude of negatively charged silica particles increases with increasing pH and ionic concentration. Aggregation rate was found out to be

decreasing with increasing pH at low ionic strengths and lowering pH at high ionic strengths. Stabilization of nanoparticle suspensions at low pH was found to be prominent for small sized nanoparticles. Such stabilization behaviour was thought to be due to presence of an additional repulsive force. The authors described the similarities and differences between DLVO predictions and experimental findings and tried to explain the dissimilarities with the help of an additional repulsion or drag force, the quantitative expression of which has not been described. Nanoparticles with largest size used in these experiments showed closest resemblance to the DLVO model predictions and non-DLVO forces effect is pronounced for smaller size nanoparticles.

DLVO theory defines particle interaction as superposition of electrostatic double layer repulsive forces and attractive van der waal force. DLVO theory suggests an increase in stability of particle suspensions with increase in surface potential and with decreasing ionic strength. The suspension behaviour of silica particles reported by several researchers has been disagreeing with DLVO theory. Since silica particle have pHzpc close to 2.5, these are expected to have very small charge at lower pH values and thus particle agglomeration should be more whereas in reality these exhibited stable particle suspensions.

Kallay and Zalac (2002) also studied the stability of nano dispersions by using Brønsted transition state theory instead of DLVO theory due to limitations of DLVO theory and found out that pH and ionic strength of electrolyte carry the most effect with regards to stability of nano dispersions. The stability of nano dispersions is also strongly related to the pHzpc of nanoparticles. The numerical simulations showed significant effect of particle size on agglomeration i.e. nanoparticles become highly unstable with decrease in size as van der waals attractive forces dominate the electric double layer repulsive force. It was seen that application of Brønsted concept (Brønsted, 1922) showed a decrease in stability of nano dispersions with the presence of electrolyte. The results of this simulation study did not cover the entire range of pH and electrolyte

concentration effect as seen from the experimental results presented by Kobayashi et al. (2005). The advantages of using Brønsted concept over DLVO or "modified" DLVO theory would have been better understood if experimental results for a broad range of pH and electrolyte concentration would have had been explained.

Guzman et al. (2006) used transparent micromodels to visually monitor the clogging of micron sized pores with nanoparticle agglomerates. Dynamic light scattering was used to measure the size of nanoparticle aggregates in suspensions. They (Guzman et al., 2006) used titania nanoparticles to investigate the effect of pH on interaction of nanoparticles and adhesion to the porous media and showed that varying pH changes the surface potential of the nanoparticles which in turn affects on particle agglomeration and particle mobility through porous media. Their results showed that over 80% of nanoparticles or their aggregates were mobile over a wide range of electrolyte pH except that when pH was close to pH of zero potential charge (pHzpc) of the nanoparticles.

In transport experiments pH 7 suspensions exhibited least amount of nanoparticle mobility and largest aggregates were visually monitored. Particle deposition was measured to be highest when pH of nanoparticle suspensions was between pHzpc of nanoparticles (5.9) and pHzpc of porous medium material (2.5), however the nanoparticles aggregates were reported to be highly mobile. At pH 12, highest attachment (in repulsive interaction zone) to porous medium surfaces was observed despite the presence of highest repulsive forces. They concluded that experimental results do not entirely match the "modified" DLVO theory (Bhattacharjee and Elimelech, 1997) of nanoparticle and aggregate interactions with porous medium surfaces.

According to DLVO theory the total interaction energy is a sum of van der waals interaction energy and electrostatic interaction due to electric double layer (EDL). However, this theory assumes that the thickness of EDL is smaller than particle radius. Iijima, M. and Kamiya, H. (2009) showed that the theoretical curve

generated by DLVO theory and measured forces from AFM colloid probe method have a good match for only higher nano meter sizes and inter-particle distances larger than few nano meters where van der Waals forces are not prominent. Due to this limitation of DLVO theory, Guzman et al. (2006) used surface element integration technique proposed by Bhattacharjee and Elimelech (1997) in their study which was thought to be valid for small particles of nano meter size but failed to replicate all the results.

Tseng and Wu (2002) performed experiments on aqueous alumina (Al_2O_3) suspensions to investigate the effect of pH of suspensions and nanoparticle concentration (in volume fractions) on particle aggregation. The pHzpc of alumina nanoparticles (γ -Al_2O_3) has been reported to be between 7-9 pH value (Reed. J. S., 1995). Sedimentation tests were performed to observe the level of settlements in these experiments. The suspensions showed good dispersion results at pH 2.

At pH 11 and relatively lower volume solid fractions (i.e. below 0.06) significant particle settlement was observed, indicating presence of dominant attractive van der waals forces over electrostatic repulsive forces. As solid fractions increased, improved suspension behaviour was seen due to formation of porous particulate network. Formation of this porous particulate network was supported with the absence of shear thickening behaviour of these high concentration suspensions over the entire shear rate range examined. Such kind of response is consistent with the high aggregation rate behaviour seen for silica nanoparticles (Kobayashi et al., 2005) and high attachment of titania nanoparticles (Guzman et al., 2006) to porous media. These observations showed domination of attractive van der waals forces at high pH values (pH>11) which facilitated the formation of nanoparticle aggregates.

Samal (2009) described that optimum pH value for stable suspensions of different nanoparticles varies with the presence and absence of surfactants. She measured the stability of the nanoparticle suspensions by taking readings of zeta-potential.

In present study, only first two methods of obtaining suspension stability and transport through porous media are studied. The effects of pH and ionic strength can be incorporated by expanding findings of this research work.

2.4 Magnetic Susceptibility

2.4.1 Definition

When a material is subjected to applied magnetic field, a magnetic moment is induced in it. This induced magnetic moment could either be positive or negative depending upon the electronic configuration of atoms or ions in a molecule. The magnetic susceptibility of a material is an indicator of its magnetization when brought into magnetic field and is defined as ratio of magnetization to applied magnetic field. Mathematically,

$$M = X_v H \qquad (2\text{-}1)$$

Where,

M = Magnetization (A/m)

X_v = Volume magnetic susceptibility

H = Magnetizing Field (A/m)

2.4.2 Classifications of Materials

Materials can be classified into following three main categories.

- Diamagnetic
- Paramagnetic
- Ferromagnetic

Diamagnetic materials generate a magnetic field opposite to applied magnetic field, thus resulting in a negative magnetization and negative magnetic susceptibility. Diamagnetism result mainly due to orbital motion of electrons and is present in all materials (Even in paramagnetic and ferromagnetic materials). However, in paramagnetic and ferromagnetic materials, negative as well as positive magnetic moments take place, but the net effect is positive magnetization.

Paramagnetic materials have net positive magnetic moments due to their tendency to align with applied magnetic field. Paramagnetic materials are only magnetized when subjected to externally applied magnetic field. The magnetization in paramagnetic materials is returned back to zero when applied magnetic field is removed. Paramagnetic materials have positive susceptibility but with a value generally lot less than susceptibility of ferromagnetic substances.

Ferromagnetic materials remain magnetized even after the applied magnetic field is removed and posses very high magnetic susceptibility. They follow a non-linear magnetization trend with applied magnetic field. However, at small applied magnetic fields there is usually a linear relationship between magnetization and applied magnetic field. At low applied magnetic field, ferromagnetic minerals typically show a higher magnetic susceptibility than at very high magnetic fields. Figure 2-1 shows magnetic hysteresis curves for ferrite nanoparticles produced by Dr. Potter’s research group at the University of Alberta for ferrite nanoparticles produced by Dr. Barron's group at Rice University, USA supplementing the above statement.

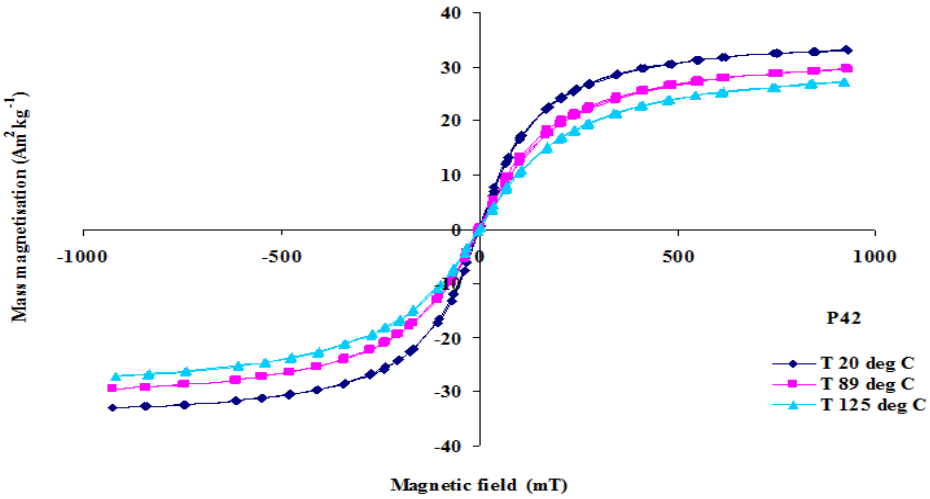

Figure 2-1: Magnetic hysteresis curves for nanoparticle spinel ferrite P42. (Courtesy: Dr. Potter's research group at the U of A)

Also shown below is a figure (figure 2-2) of magnetic susceptibility of some common reservoir minerals and fluids measured at low magnetic fields.

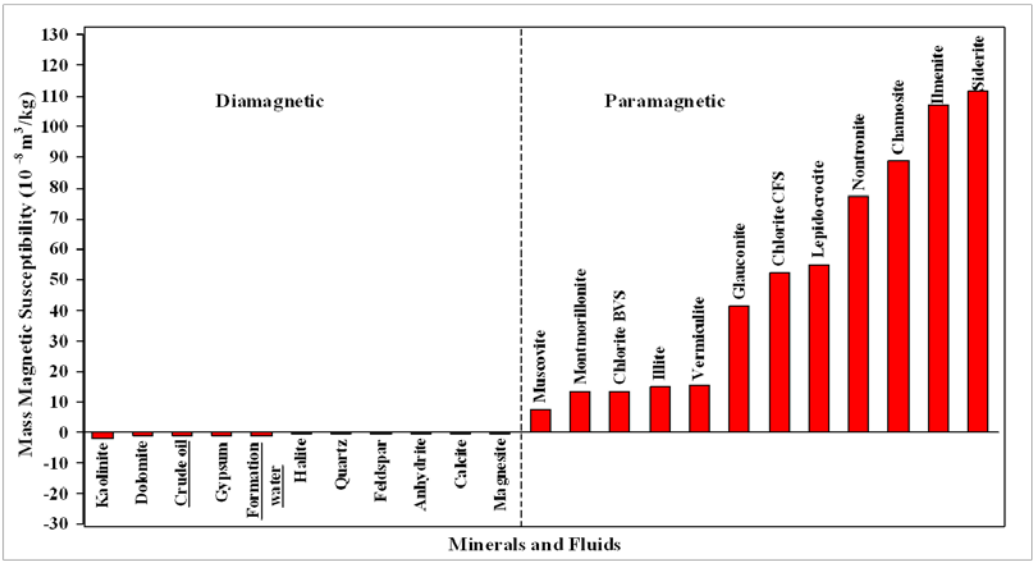

Figure 2-2: Magnetic Susceptibility of diamagnetic and paramagnetic materials and fluids (Ivakhnenko and Potter, 2004).

It is obvious from figure 2-2 that most of the diamagnetic and paramagnetic materials/ fluids frequently found in reservoir have a magnetic susceptibility close to zero. Ferromagnetic materials typically have mass magnetic susceptibility of the order of 10^{-05} to 10^{-03} SI units which is way higher than generally found diamagnetic and paramagnetic materials.

2.4.3 Application of Magnetic Susceptibility in Study of Suspension Stability and Their Transport through Porous Media

The magnetic susceptibility of the materials is a useful characteristic that may be exploited to locate the concentration of high magnetic susceptibility material in low magnetic susceptibility media. High susceptibility contrast between ferromagnetic or super-paramagnetic material and commonly found diamagnetic and paramagnetic material can make it a potential tracer material in fluid flow, fracture diagnostics and any other techniques requiring tracer. High magnetic susceptibility of nanoparticles (NPs) can be used as a contrast agent to estimate the concentration of nanoparticles in nanoparticle suspensions. Also, the time based measurements of magnetic susceptibility may be used to estimate the particle suspension characteristics or in other words to determine the stability of nanoparticle suspensions. The magnetic susceptibility response may also be used in estimation of concentration of nanoparticles in porous media which in turn can be used in the study of transport of nanoparticle and their retention behaviour.

2.5 Application of Magnetic Susceptibility Technique for Determining the Transport Behaviour of Nanoparticle Suspensions

Darko-Kagya and Reddy (2010) were the first to use magnetic susceptibility technique to investigate the transport and retention behaviour of high susceptibility nanoparticles. They used 135 mm diameter Bartington's MS2C core logging sensor to investigate the real time transport of nano sized iron particles through a column of sand pack. The flow column consisted of 35 mm ID Plexiglass® tubing of 135 mm length. They checked the effect of two different

flow rates, two different concentrations of nanoparticles and addition of aluminum lactate as dispersant on the transport and adhesion behaviour of nanoparticles. The study was primarily focussed towards increasing the transport characteristics of iron nanoparticle suspensions through soils which basically acts as decontaminant. They took magnetic susceptibility measurements with a lower resolution of 1.0 SI units. Also, the diameter of sensor was more than 3 times the diameter of flow column which also would have contributed in poor resolution and shall be more affected by the nanoparticles distribution away from the point of measurement than using a higher flow column diameter to sensor diameter ratio. Darko-Kagya and Reddy (2010) concluded that increase in flow rate increased the transport of nanoparticles. The magnetic susceptibility trends showed relatively very high susceptibility at the inlet point of vertical column even for aluminum lactate treated suspensions which is an indicator of particle adsorption to the surfaces of porous media. However, the high magnetic susceptibility at inlet point was relatively lower for aluminum lactate treated nanoparticle suspensions.

Figure 2-3 shows the susceptibility response at the end of four experiments performed by Darko-Kagya and Reddy (2010) with and without aluminum lactate modified nanoparticle suspensions. Although the aluminum lactate modified suspensions for high concentration of nanoparticles show relatively better distribution of nanoparticles, any significant improvement is not evident; this raises the question about the suitability of aluminum lactate towards its transport through porous medium. Although the suspensions were reported to be quite stable (Cameselle et al., 2008), they did not work that well in porous media. Therefore it may be concluded that although nanoparticle suspensions are found stable these might not prevent adsorption to the surfaces of another medium, when brought in contact with it. This would primarily be due to difference in surface potential of nanoparticles and porous medium surfaces.

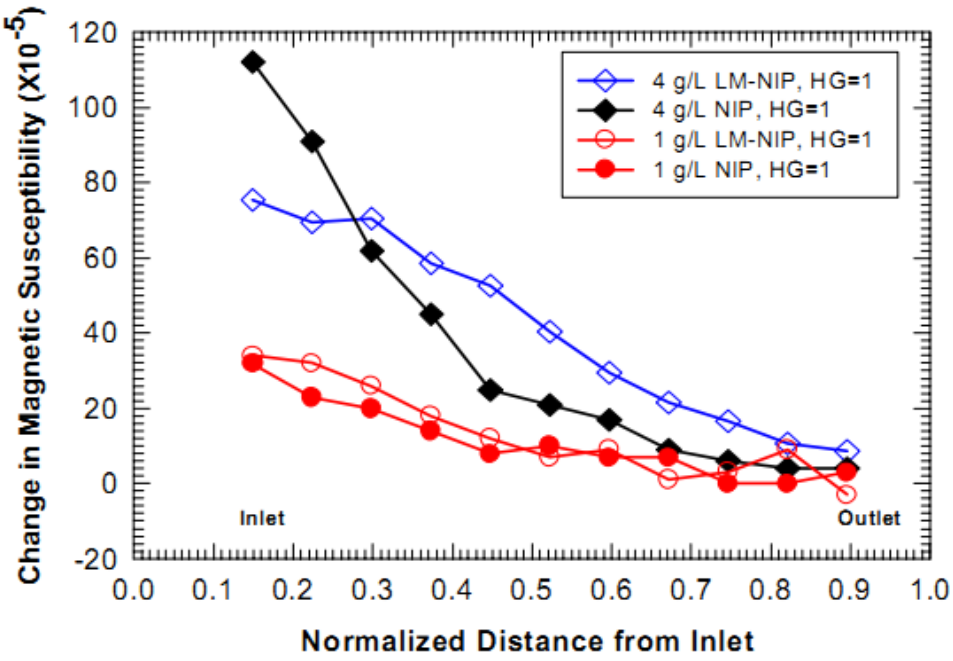

Figure 2-3: Magnetic Susceptibility values after the end of four flow experiments with and without lactate modified nano iron particles at same hydraulic head.

(Courtesy: Darko-Kagya and Reddy, 2010)

Darko-Kagya and Reddy (2010) used vertical column of porous media for suspensions flow, which was specifically designed to address the soil decontamination issues. Whereas, this study is aimed at transport of nanoparticles in reservoir that required experimentation work to be performed on horizontal flow cell. Appropriate sizing of the flow cell is used to enhance the sensing resolution which was relatively poor in Darko-Kagya and Reddy's (2010) experimental work due to high sensor to flow cell diameter ratios. Furthermore, Darko-Kagya and Reddy (2010) performed only few transport experiments wherein high amount of nanoparticle retention is seen. They used nanoparticle concentration, flow rates and suspension with and without dispersant treatment (aluminum lactate) as variables in their study. In comparison to their study, this study investigates the effect of extensive range of parameters including flow rates,

lithology, permeability, type of dispersant, suspensions preparation methods, concentration of nanoparticles etc.

3 MATERIALS, EQUIPMENT AND EXPERIMENTAL PROCEDURES

The materials, equipments and experimental procedures used in the project are discussed in this chapter.

3.1 Materials

3.1.1 Nanoparticles (NPs)

Five types of nanoparticles from MTI Corporation, USA were used in nanoparticle suspension stability and their flow experiments through porous media. Physical properties of these nanoparticles are presented in Table 3-1 through Table 3-5.

Table 3-1: Physical properties of Hematite (α-Fe_2O_3) NPs.

Property	Description
Appearance	Red brown
Purity	99.5%
Morphology	Spherical
Average Particle Size (APS)	30 nm
Specific Surface Area (SSA)	> 50 m2/gm
Bulk density	1.2 gm/cm3
True density	5.24 gm/cm3

Table 3-2: Physical properties of Maghemite (γ -Fe_2O_3) NPs.

Property	Description
Color	Red brown
Purity	99+%
Morphology	Spherical
Average Particle Size (APS)	20 nm
Specific Surface Area (SSA)	>30 m2/gm
Bulk density	1.20 gm/cm3
True density	5.24 gm/cm3

Maghemite is prepared by oxidation of magnetite. It has a chemical structure similar to magnetite but iron and oxygen atoms in compound same as hematite.

Table 3-3: Physical properties of Magnetite (Fe_3O_4) NPs.

Property	Description
Color	Black
Purity	99.9%
Morphology	Spherical
Average Particle Size (APS)	20 nm
Specific Surface Area (SSA)	>60 m2/gm
Bulk density	0.84 gm/cm3
True density	5.0 gm/cm3

Table 3-4: Physical properties of Cobalt Ferrite ($CoFe_2O_4$) NPs.

Property	Description
Color	Black
Purity	99.9%
Morphology	Spherical
Average Particle Size (APS)	40 nm
Specific Surface Area (SSA)	Information not available
Bulk density	0.41 – 0.51 gm/cm3
True density	5.3 gm/cm3

Table 3-5: Physical properties of Nickel Ferrite ($NiFe_2O_4$) NPs.

Property	Description
Color	Black
Purity	99.5%
Morphology	Nearly spherical
Average Particle Size (APS)	40 nm
Specific Surface Area (SSA)	59 m2/gm
Bulk density	0.89 gm/cm3
True density	5.368 gm/cm3

3.1.2 **Glass beads and sand**

Following mesh sizes of glass beads and sand with corresponding equivalent size in micrometer were used in fluid flow experiments. The glass beads and sand were purchased from SIL Industries Minerals, Canada.

Table 3-6: Description and sizes of sand and glass beads.

Material Description	Mesh Size	Equivalent Size (µm)
SIL 40-70 glass beads	40-70	210-400
SIL 50-80 glass beads	50-80	177-297
SIL 100-170 glass beads	100-170	88-149
SIL 170-325 glass beads	170-325	44-88
SIL-4 sand	30-60	250-595

3.1.3 **Chemicals and Dispersants**

Nickel Chloride Hexahydrate ($NiCl_2.6H_2O$):

Nickel chloride is a paramagnetic water soluble salt that was used for calibration of MS2C sensor and to see the effect of lateral distribution of uniformly distributed paramagnetic mixture. Nettleton and Sugden (1939) showed that this paramagnetic salt exhibit a susceptibility response consistent with change in the concentration and developed an empirical formula relating molar concentration of nickel chloride with magnetic susceptibility.

Dispersants:

Xantham gum polymer and three different types of surfactants were tried in different concentrations in nanoparticle suspensions to observe the change in stability of nanoparticle suspensions and their transport behaviour (adhesion/ retention) through porous media. The dispersants (polymer and surfactants) used in this study are listed below. Specifications of the polymer and surfactants used for dispersion of nanoparticle suspensions are tabulated below.

Table 3-7: Specifications of Xanthan Gum polymer used as dispersant.

Property	Description
Color	White to tan
Solubility	Soluble in water
Bulk density	~0.80 gm/cm3

Table 3-8: Specifications of surfactants used as dispersant.

Description	Type	Appearance
Cetyltrimethyl Ammonium Bromide (CTAB)	Cationic	White powdered
Sodium Dodecylbenzeno Sulfonate (DDBS)	Anionic	White granular
Tergitol (TGT)	Non-ionic	Clear, liquid

3.2 Equipment

3.2.1 **Magnetic Susceptibility Core Logging System**

The magnetic susceptibility measuring system from Bartington Instruments was used in NP mixture stability study and fluid flow experiments. The system mainly comprises of an 80 mm diameter/ aperture MS2C sensor and an MS2 meter which are connected through a signal transmission cable. The system works on a very simple principle that when a material is subjected to an applied magnetic field, it is negatively or positively magnetized, depending upon the type of material. The magnetic susceptibility is a function of magnetization which is then determined from frequency of oscillation sensed by an inductor in the sensor (MS2 manual, Bartington® Instruments). The meter has an option to display readings both in SI and CGS systems and has a high resolution susceptibility reading option (0.1 range that takes 11 seconds to take one reading) and a low resolution (1.0 range that takes reading in only 1.1 seconds). The measuring range of the MS2 magnetic susceptibility system is 1-9999 x 10^{-5} in SI units and 1-9999 x 10^{-8} in CGS units.

The size of the MS2C sensor (80 mm) was selected relative to the size of flow cell (63.5 mm OD, 57 mm ID) to provide sufficient clearance. This clearance was essentially needed to avoid any obstruction during movement of MS2C sensor across the full length of flow cell and also to keep the option for installation of any pressure/ temperature ports open. Most importantly, the internal diameter (ID) of the flow cell to sensor aperture ratio would require no correction and shall give true susceptibility directly at a point in homogenous media where distance to either sides of point of measurement is greater than diameter/ aperture of the MS2C sensor.

Figure 3-1 and Figure 3-2 are pictures of MS2C sensor and MS2 meter respectively.

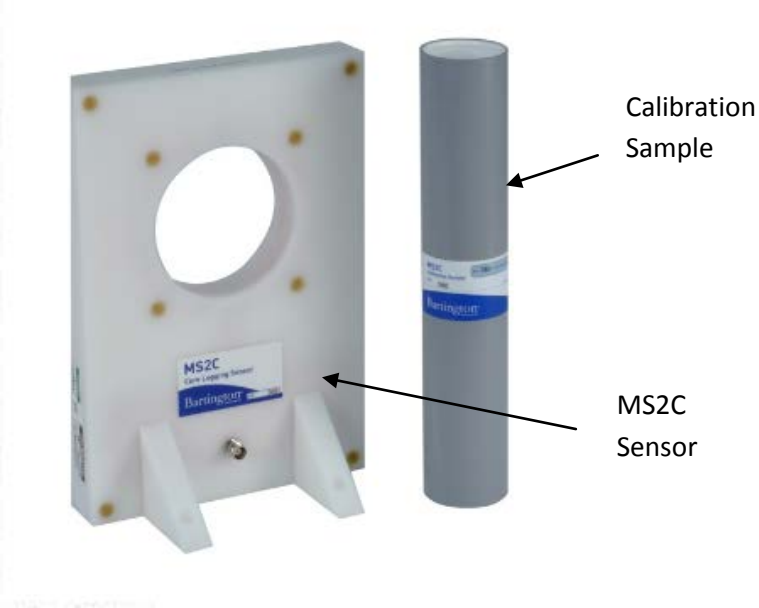

Figure 3-1: Magnetic susceptibility core logging sensor.

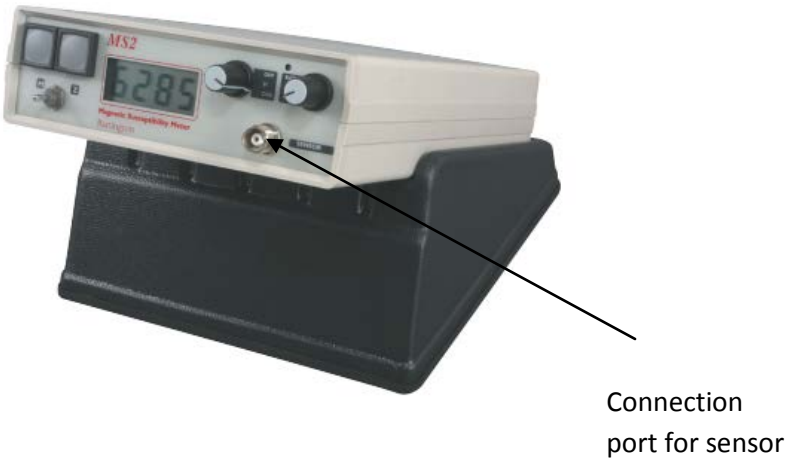

Figure 3-2: MS2 magnetic susceptibility meter.

3.2.2 **Sonicator**

Misonix model 3000 sonicator was used to disintegrate the NPs in the base fluid. The sonicator consists of three major components, the generator that converts 110

V and 50/60 Hz input power supply to 20 KHz output energy, the convertor that converts electrical energy to longitudinal vibrations and lastly the probe which amplifies and transmits the high frequency vibrations to liquid mixture. As a result of this process, cavitations take place in the liquid mixture, generating tiny bubbles which implodes and produce shock waves (Manual Misonix model 3000 sonicator). These shock waves help in disintegration of micron sized clusters of nanoparticles. Figure 3-3 is a picture of Misonix model 3000 sonicator with its major components marked therein.

Figure 3-3: Misonix model 3000 sonicator.

3.2.3 **Flow Cell and Associated Equipment**

A non-metallic flow cell made of acrylic tube and acrylic blocks was designed and constructed for fluid flow experiments to observe the transport behaviour of nanoparticles through glass beads and sand packs. Acrylic blocks were machined to fit into the internal diameter of the tube, as push-in type end caps. Provision of

two ports at both ends of flow cell (i.e. end caps) was kept for study of simultaneous flow of two fluids. Filter papers were used at the inlet and outlet end of flow cell to prevent the flow of glass beads or sand.

Dimensions (i.e diameter and length) of the flow cell were selected to get improved measured susceptibility, reasonable number of measurement points and ease in flow cell handling and packing/ un-packing. Smaller diameter flow cell results in a lower measured susceptibility response, which would amplify any error in the susceptibility measurements after corrections are applied to obtain true susceptibility. The length of flow cell (200 mm or 8 inches) provides sufficient measurement points to closely monitor the transport behaviour of the nanoparticle suspensions with distance from injection/ withdrawal ends. Specifications of the flow cell are presented below in table 3-9.

Table 3-9: Specifications and dimensions of acrylic core holder.

Outer diameter	2.5 inches
Inside diameter	2.25 inches
Wall thickness	0.125 inches
Length	8 inches
Volume	521 cc
Pressure Rating	>50 psi
Injection/ withdrawal port sizes	0.25 inches (2 each)

Figure 3-4 is a picture of flow cell/core holder used in the fluid flow experiments and figure 3-5 shows the schematic of flow cell.

Figure 3-4: Components of flow cell (Acrylic pipe and end caps).

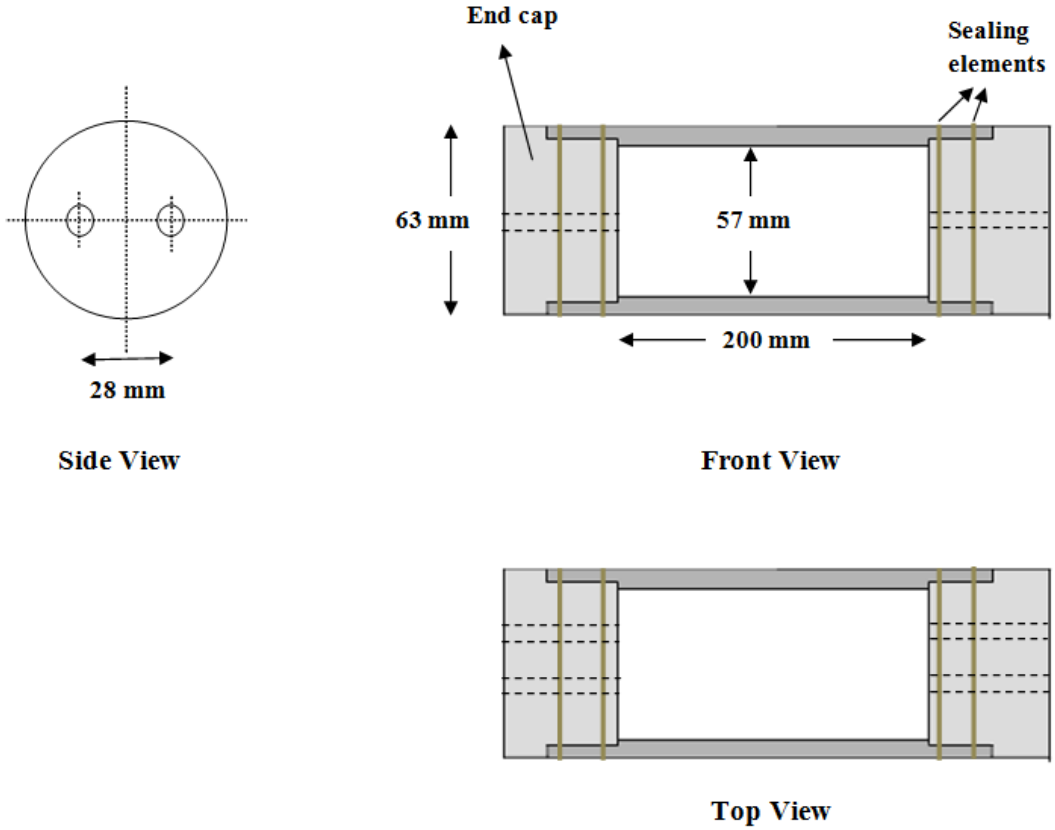

Figure 3-5: Schematic of acrylic flow cell

Associated equipment was also non-metallic and made of wood. The associated equipment was used to hold the flow cell and to keep it concentric to the aperture of MS2C sensor. Keeping flow cell was necessary in order to avoid any errors associated with eccentricity of the flow cell. Figure 3-6 is a laboratory picture of experimental set up used for magnetic susceptibility measurements, showing flow cell, its holding apparatus and MS2C sensor.

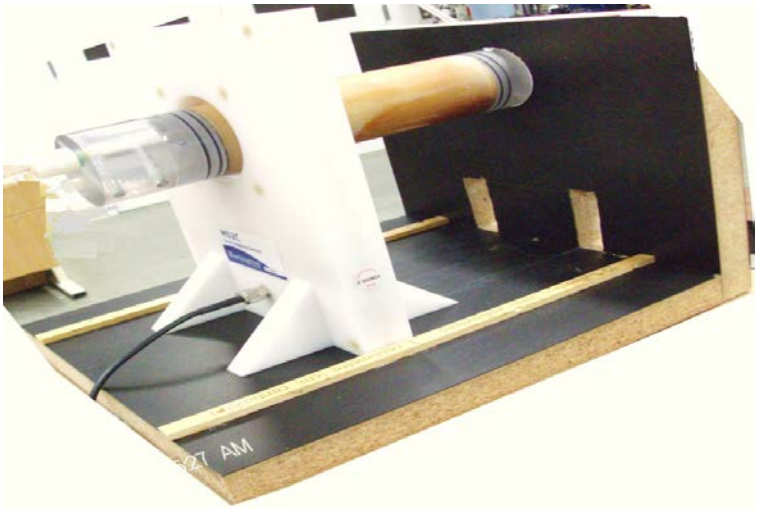

Figure 3-6: Laboratory picture of fluid flow apparatus.

3.2.4 **Syringe Pump**

Syringe pump was used for pumping of water and nanoparticle suspensions through porous media during dynamic/ fluid flow experiments. The syringe pump is a constant injection/withdrawal rate pump having 55 mm diameter, injection capacity of 249.5 ml and discharge rate range of 0.00069 ml/min to 423.37 ml/min. Figure 3-7 is a laboratory picture of the syringe pump.

Figure 3-7: Laboratory picture of syringe pump.

3.2.5 **Data Logging System**

The data logging system used in the flow experiments consisted of a pressure transducer from Omegadyne, data acquisition system NI USB-9219 from National Instruments and Labview Signal Express software that too provided by National Instruments. The pressure transducer had a pressure sensing range of 0-100 psi. Signals from pressure transducer were sent to computer through NI USB-9219 data acquisition system, where these were recorded in the form of pressure versus time plots by Labview Signal Express software.

3.2.6 **Water Purifier**

De-ionized water used for the nanoparticle suspension stability and flow experiments through porous medium was taken from PURELAB Ultra water purifier. The water purifier removes impurities from water and brings down the concentration of ionic components. The water purifier gives the processed water resistivity of 18.2 MΩ-cm. Figure 3-8 is the picture of PURELAB Ultra water purifier.

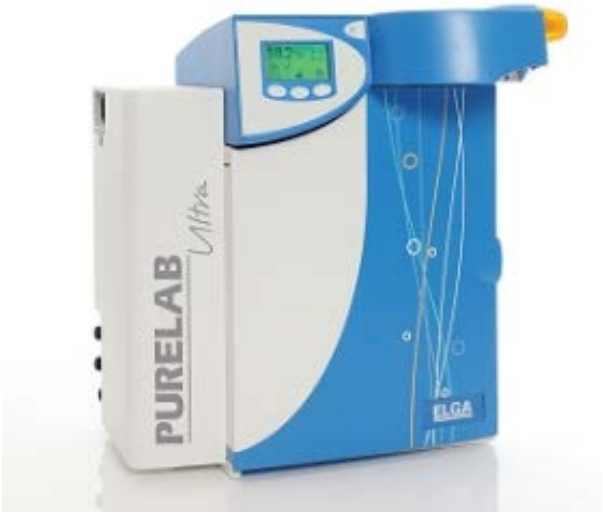

Figure 3-8: PURELAB ® Ultra water purifier.

3.2.7 **Digital Weighing Balance**

Mettler model AE 160 scale was used for weighing the NPs and dispersants with 0.0001 gm measuring accuracy. The weighing balance has a mass measuring range of 0 to 162 grams. Figure 3-9 is the picture of the digital weighing balance.

Figure 3-9: Mettler model AE 160 weighing scale.

3.2.8 **Homogenizer**

Polytron PT 6100 is a powerful homogenizer/ mixer with 1700 watt power drive that can achieve high speeds up to 24,000 rpm. The homogenizer was used to prepare mixture of NPs with water and dispersants (polymers / surfactants). Figure 3-10 is the picture of Polytron PT 6100 homogenizer.

Figure 3-10: Polytron PT 6100 Homogenizer.

3.2.9 **Rheometer**

BOHLIN CVOR rheometer was used in viscosity measurement of nanoparticle suspensions. The rheometer has shear rate operating range of 0.0001 to 10,000 per second. The viscometry of samples was performed with cone and plate arrangement, wherein sample is placed in 150 μm gap between the base plate and upper cone with 4^{o} angle. Figure 3-11 is the picture of BOHLIN CVOR rheometer.

Figure 3-11: Bohlin CVOR rheometer with cone and plate arrangement.

3.3 Experimental Setup (Schematics)

Figures 3-12 and 3-13 are schematics of experimental setups used for nanoparticles stability and suspension flow experiments respectively.

In nanoparticle suspensions stability experiments a 250 ml graduated cylindrical tube was used which was filled with nanoparticle suspensions were filled up to a certain level and susceptibility measurements with magnetic susceptibility sensor were taken at different time to see the change in susceptibility response with time. Change in susceptibility was thought to be an indicator of stability of suspensions; i.e. less the susceptibility change, higher the suspensions stability. As the suspensions become unstable, nanoparticle agglomerates and tends to settle down at the bottom of tube rapidly, giving a change in susceptibility response along the height of the tube. This change in response would be higher near the base of the tube where settlement of nanoparticles and their agglomerates will be taking place.

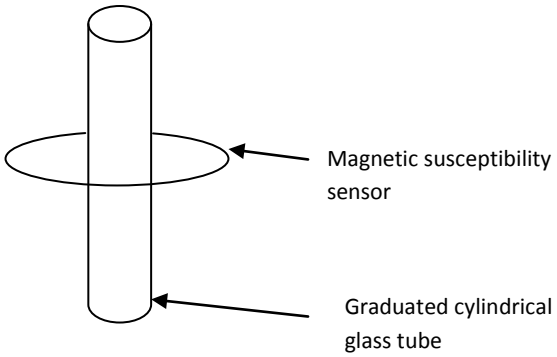

Figure 3-12: Schematic of stability experiment set up on nanoparticle suspensions.

In flow experiments water or nanoparticle suspensions are injected from syringe pump and effluent collected from the outlet end of core. Meanwhile, susceptibility measurements at different points along the length of core are measured, when needed. Pressure sensing is performed to measure and absolute permeability of glass beads/ sand pack and any variation due to injection of nanoparticle suspensions. In these experimental set-ups non-metallic equipment is used which is diamagnetic or slightly paramagnetic in nature, so that when nanoparticles of high magnetic susceptibility are introduced in the system, a high change in magnetic susceptibility is observed.

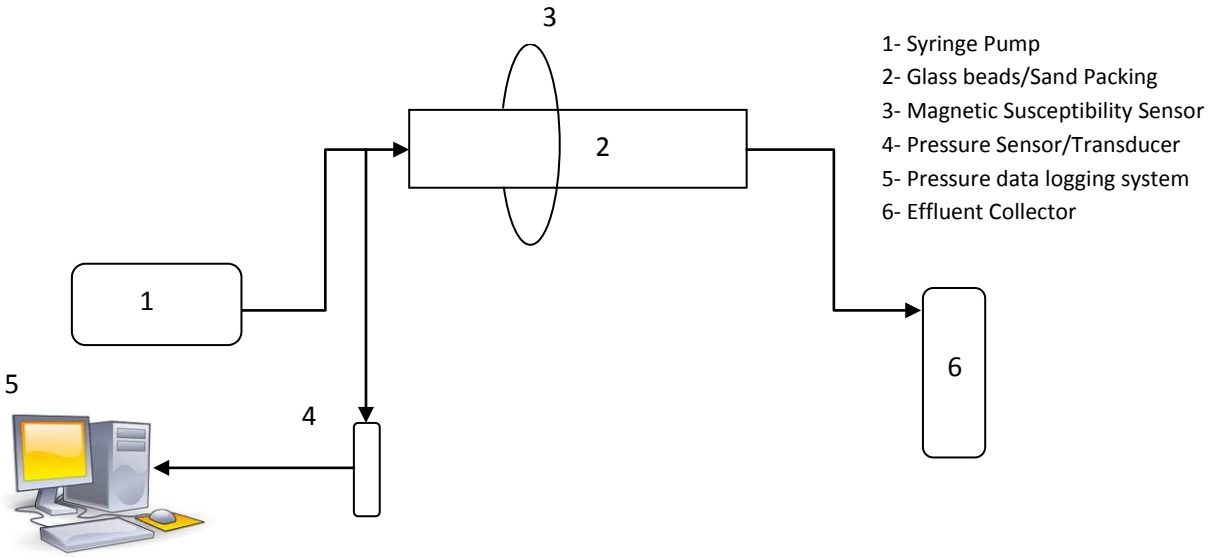

Figure 3-13: Schematic of fluid flow experimental set up.

3.4 Experimental Procedures

In this section, procedures followed in experiments concerning stability and transport of nanoparticle suspensions are presented under static experiments and dynamic experiments headings respectively.

3.4.1 Static Experiments

Series of experiments were performed for determining the effect of following factors on magnetic susceptibility response and stability of nanoparticle suspensions.

i. Concentration of nanoparticles (NPs)
ii. Sonication and/or dispersion
iii. Sonication time
iv. Type and concentration of dispersants
v. Sonication power
vi. Method of sample preparation
vii. Applied magnetic field duration

Objective of this study was to find out stable nanoparticle suspensions with better dispersion of nanoparticles or their agglomerates. Dispersion of these nanoparticles are likely to be affected by the methods of preparation. These methods of dispersing nanoparticles were expected to result in different sizes of nanoparticle agglomerates, which may therefore show different stability of prepared nanoparticle suspensions. Better nanoparticle dispersions are likely to exhibit better transport behaviour through porous media properties due to smaller size of nanoparticle agglomerates in prepared suspensions.

Generally, following procedure was adopted for most of the samples shown in table 3-10 (samples 1 through 30). However, some samples were prepared with deviations from the below mentioned procedure and these deviations are specified in the sample recipe table (table 3-10).

a) Weighed the desired amount of NP and mixed in 300 ml of water at 4500 rpm for 4-5 minutes.
b) Sonicated the sample for specific period of time at fixed sonication power.
c) Added known weight of dispersant (CTAB or XG) and mixed for 4-5 minutes using homogenizer at 4500 rpm.
d) Took 250 ml of mixture in graduated glass cylinder of 25 mm diameter and took readings soon after the suspensions preparation and after a set fixed time (i.e. 54 hours) for each sample.

Table 3-10: Effect of different parameters on stability of NP suspensions.

Sr. #	NPs		Water	Dispersant		Sonication		Remarks
	Type	(gm)	(ml)	Type	Wt. (gm)	(Mins)	(Watt)	
1	Fe_3O_4	0.2	300	CTAB	0.2	30	70	Sonicated then dispersed.
2		0.3			0.3			
3		0.5			0.5			
4		1.0			1.0			
5	$CoFe_2O_4$	0.2			0.2			
6		0.3			0.3			
7		0.5			0.5			
8	$NiFe_2O_4$	0.2			0.2			
9		0.3			0.3			
10		0.5			0.5			
11	γ - Fe_2O_3	0.2			0.2			
12		0.3			0.3			
13		0.5			0.5			
14		0.2		x	x	x	x	No Sonication, No dispersion
15				x	x	30	70	No dispersant.
16				CTAB	0.2	x	x	No sonication.
17					0.2	30	70	Dispersed then sonicated.
18				x	x	15		Less sonication time.
19				x	x	45		More Sonication time.
20				XG	0.25	30		2:5 XG to NP ratio
21					0.5			1:5 XG to NP ratio
22					1.0			1:1 XG to NP ratio
23				CTAB	0.2	15	100	High sonication power.
24					0.2	15	40	Low sonication power.
25					0.1	30	70	1:2 CTAB to NP ratio
26					0.4			2:1 CTAB to NP ratio
27		0.5			0.25			1:2 CTAB to NP ratio
28		0.5			1.0			2:1 CTAB to NP ratio
29		0.2		XG	0.5			Dispersed then sonicated.
30		0.2		CTAB	0.2			Longer exposure to magnetic field.

After carrying out the initial study on stability of nanoparticle suspensions by varying various parameters such as sonication power sonication time, concentration of nanoparticles, concentration of dispersants, sequence of preparation etc., following procedure was used for further sample preparations (sample 31 through sample 45). This procedure was opted on the basis of better suspension stability and magnetic susceptibility response, determined from first set of suspensions stability experiments (i.e. table 3-10). Results of these suspension stability experiments are discussed in detail in Chapter 4. In these samples (sample 31 through sample 45) effect of cationic, anionic and non-ionic surfactants were also examined on stability of suspensions. Description of various parameters used in sample preparation and any deviations from below mentioned procedure are presented in table 3-11.

a) Weighed the desired amount of NPs and mixed in 300 ml of water at 4500 rpm for 4-5 minutes.
b) Added known weight of dispersant (CTAB, DDBS, TGT and/or XG) and mixed for 4-5 minutes using homogenizer at 4500 rpm.
c) Sonicated the sample for specific period of time at constant sonication power.
d) Took 250 ml of mixture in graduated glass cylinder of 25 mm diameter and took readings soon after the mixture preparation and after a set fixed time (i.e. 54 hours) for each sample.

Table 3-11: Stability of nanoparticle suspensions with XG and cationic, anionic and non-ionic surfactants.

Sr. #	NPs		Water	Dispersant		Sonication		Remarks
	Type	(gm)	(ml)	Type	Wt. (gm)	(Mins)	(Watt)	
31	ɣ - Fe_2O_3	0.3	300	CTAB	0.5	30	70	Dispersed then sonicated.
32		0.5			0.5	30	70	
33		1.0			0.5	30	70	
34		1.0			0.5	30	130	
35		1.0		CTAB/ XG	1.0/ 0.5	30	130	
36		0.2		DDBS	0.2	30	70	
37		0.2			0.5	30	70	
38		0.2			1.0	30	70	
39		0.2		DDBS/ XG	1.0/ 0.5	30	70	
40		0.2		TGT	2 (ml)	30	70	
41		0.2			5 (ml)	30	70	
42		0.2			20 (ml)	30	70	

3.4.2 **Dynamic Experiments**

Dynamic experiments were aimed to investigate the nanoparticle adhesion/ sticking to the surfaces of material (sand/ glass beads), during flow through porous media. Similar to the static experiments, dynamic experiments were performed using different sample recipes to understand the effect of individual parameters on transport characteristics (i.e. adhesion/ sticking, agglomeration) of nanoparticle suspensions.

Following procedure was used for performing the suspension flow experiments.

a) Prepared 600 ml nanoparticle suspensions by mixing desired weight of nanoparticles in 600 ml of water, adding dispersant (CTAB, DDBS, TGT or XG) in varied quantities and finally sonicating the suspensions. (Few initial flow experiments were performed with nanoparticle suspension prepared by first sonicating and then adding dispersants).
b) Packed flow cell with known mesh glass beads or sand.

c) Saturated the glass beads/ sand filled flow cell with de-ionized water and measured the porosity.
d) Attached pressure transducer at the inlet of core holder and flowed de-ionized water of known viscosity and took pressure measurements at different flow rates to measure absolute permeability of glass beads/ sand pack.
e) Pumped 3 pore volumes of nanoparticle suspensions through porous media at certain flow rate and measured susceptibility response along the length of flow cell at every 1 cm interval after every pore volume injection.
f) After injection of nanoparticle suspensions, the flow cell (glass beads/ sand pack) was flushed with 4 pore volumes of de-ionized water at the same flow rate, the nanoparticle suspensions were pumped through the flow cell. Magnetic susceptibility measurements were taken after 1 PV and 4 PV injections of de-ionized water to estimate the ultimate retention/ adhesion of nanoparticles in the flow cell.

4 STATIC EXPERIMENTS (RESULTS AND DISCUSSION)

Main emphasis of this chapter is to discuss effects of various parameters on the stability of the nanoparticle suspensions in terms of magnetic susceptibility response. However, prior discussing that, it is important to know the effect of radial and axial distribution of material/ fluid on measured susceptibility response.

4.1 Dependence of Magnetic Susceptibility Response on Axial and Radial Distribution of Materials/ Suspensions

Figure 4-1 shows the volume susceptibility response of 2.8 molar nickel chloride solution in a vertical cylindrical tube of 35 mm diameter. Nickel chloride is soluble in water and provides a homogenous mixture with uniform susceptibility characteristics. It can be noticed that despite the homogenous nature of the mixture, response along the length of the fluid column varies, indicating that the sensor not only sense the fluid inside the aperture/ diameter but also its response is affected by the fluid adjacent to it. The susceptibility response is maximum at the center of the tube where paramagnetic solution is present on either sides of the sensing point. Sensor also measures some susceptibility even when it is taken past the fluid column height.

Nickel chloride is a stable paramagnetic substance which has in past shown to exhibit linear susceptibility response with increasing concentrations (Nettleton and Sugden, 1939). The susceptibility measurements are recorded at different fluid column heights, first by centering the cylindrical tube and then by off-centering it by 10 mm. It can be seen from figure 4-1 that off-centered tube has shown higher susceptibility readings, indicating that the fluid closer to the sensor body influence more on the susceptibility readings. It is shown that magnetic susceptibility response varies with relative positioning of sensor to the sensing material both axially and radialy therefore it may not be practically possible from susceptibility response to know the exact concentration of nanoparticles in suspensions at different points along the length of the media. Different

susceptibility response may actually correspond to same tracer saturation but different radial/ axial fluid distribution and vice versa.

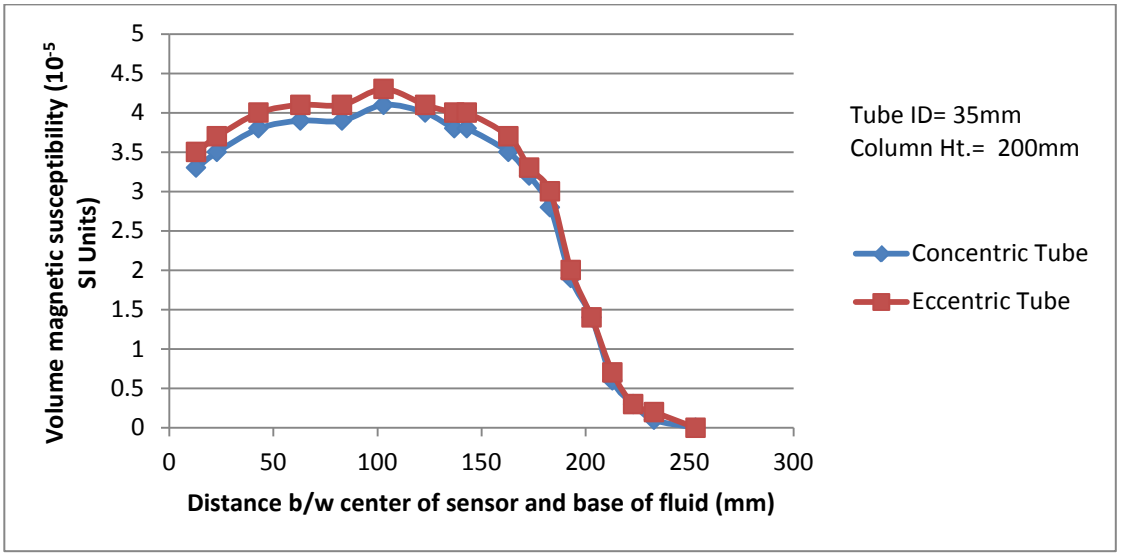

Figure 4-1: Volume magnetic susceptibility of 2.8 molar nickel chloride solution.

4.2 Suspension Stability without Sonication and Dispersion

The particle settlement behaviour of two nanoparticle suspensions prepared in water with mixing only at 4500 to 5000 rpm for 3 to 4 minutes is shown in figures 4-2 and 4-3. These suspensions were highly unstable and settled at a very high rate which corresponded to presence of quite big size of particles. If the effective size of particles was truly of nano meter size, the nanoparticle suspensions would have had, according to stokes law, very low terminal settling velocity and a very good particle suspension characteristics.

The Stokes Equation of terminal velocity is shown below:

$$v_s = \frac{2(\rho_s - \rho_f) g r^2}{9\mu} \qquad (4\text{-}1)$$

Where,

v_s = Terminal velocity of solid particles (m/s)

ρ_s = Density of solid particles (Kg/m^3)

ρ_f = Density of fluid (Kg/m^3)

g = Gravitational acceleration (m/s^2)

r = Radius of spherical solid particles (m)

μ = Dynamic viscosity ($N\text{-}s/m^2$)

The anticipated terminal velocities of two types of nanoparticles in water are shown in table 4-1.

Table 4-1: Terminal Settling Velocities of Nanoparticles according to Stokes Law

Nanoparticles Type	NP density (Kg/m3)	NP radius (nm)	Terminal velocity (m/s)	Terminal velocity (mm/hr)	Settlement time (hr/mm)
γ -Fe_2O_3	5240	10	9.22×10^{-10}	0.0033	301.1
$CoFe_2O_4$	5300	20	3.74×10^{-9}	0.0135	74.2

The actual settlement of nanoparticles appeared to be much faster than anticipated. Majority of particles settled down in first hour after preparing the mixture corresponding to particle of micron sizes. The particle settlement behaviour in nanoparticle suspensions is presented in figures 4-2 and 4-3 showing pictures taken at different time intervals.

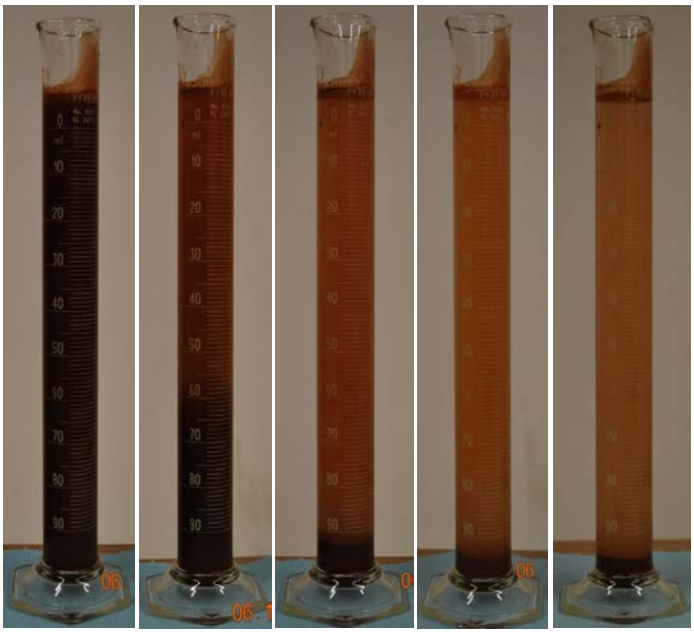

a):1 min b):5 mins c):10 mins d):30 mins e):2 hours

Figure 4-2: Settlement of 20 nm ɣ -Fe_2O_3 (Maghemite) nanoparticles in water

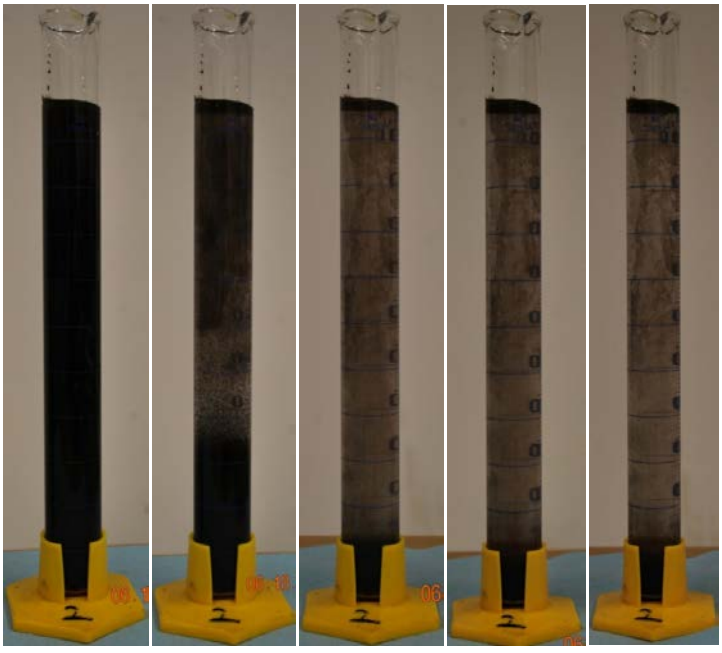

a)1 min b) 5 mins c) 10 mins d) 30 mins e) 2 hours

Figure 4-3: Settlement of 40 nm $CoFe_2O_4$ nanoparticles in water

The high particle settlement rate was also supported by the electron microscopy images of the particles, pointing high affinity of nanoparticles particles to coalesce and form agglomerates. The SEM image of γ-Fe_2O_3 nanoparticle sample (figure 4-4) shows the nanoparticles clumped together.

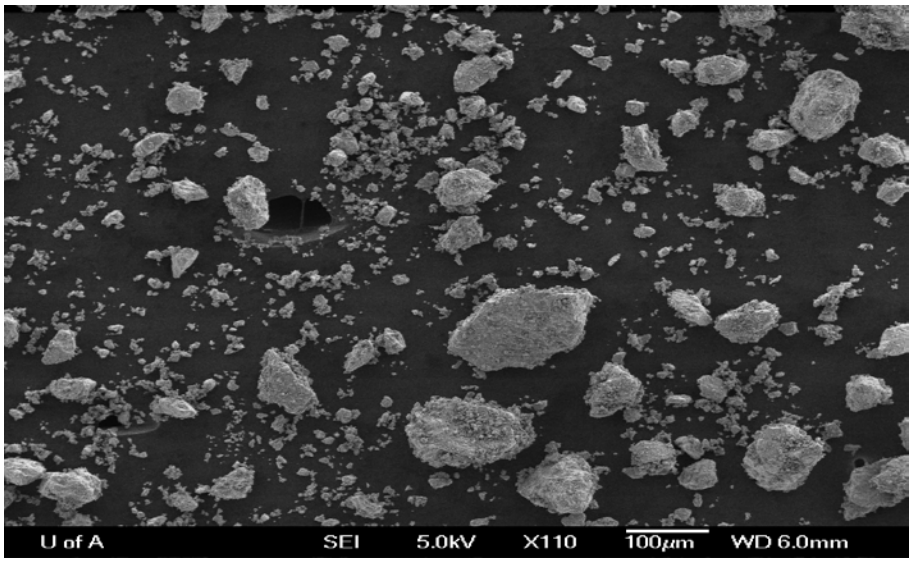

Figure 4-4: SEM image showing agglomerates of 20 nm γ-Fe_2O_3 (Maghemite) Nano Particles (NPs)

The effects of various parameters studied in these static experiments are discussed below. The stability of the nanoparticle suspensions is determined by taking magnetic susceptibility readings at least at two different times. First reading was taken soon after preparation of the suspension and second after 54 hours. The concept behind using the time based magnetic susceptibility response for stability measurement is that when suspensions are not stable these will have large agglomerates in it resulting in higher particle settlement rates and thus a greater change in susceptibility readings. Whereas, stable nanoparticle suspensions will show minimal or no susceptibility change with time. For method of preparation of each sample, please refer back to section 3.4.1.

4.3 Concentration of Nanoparticles (NPs): (Samples 1-13)

Samples of nanoparticle suspensions were prepared using different concentrations of nanoparticles. Following four types of nanoparticles were used in preparing nanoparticle suspensions. Hematite (α-Fe_2O_3) was found "not suited" for suspensions stability and flow experiments owing to its very small magnetic susceptibility contrast.

Table 4-2: Nanoparticles used in measuring the effect of NPs concentration on magnetic susceptibility and suspension.

NPs Type	Chemical Formula	APS (nm)	True Density (g/cc)	Samples
Magnetite	Fe_3O_4	20	5.0	1-4
Cobalt Iron Oxide	$CoFe_2O_4$	40	5.3	5-7
Nickel Iron Oxide	$NiFe_2O_4$	30	5.368	8-10
Maghemite	γ -Fe_2O_3	20	5.24	11-13

The cobalt iron oxide suspensions were highly unstable and possessed relatively poor magnetic susceptibility characteristics. They did not seem to have much effect of sonication and dispersion as compared to the other samples. Due to their low susceptibility response and high particle settlement, their results were of no interest and are therefore not presented here.

Concentration versus susceptibility plots for these nanoparticle suspensions have also been generated from the susceptibility measurement taken at the center of suspension filled graduated tube. The susceptibility readings used in these NPs concentration versus susceptibility response was taken soon after the preparation of suspensions, where it was believed that nanoparticles are uniformly distributed

within the suspensions column. The magnetic susceptibility responses for each NP type (other than cobalt iron oxide) with various concentrations (at time 0 hour and 54 hours) and concentration versus susceptibility plots are presented below in figures 4-5 through 4-17.

Magnetite: (Samples 1-4)

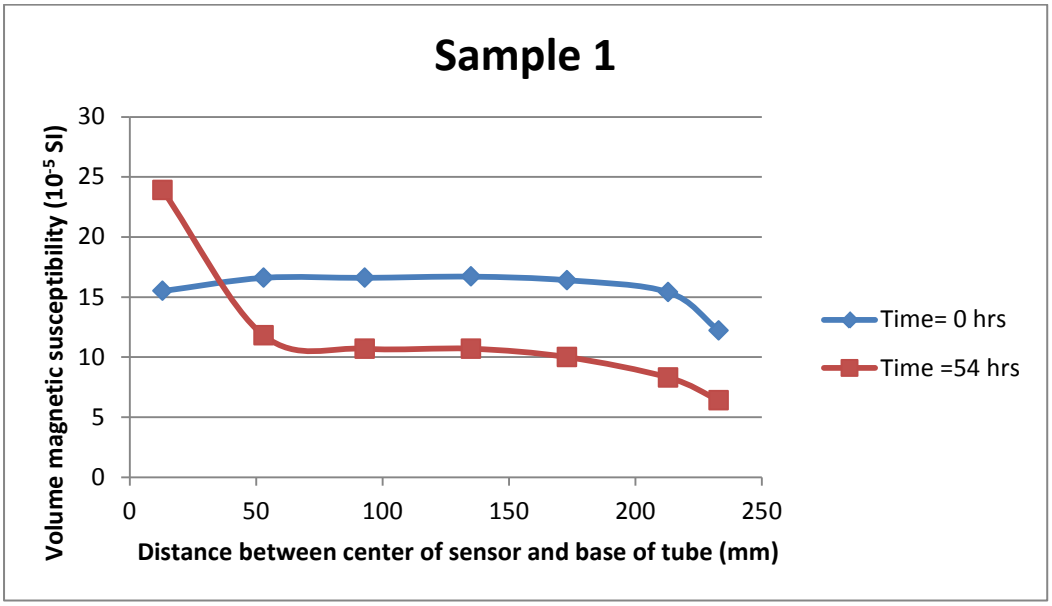

Figure 4-5: Susceptibility response of 0.2 gm Magnetite NPs with water and 0.2 gm CTAB.

The blue curve in the above figure is produced from the susceptibility measurements taken soon after the suspension preparation. It is showing a typical decreasing trend towards the ends of the tube. The second trend shows increase in measured magnetic susceptibility near the base of the tube and decrease in susceptibility away from the base, pointing to nanoparticle settlement. Higher the particle settlement rate, higher will be the separation between the measured susceptibility trends.

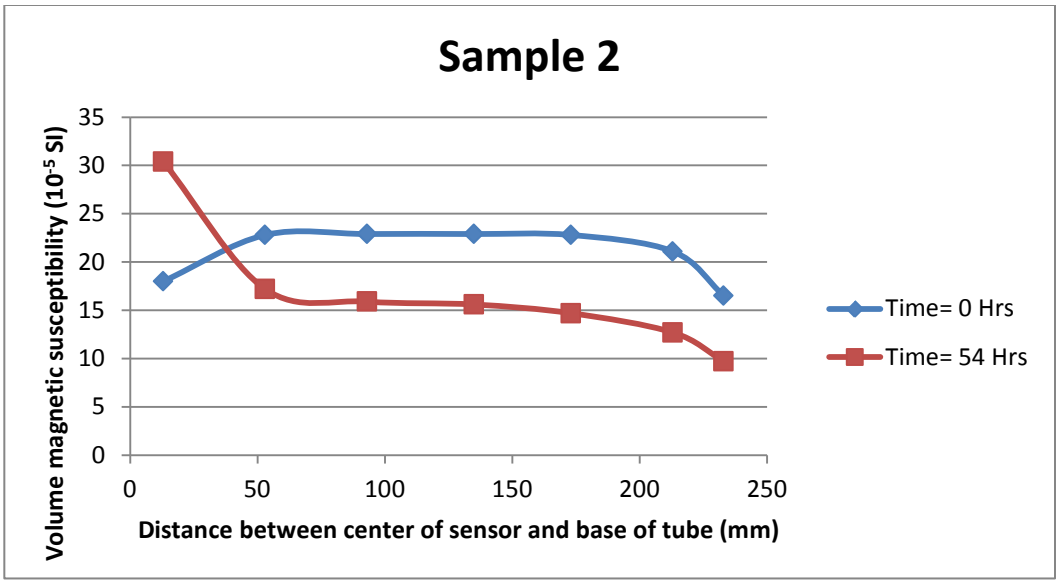

Figure 4-6: Susceptibility response of 0.3 gm Magnetite NPs with water and 0.3 gm CTAB.

The magnetic susceptibility response of the sample 2 is similar to that of the sample 1 except that the measured values are proportionately higher due to different concentration of NPs.

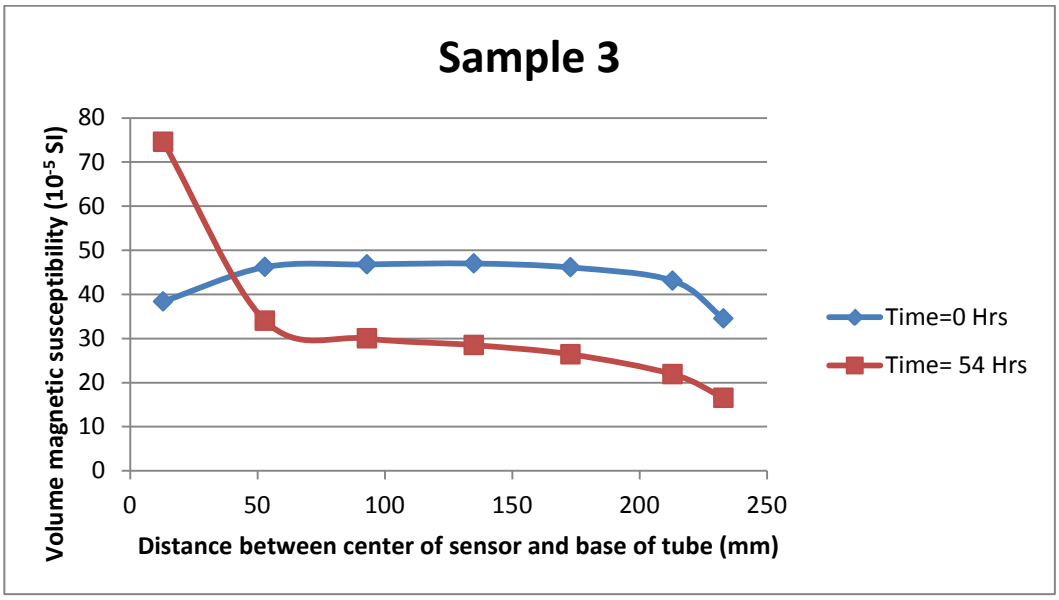

Figure 4-7: Susceptibility response of 0.5 gm Magnetite NPs with water and 0.5 gm CTAB.

The susceptibility trends in the above figure are somewhat different than earlier two plots since a relative increase in separation between time based susceptibility trends can be seen. Such an increase in separation may be explained with the reasoning that at higher concentration of nanoparticles, the tendency of nanoparticles to coalesce increases. Therefore, higher concentration of nanoparticles under same conditions of suspension preparation may show relatively poor stability and in order to achieve stability similar to that of lower concentration suspensions, a better dispersion technique may be required.

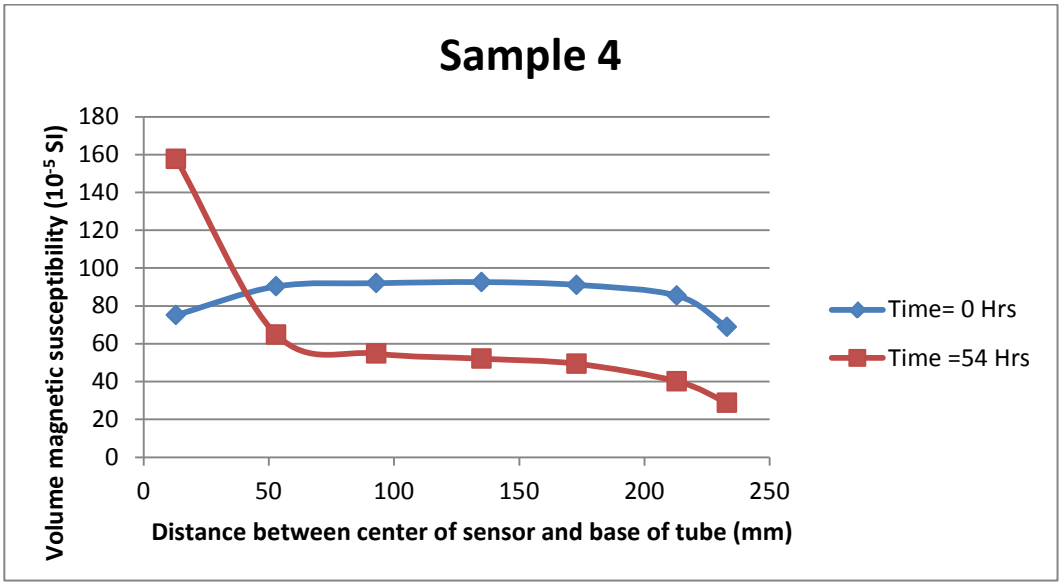

Figure 4-8: Susceptibility response of 1.0 gm Magnetite NPs with water and 1.0 gm CTAB.

Figure 4-8 also supplement the above discussed finding of poor suspension stability at higher nanoparticle concentrations. The suspension stability is poorest in sample 4 among all four samples discussed above.

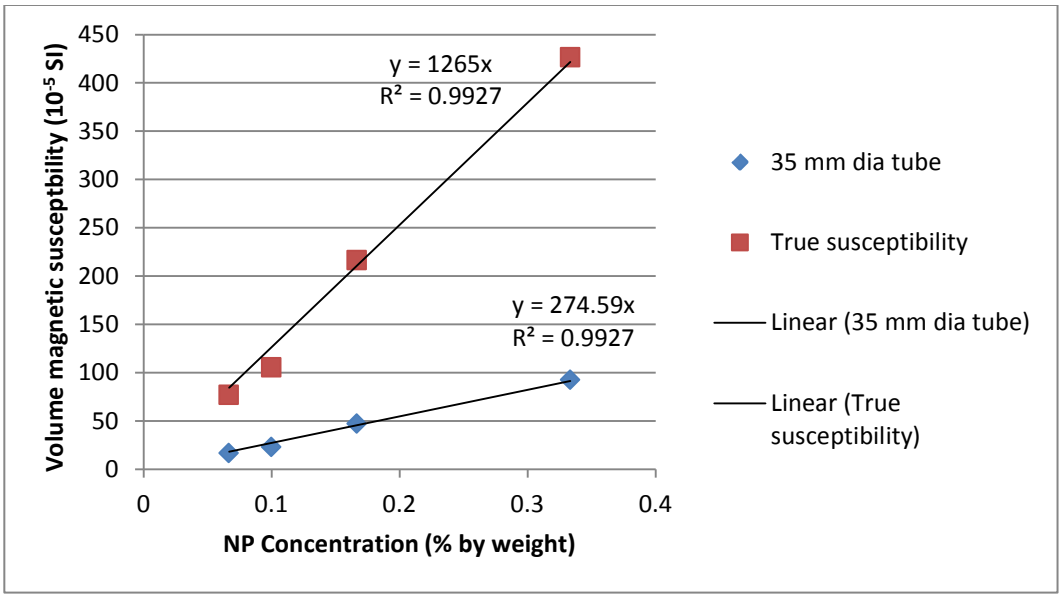

Figure 4-9: Concentration versus susceptibility plot for Magnetite NP suspensions.

Figures 4-9, 4-13 and 4-17 show the susceptibility response of three different type of nanoparticle suspensions, as function of nanoparticle concentration, in 35 mm internal diameter cylindrical tube indicating a fairly linear response. The true susceptibility trends, corrected for internal diameter of tube, are also shown in these plots. The true susceptibility values in these plots are calculated using following relation.

$$X_v = \frac{X_{mv}}{3.45(d/D)^3} \qquad (4\text{-}2)$$

Where,

X_v = True Volume Susceptibility

X_{mv} = Measured Volume Susceptibility

d = diameter of the measuring tube

D = Sensor Aperture + 8 mm

This relation is valid for a uniform, homogenous mixture with length of the mixture on either side of the sensing point greater than the size of the sensor aperture plus 8mm (8 mm is to account for the body thickness next to sensing coils).

The true susceptibility plots such as in figures 4-9, 4-13 and 4-17 can be used to estimate the concentration of nanoparticles provided nanoparticle suspensions are homogeneously distributed and the length of media containing these suspensions is more than twice the size of diameter of sensor.

Nickel Iron Oxide: (Samples 8-10)

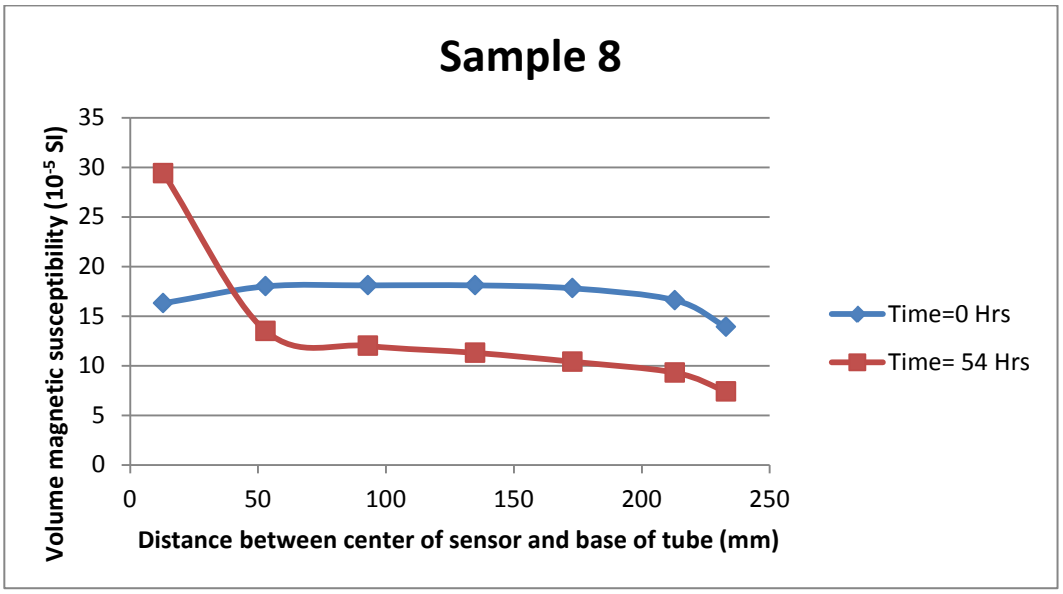

Figure 4-10: Susceptibility response of 0.2 gm Nickel Iron Oxide NPs with water and 0.2 gm CTAB.

The initial and final susceptibility responses of sample 8 are almost same as that of sample 1, indicating same stability and magnetic susceptibility characteristics. Slight variations are expected though due to errors associated with nanoparticle weighing, exact positioning of the sensor, eccentricity of the graduated cylindrical tube, sensor drift etc.

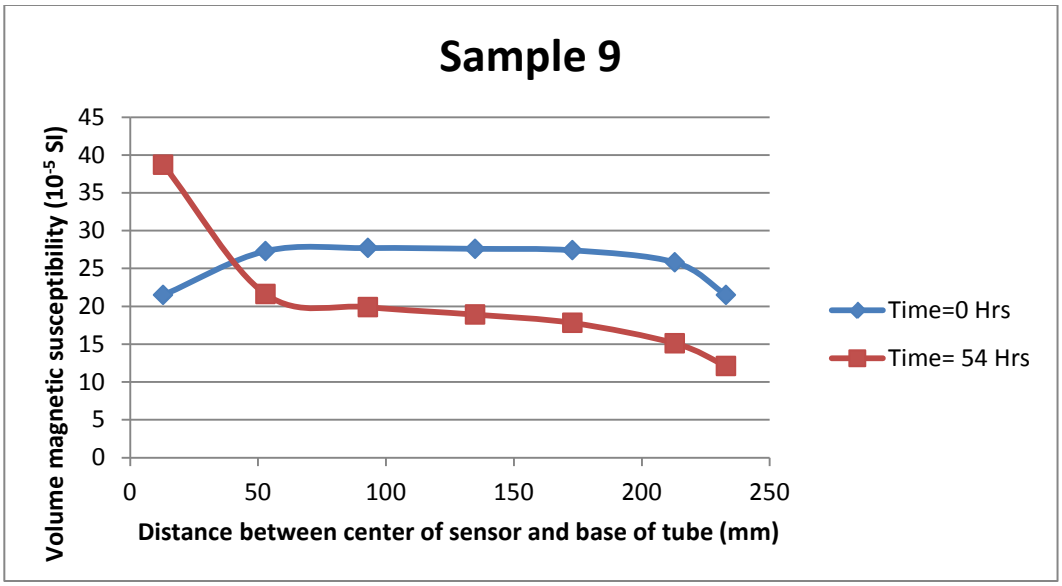

Figure 4-11: Susceptibility response of 0.3 gm Nickel Iron Oxide NPs with water and 0.3 gm CTAB.

The susceptibility trends of sample 9 are similar to the susceptibility trends of sample 8, pointing to same nanoparticle stability. The only difference is the higher susceptibility values for larger concentration of nanoparticles.

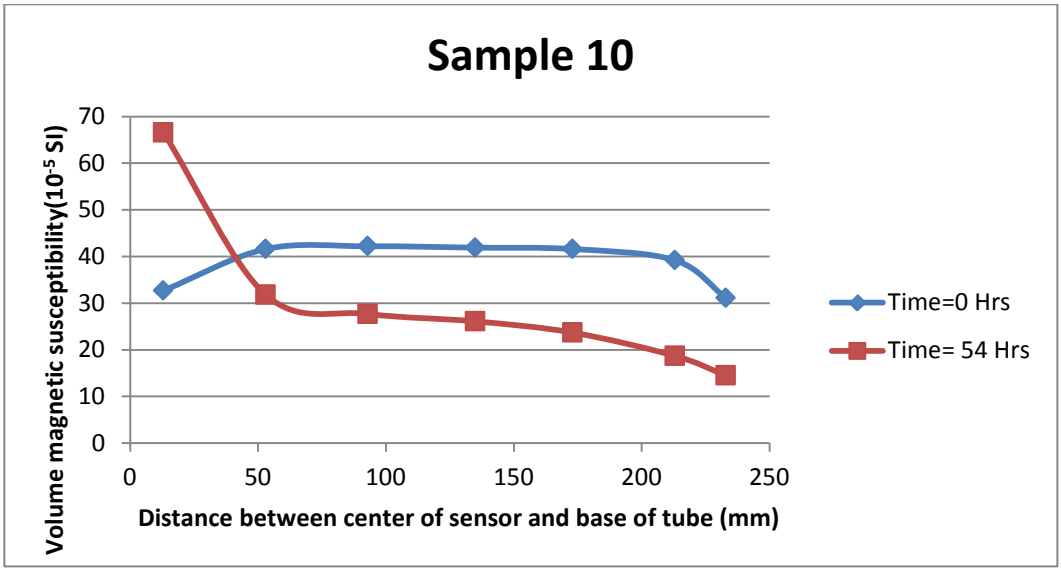

Figure 4-12: Susceptibility response of 0.5 gm Nickel Iron Oxide NPs with water and 0.5 gm CTAB.

Again, the differences between susceptibility trends are increased as nanoparticle concentration in suspensions is further increased, which is supplementing our earlier conclusion of decrease in suspension stability with increase in nanoparticle concentration. However, this decrease in stability is observed after the concentration exceeds a certain critical value (i.e. 0.3 gms in above experiments).

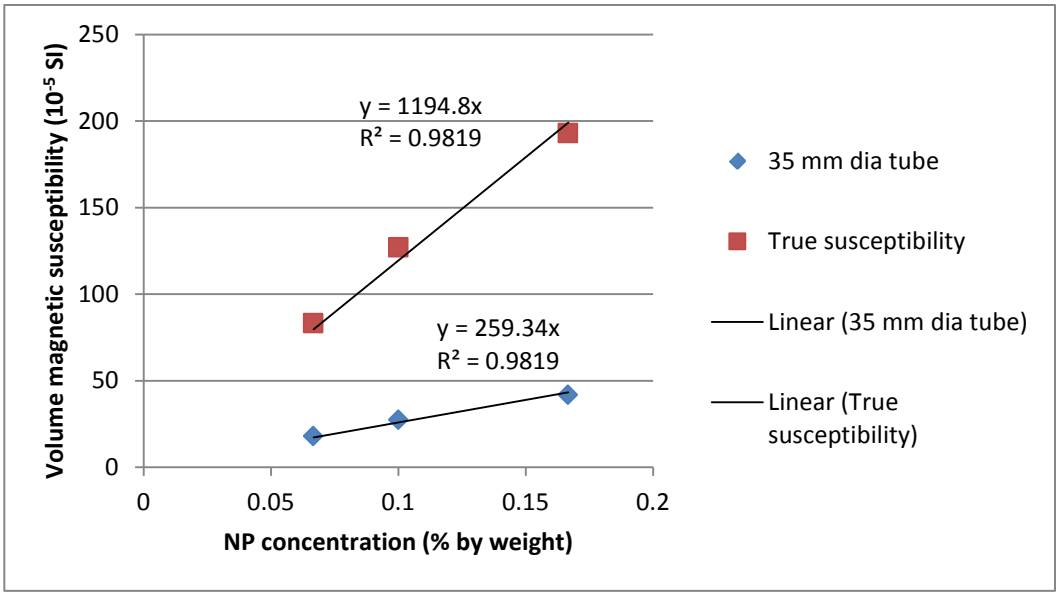

Figure 4-13: Concentration versus susceptibility plot for nickel iron oxide NP suspensions.

Figure 4-13 shows concentration versus susceptibility plot for nickel iron oxide nanoparticle suspensions. The points plotted in the above figure corresponds to the susceptibility measurements taken at time=0 hrs and at the middle of graduated tube. The true susceptibility values are also calculated from measured response using equation 4-2. Comparison of the figures 4-13 and 4-9 shows that both magnetite and nickel iron oxide posses same magnetic characteristics with the present method of suspension preparation.

Maghemite: (Samples 11-13)

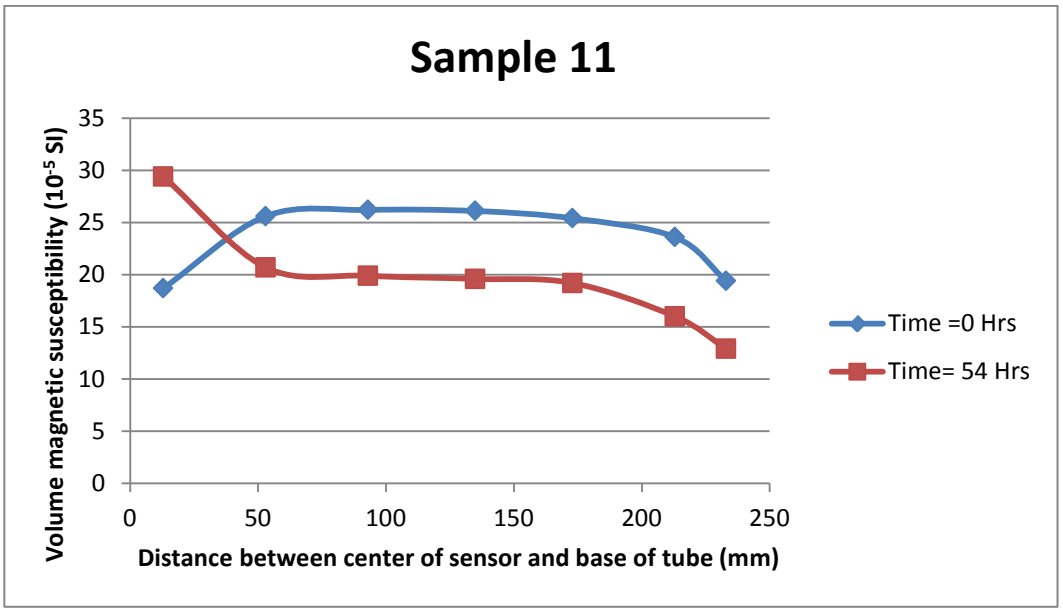

Figure 4-14: Susceptibility response of 0.2 gm Maghemite NPs with water and 0.2 gm CTAB.

Maghemite possess higher magnetic susceptibility characteristics than the other two types of nanoparticles (i.e. Magnetite, Nickel iron oxide). The initial susceptibility values of 0.2 gm Maghemite nanoparticle suspensions are higher than the susceptibility values from same concentration of other type of nanoparticle suspensions (figures 4-2, 4-7). The stability of the Maghemite nanoparticle suspensions looks not very different from the other two suspensions types discussed earlier, however, on close analysis one may find relatively better stability in Maghemite nanoparticle suspensions.

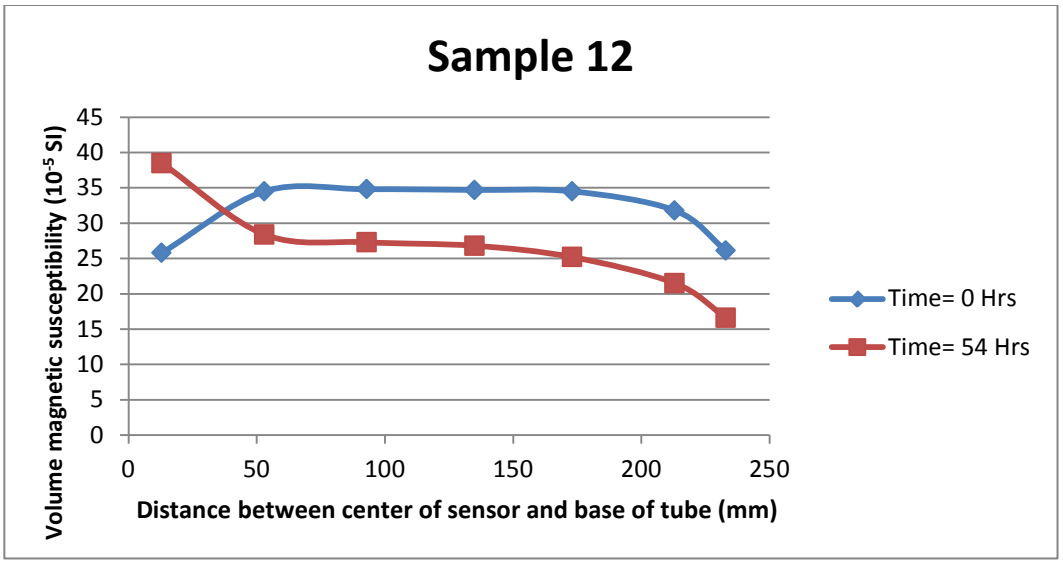

Figure 4-15: Susceptibility response of 0.3 gm Maghemite NPs with water and 0.3 gm CTAB.

Figure 4-15 also looks fairly similar to previous susceptibility trends with same nanoparticle concentration. The initial susceptibility response is however greater than what is seen for the other two nanoparticle suspension types.

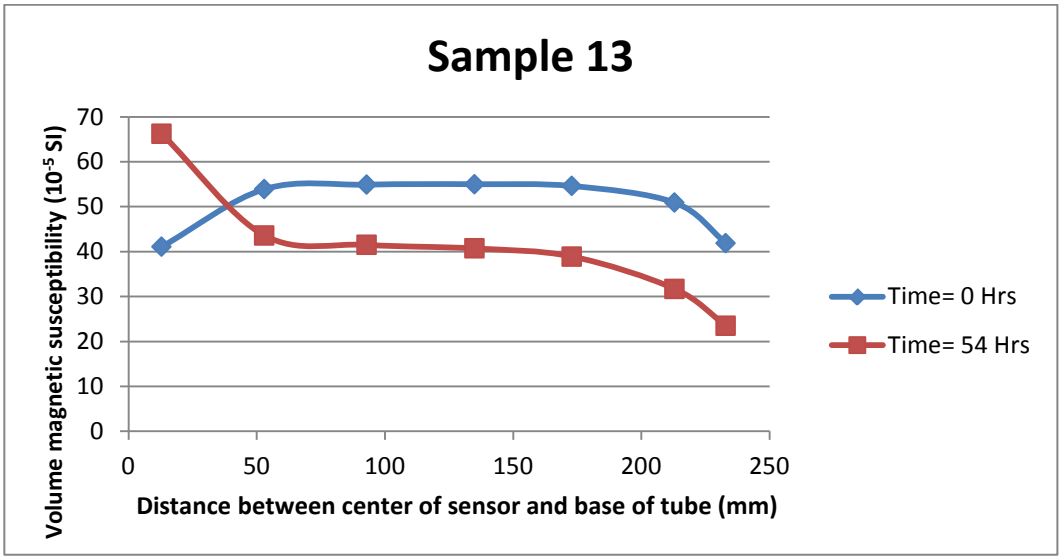

Figure 4-16: Susceptibility response of 0.5 gm Maghemite NPs with water and 0.5gm CTAB.

The separation between initial and final susceptibility trends is slightly increased in figure 4-16 as compared to separation observed for figures 4-14 and 4-15. However, the stability improvement for Maghemite nanoparticle suspensions is seen when compared with figures 4-7 and 4-12.

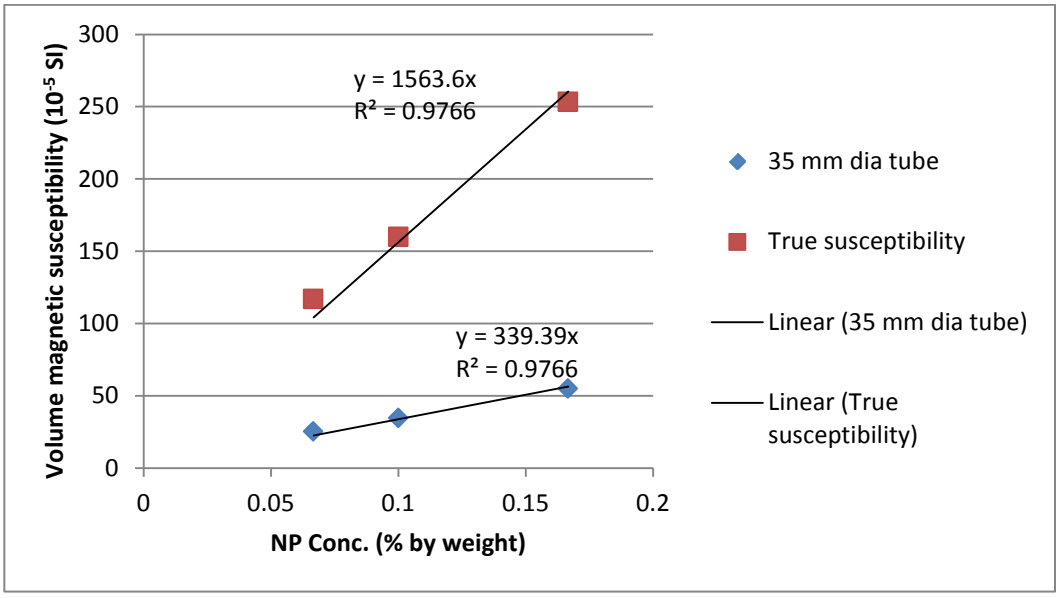

Figure 4-17: Concentration versus susceptibility plot for Maghemite NP suspensions.

Figure 4-17 like figures 4-9 and 4-13, also shows a good linear relation between magnetic susceptibility and nanoparticle concentration. The magnetic susceptibility to nanoparticle concentration slope is highest for Maghemite nanoparticles. Owing to the higher magnetic susceptibility and relatively better stability of Maghemite nanoparticle suspensions, Maghemite nanoparticles are used in further investigation studies to determine the effects of various other parameters.

4.4 Effect of Sonication and/or Dispersion: (Samples 11, 14-17)

To see the effect of sonication and dispersion, following samples were prepared.

i. No sonication, no dispersion (Sample 14)
ii. Only sonication (Sample 15)
iii. Only dispersion (sample 16)
iv. Sonication then dispersion (Sample 11)
v. Dispersion then sonication (Sample 17)

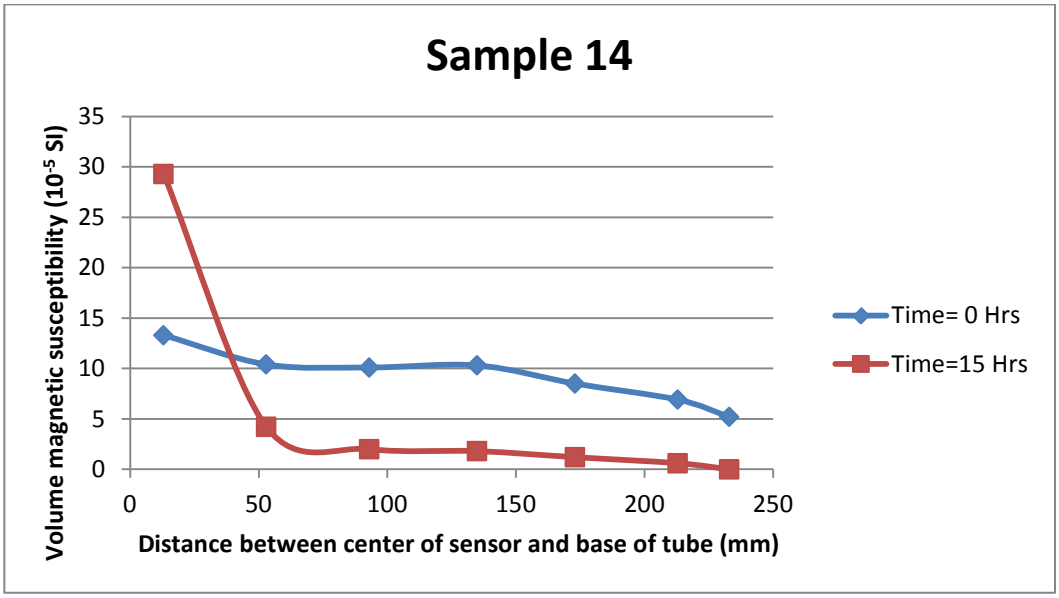

Figure 4-18: Susceptibility response of 0.2 gm Maghemite NPs with water and 0.2 gm CTAB (Without sonication and dispersion).

Sample 14 is extremely unstable. Even though the initial measurements were taken soon after the suspension preparation, typical susceptibility trend wherein susceptibility values are dropped towards the end is missing. The rise in the initial susceptibility trend near the base of the tube is indicative of the fact that settlement has already started taking place. The second susceptibility trend is constructed from susceptibility measurements taken much earlier (i.e. after 15 hrs instead of typically used time of 54 hours). Even then, the susceptibility values are approaching zero at various points away from the base of the tube. This highly

unstable behaviour of nanoparticle suspensions with mixing only demands other techniques to be employed to improve the stability of nanoparticle suspensions.

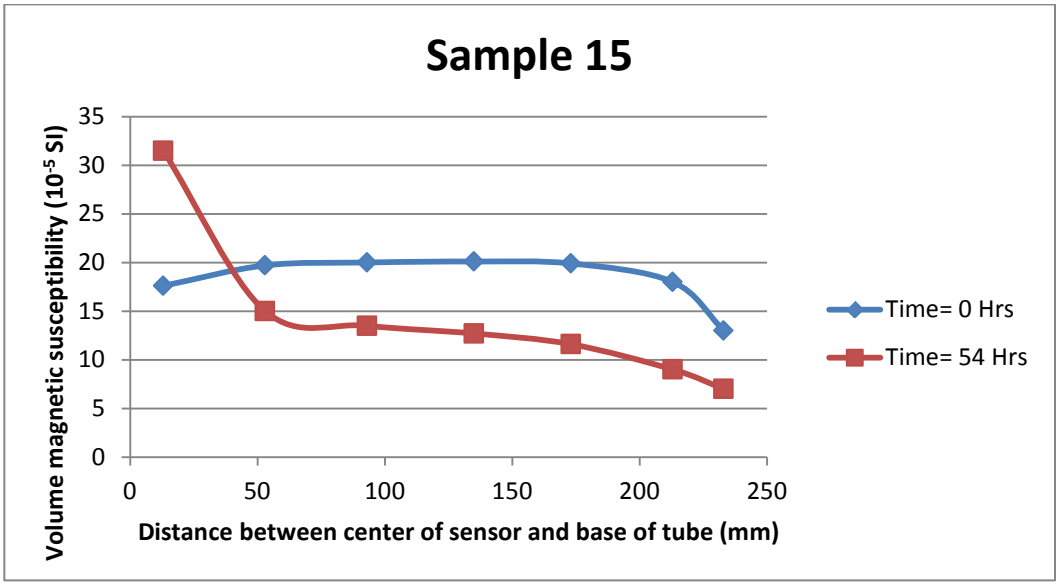

Figure 4-19: Susceptibility response of 0.2 gm Maghemite NPs with water (Without dispersants).

Figure 4-19 shows the stability behaviour of nanoparticle suspensions prepared with mixing and sonication only. It should be noted that in order to see the effects of various parameters on stability of nanoparticle suspensions, type and the concentration of nanoparticles is kept same in majority of the experiments. It is established from comparison of sample 14 and 15 that sonication, not only increases the stability of nanoparticle suspensions but also enhances the magnetic susceptibility response. Increase in initial/ final susceptibility response is thought to be due to disintegration of nanoparticle agglomerates into smaller agglomerates.

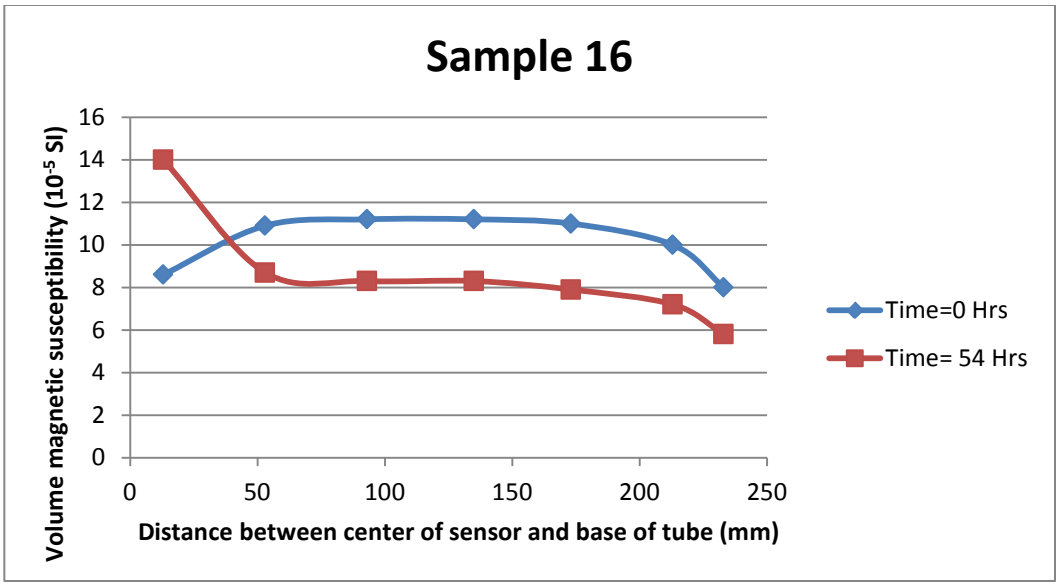

Figure 4-20: Susceptibility response of 0.2 gm Maghemite NPs with water and 0.2 gm CTAB (Without sonication).

Sample 16 was prepared by mixing and addition of cationic, CTAB surfactant. It shows significantly enhanced stability of the suspension in comparison to sample 14. On the other hand, the susceptibility values remained low. It may therefore be concluded that addition of surfactant did not play any role in disintegration of nanoparticles. However, it did improve the stability of the nanoparticle suspensions by forming a thin film around the agglomerates and prevented from further coalescing. The increased hydrodynamic radius of nanoparticle agglomerates would have also contributed in low settlement velocities and thus improved stability.

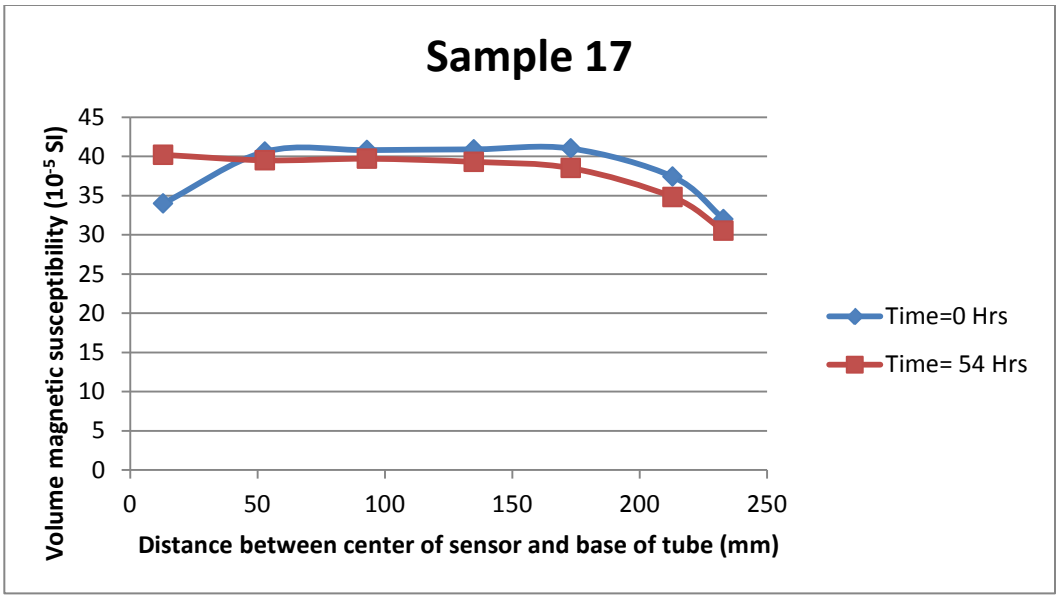

Figure 4-21: Susceptibility response of 0.2 gm Maghemite NPs with water and 0.2 gm CTAB (Dispersion followed by sonication).

It is evident from comparison of the above plots that the sample without sonication and dispersion is least stable. Sample 17 representing dispersion followed by sonication appeared to be the most stable suspension of all, as the curves are almost overlapping each other. The high susceptibility response and smallest separation observed between the two trends indicate that this method of sample preparation gives smallest agglomerate sizes and effective dispersion, offering best stability among all other methods tried and discussed above.

Figure 4-22 shows the initial susceptibility responses of different methods of suspension preparation. Comparison of initial susceptibility trends may also be used as a criterion for the stability of the nanoparticle suspensions. Higher initial susceptibility response will point towards smaller sizes of nanoparticle agglomerates which in turn gives better suspension and stability, provided same ingredients are used in preparing the suspension recipe.

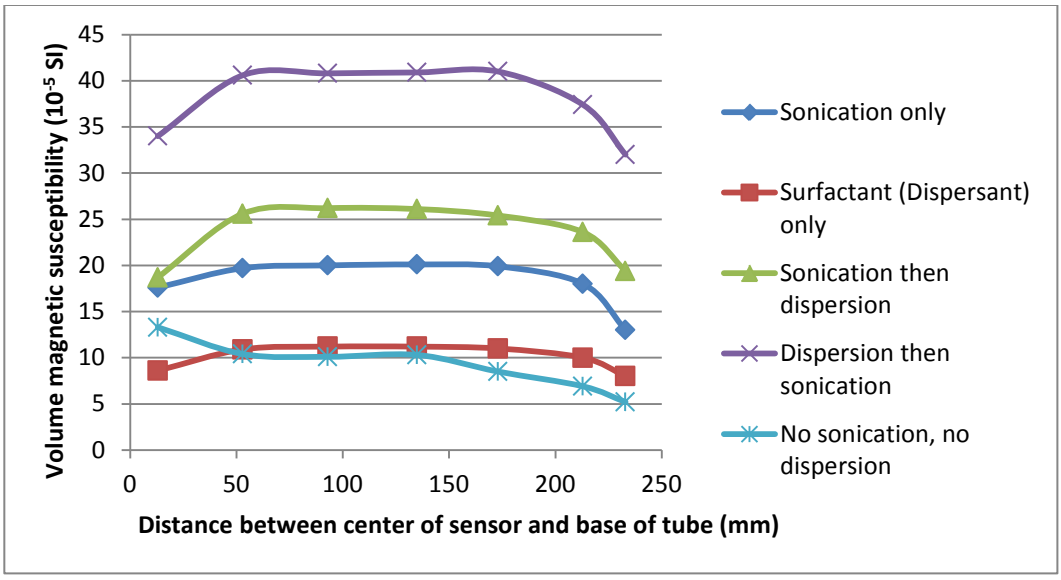

Figure 4-22: Effect of dispersion and/or sonication on stability of Maghemite NP suspensions.

Summing up together, we may say that addition of surfactant (sample 16) did not bring any appreciable change to initial susceptibility response when compared with sample without surfactant (sample 14); however it increased the stability of nanoparticle suspensions. Sonication caused an increase in volume susceptibility response and stability of the suspension. High susceptibility response was thought to be due to better dispersion of nanoparticle or their agglomerates (i.e. smaller size). Samples with dispersion followed by sonication (sample 11) exhibited slightly higher initial susceptibility response but much improved stability than of the sample with sonication only. Such an improved stability is understandable due to formation of dispersant layer of surfactant which provides steric repulsive force between nanoparticles and prevents them from agglomeration. Another factor in the stability of the nanoparticles could be the increase in electrostatic repulsive force resulting from change in pH of the suspension with the addition of ionic surfactant. The most stable solution was found to be one with dispersion followed by sonication. The susceptibility response of this suspension was many folds in contrast to other samples of same NP concentration. A plausible explanation for such a higher response is that nanoparticle or their agglomerates are smaller in size when sonication is applied after adding dispersants. Thapa et al. (2004)

demonstrated for magnetite nanoparticles that decreasing the nanoparticle size down to 10 nm improved the magnetization properties of material. Their (Thapa et al., 2004) results support the high susceptibility response as a consequence of better disintegration of nanoparticle agglomerates. With the presence of dispersant, nanoparticle agglomerates, disintegrated by sonication stay dispersed in suspension whereas in sample with dispersion after sonication, sonication results in disintegration of NP clusters/ agglomerates but before the addition of dispersant, the small sized nanoparticle agglomerates re-form larger nanoparticle agglomerates because of the absence of steric and electrostatic repulsive forces.

4.5 Effect of Sonication Time: (Samples 11, 16, 18-19)

To see the effect of sonication time, NP suspensions were prepared using same recipe but different sonication times (i.e. 0 mins, 15 mins, 30 mins and 45 minutes). The stability trends for 30 minutes sonication time and no sonication have already been presented above (sample 11 and 16 respectively). The susceptibility plots for 15 minutes and 45 minutes sonication are shown below followed by a comparison drawn for the effect of these different sonication times.

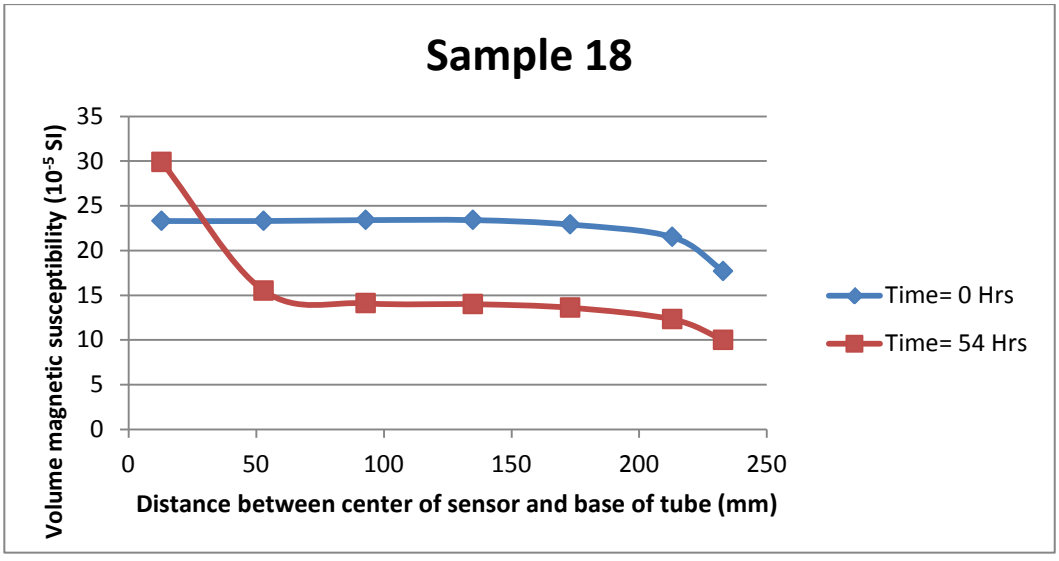

Figure 4-23: Susceptibility response of 0.2 gm Maghemite NPs with water and 0.2 gm CTAB (Sonication time=15 mins).

Comparison of susceptibility plots for sample 11, 14 and 18 (figures 4-14, 4-18 and 4-23) show that as sonication time is increased, stability of the suspension is improved. It was therefore anticipated that increasing the sonication time would further improve the stability. However, the NP suspensions did not behave as expected when sonication time was increased to 45 minutes (figure 4-24).

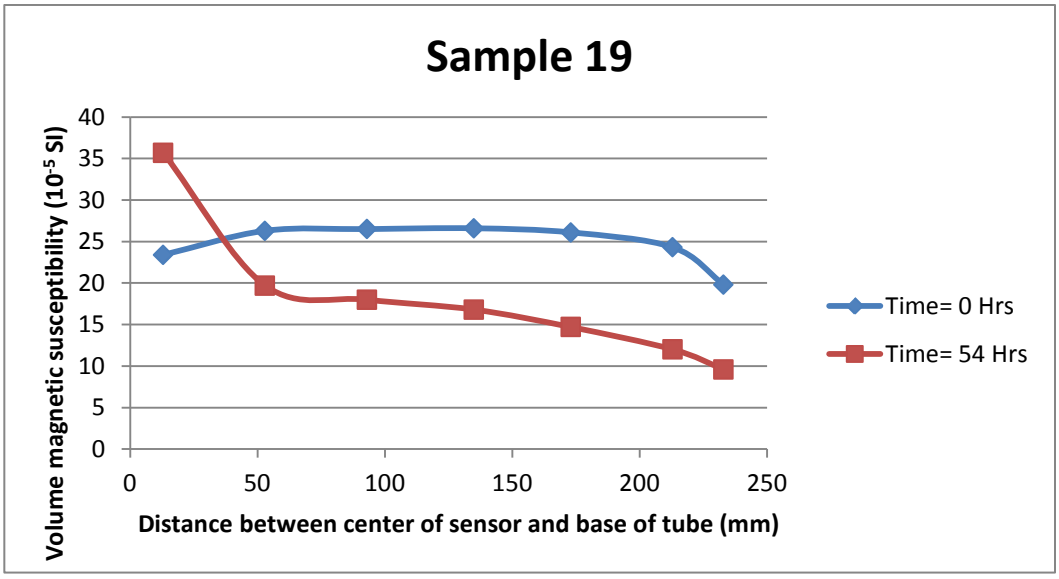

Figure 4-24: Susceptibility response of 0.2 gm Maghemite NPs with water and 0.2 gm CTAB (Sonication time=45 mins).

The lower stability behaviour of 45 minutes sonication sample (figure 4-24) as compared to 30 minutes sonication sample (figure 4-14) could be explained with the rise in the temperature of suspension as a result of prolonged sonication which would have facilitated the particle agglomeration. As we are aware that van der waals attractive forces play a key role in particle agglomeration. The three dimensional mean transfer distance which is represented by Δx is a measure of intensity of Brownian motion which is given by Equation (4-3).

$$\Delta x = \sqrt{6 D_B \Delta t} \qquad (4\text{-}3)$$

Where,

Δx = Three dimensional mean transfer distance

D_B = Brownian diffusion coefficient

Δt = Time change

The Brownian diffusion coefficient is defined by following expression.

$$D_B = kT/3\pi\mu d_p \quad (4\text{-}4)$$

Where,

k = Boltzmann constant

T = Absolute temperature

μ = Viscosity of the media/ base fluid

d_p = Size of the particle

From equations 4-3 and 4-4, one may infer that the Brownian motion, which plays a vital role in particle agglomeration is increased not only when the particle size is reduced but also when the temperature of the base fluid is increased. Kawashima et. al (1984) also reported generation of large agglomerates of salicylic acid crystals at higher temperatures. They also showed that growth rate of agglomerates increased with increasing temperature.

A precaution may therefore be used to keep the suspension cooled during sonication in order to obtain better suspension stability. Shown below is a comparison of initial volume susceptibilities of the nanoparticle suspensions prepared with different sonication times.

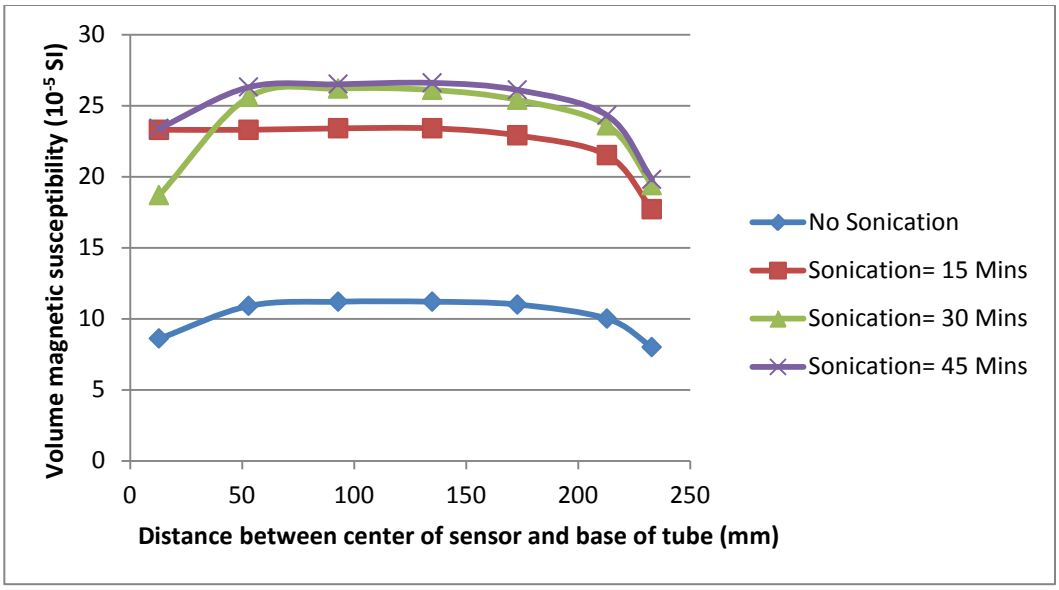

Figure 4-25: Effect of sonication time on stability of nanoparticle suspensions with CTAB.

It is clear from above figure that increasing the sonication time helps in improving the initial susceptibility response and thus the suspension stability but the improvement in the initial susceptibility response decreases exponentially with increase in sonication time. For example susceptibility change and hence stability change is much higher between no sonication and 15 minutes sonication samples than between 30 minutes and 45 minutes sonication samples. It can be seen from figure 4-25 that beyond certain sonication time, sonication might not help much in disintegration/ dispersion of NP agglomerates. In fact, higher sonication would increase the temperature of the nanoparticle suspensions, if necessary measures are not taken, that would result in poor suspension stability as observed for sample 19 above.

4.6 Effect of Sonication Power: (Samples 23, 24)

To see the effect of sonication power two similar samples were sonicated for 15 minutes at different sonication powers. Figures 4-26 and 4-27 are graphs of nanoparticle suspensions with high and low sonication powers respectively.

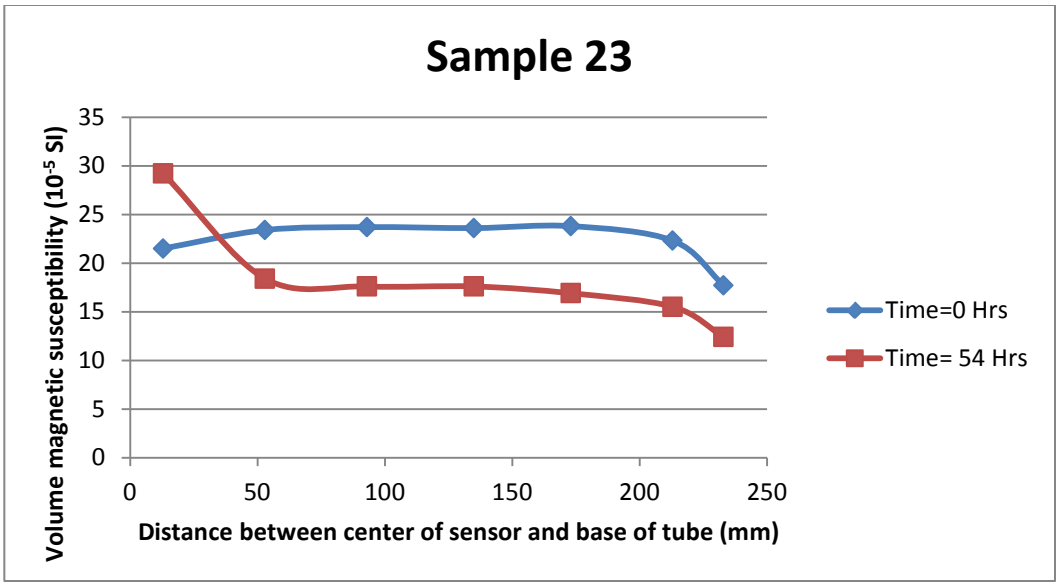

Figure 4-26: Susceptibility response of nanoparticle suspensions (Sonication Power = 100 Watts, Sonication time=15 mins).

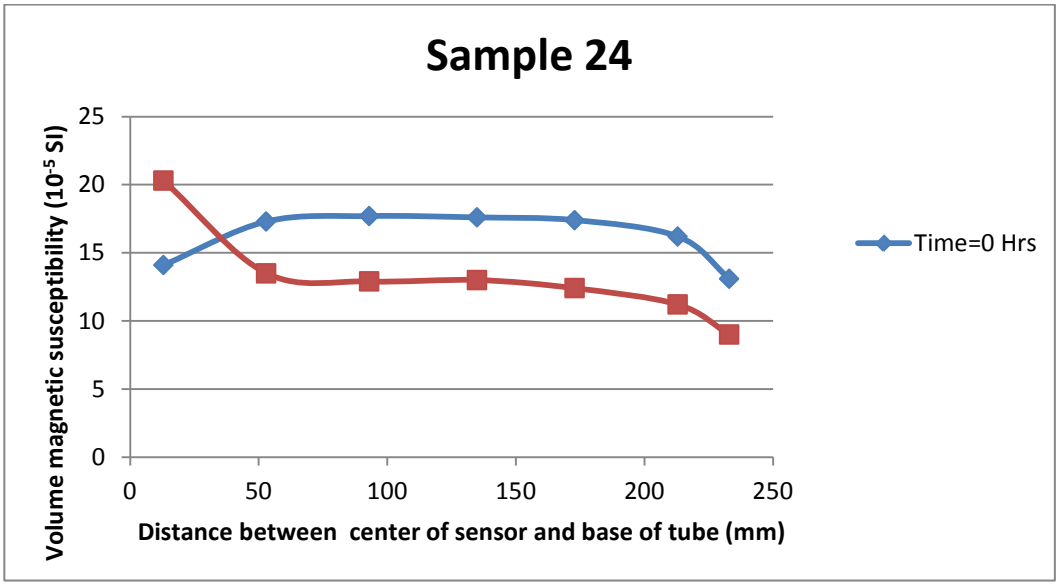

Figure 4-27: Susceptibility response of nanoparticle suspensions (Sonication Power = 40 Watts, Sonication time=15 mins).

Susceptibility trends of both the samples were similar except that the suspension samples treated at high sonication power showed higher initial susceptibility response. This implies that high sonication power/ energy results in better

disintegration/ dispersion of nanoparticles. Furthermore, comparison of sample 23 (sonication power 100 watts, sonication time 15 mins) and sample 11 (sonication power 70 watts, sonication time 30 mins) showed more or less same initial susceptibility response. Therefore, one may be conclude that it is not just the sonication time or sonication power that affects on the stability of nanoparticle suspensions but actually a composite effect of both (i.e. sonication energy = sonication power x time).

In order to find out what would be the optimum sonication power the initial susceptibility values of samples 11, 16, 18, 19 and 24 were plotted against the sonication energy applied on each of these samples. Sonication energy is calculated from multiplication of the respective sonication power and time (figure 4-28).

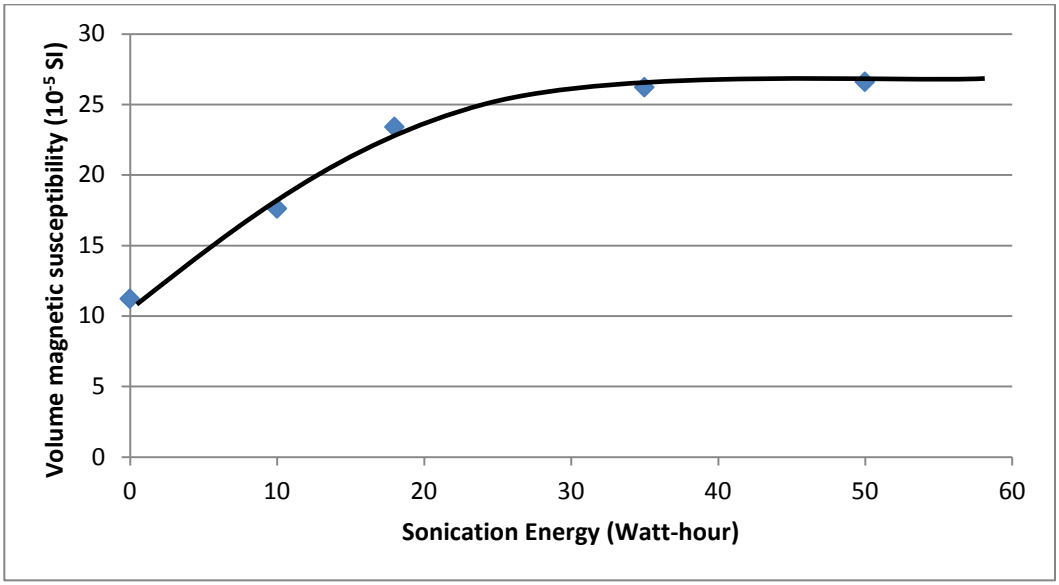

Figure 4-28: Initial susceptibility responses of nanoparticle suspensions with different concentration of CTAB surfactant in 300 ml water.

From above graph, sonication energy of 30 watt-hour should be sufficient for 300 ml suspension having 0.2 gms of Maghemite nanoparticles in it.

4.7 Effect of Type and Concentration of Dispersants: (Samples 11, 20-22, 25-28)

Initially only Xanthan Gum polymer and CTAB surfactant were used in the suspension stability study. However, later on two other types of surfactants, TGT and DDBS were also experimented those shall be discussed later in this chapter.

The initial susceptibility response is shown in figure 4-29 for different concentrations of CTAB and XG. Increasing dispersant concentration has shown improvement in initial susceptibility response. Considerably less concentration of CTAB surfactant is required to achieve same initial susceptibility response (same level of dispersion) than by Xanthan Gum polymer.

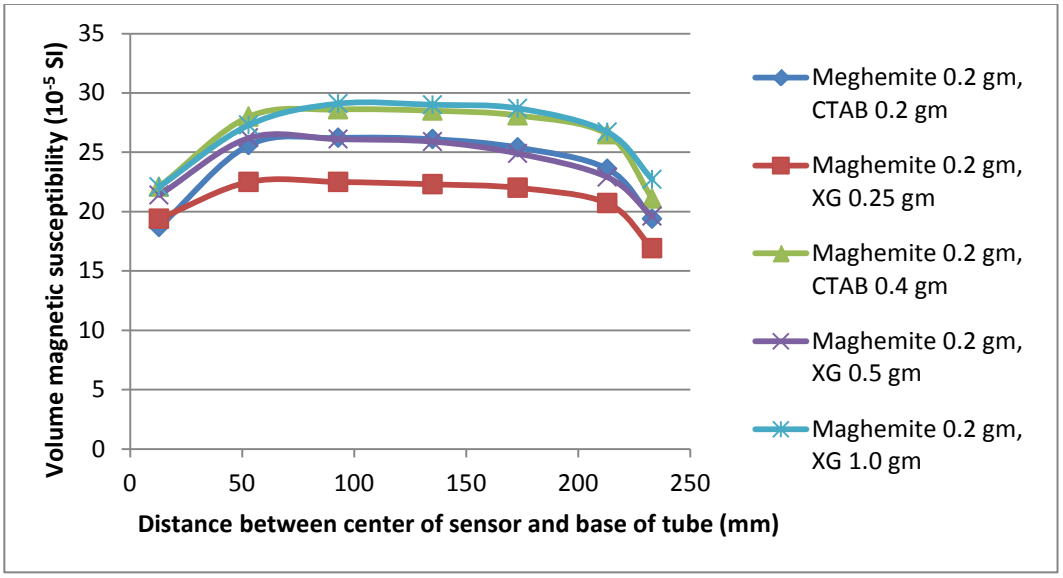

Figure 4-29: Effect of dispersant type and concentration on stability of nanoparticle suspensions.

Change in susceptibility response with time is less for suspensions with XG as dispersant, mainly due to its initially high low shear rate viscosity (LSRV) that results in drop of terminal settling velocity of nanoparticles/ agglomerates. Table 4-2 shows the LSRV of nanoparticle suspensions with XG, measured from Bohlin viscometer.

Table 4-3: LSRV table of nanoparticle suspensions with XG.

Sample #	NP wt. (gm)	Additive type	Additive wt. (gm)	LSRV (cp)
20	0.2	XG	0.25	350
21	0.2	XG	0.5	1050
22	0.2	XG	1.0	3000

Increasing the XG concentration can significantly influence the viscosity and other rheological properties of the nanoparticle suspensions. Therefore, this factor should also be taken into account, particularly when nanoparticle suspensions are prepared for flow. Figures 4-30 through 4-32 show volume magnetic susceptibility response of suspensions with XG, whereas figures 4-33 to 4-36 are for nanoparticle suspensions with CTAB as dispersant.

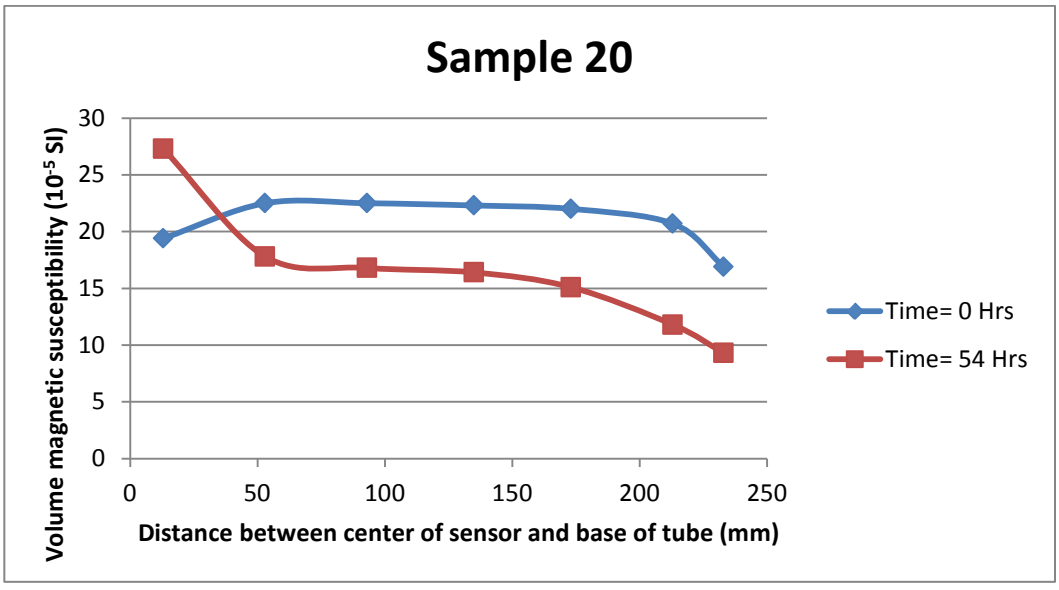

Figure 4-30: Susceptibility response of nanoparticle suspension with XG as dispersant (XG=0.25 gm).

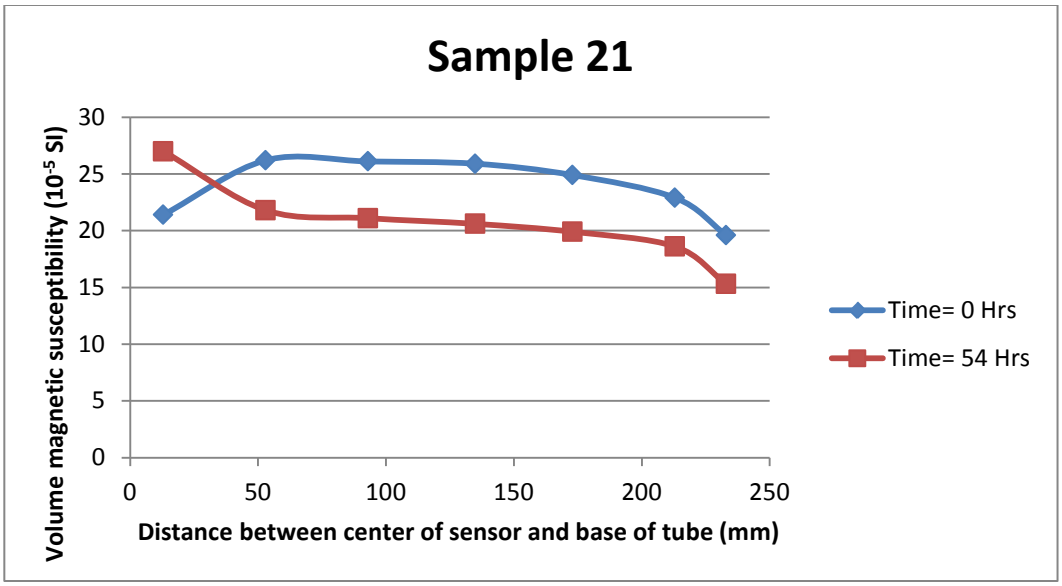

Figure 4-31: Susceptibility response of nanoparticle suspension with XG as dispersant (XG=0.50 gm).

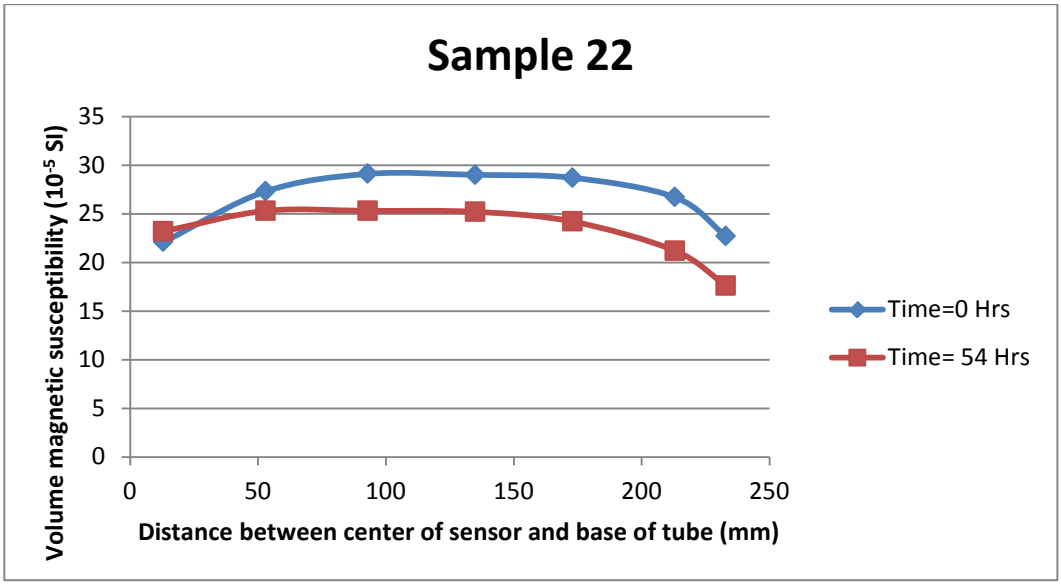

Figure 4-32: Susceptibility response of nanoparticle suspension with XG as dispersant (XG=1.0 gm).

The gap between initial and final susceptibility values is decreasing with increase in concentration of XG polymer. On the other hand, there isn't any appreciable increase in the initial volume susceptibility of the suspensions, which is

considered to be an indicator of better disintegration/ dispersion of the nanoparticle agglomerates. Therefore, it is obvious that small change in separation between the two susceptibility trends with increase in XG concentration is primarily due to LSRV of the base fluid.

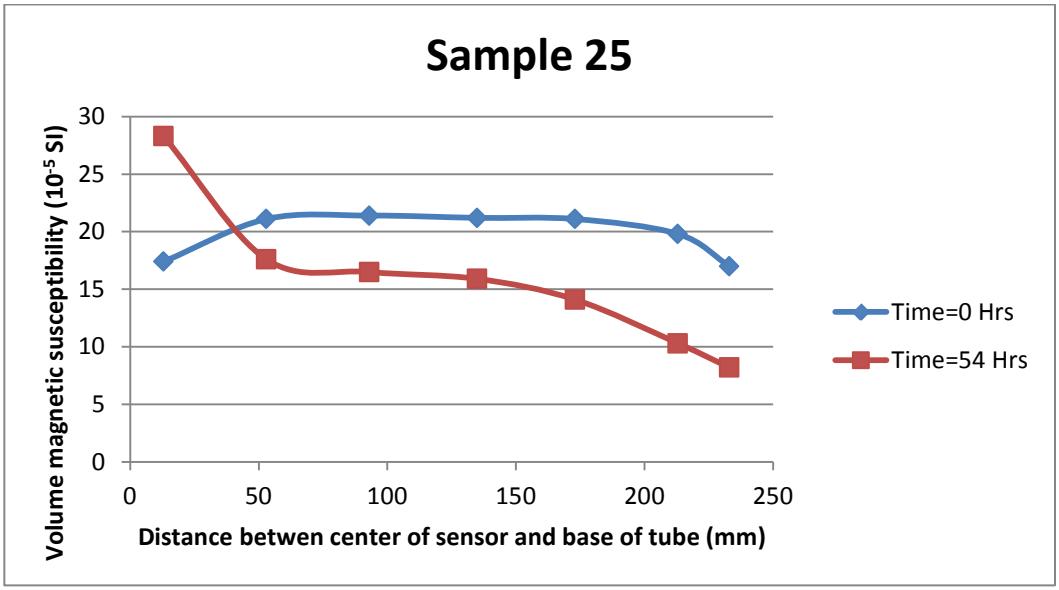

Figure 4-33: Susceptibility response of nanoparticle suspensions with CTAB as dispersant (NPs=0.2 gm, CTAB=0.1 gm).

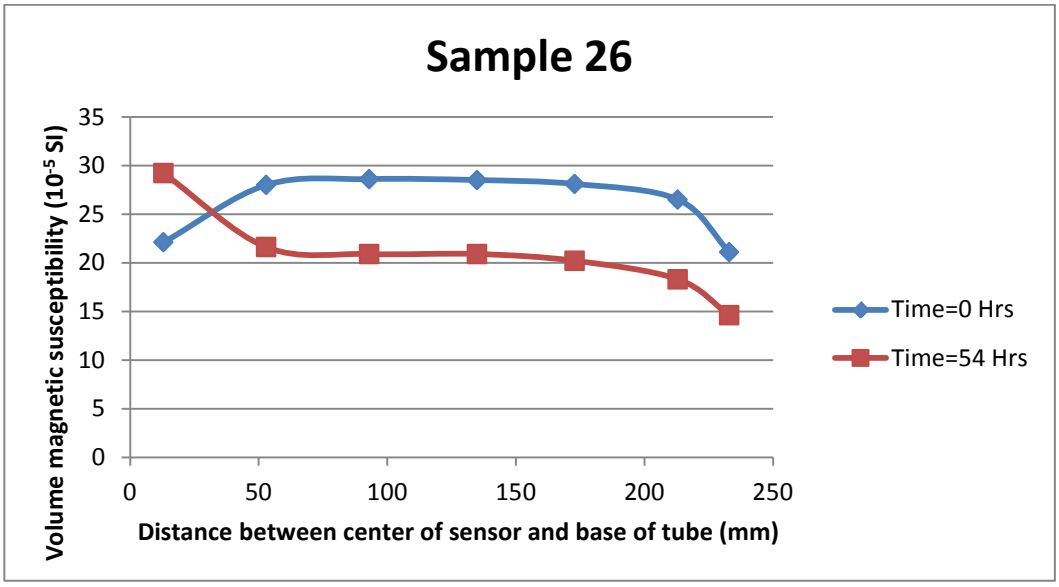

Figure 4-34: Susceptibility response of nanoparticle suspensions with CTAB as dispersant (NPs=0.2 gm, CTAB=0.4 gm).

Comparison of plots for samples 25 and 26 shows high initial susceptibility response and relatively better nanoparticle suspensions stability for high concentration of CTAB surfactant. The separation between initial and final susceptibility trends is not as close as seen for the suspensions with XG as dispersant, primarily due to high LSRV of XG based suspensions.

In order to figure out that whether the stability of the suspensions is a direct function of nanoparticle to surfactant ratio, few more samples with higher nanoparticle concentration but same nanoparticle to surfactant ratio were prepared. Unlike sample 25 and sample 26 where initial susceptibility response and suspension stability was better with higher concentration of CTAB, sample 27 and 28 showed more or less same suspension stability regardless of increase in CTAB concentration.

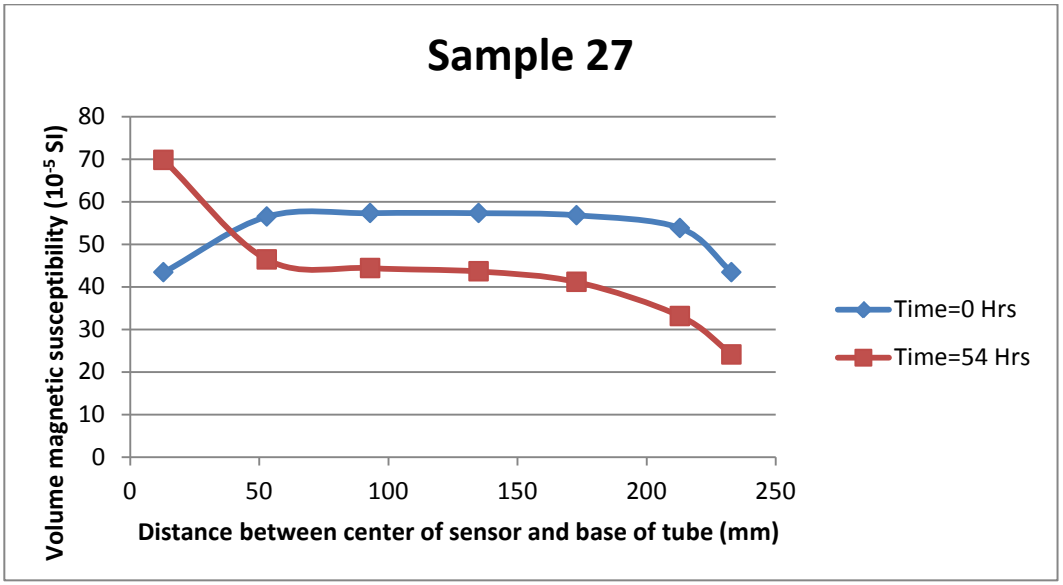

Figure 4-35: Susceptibility response of nanoparticle suspensions with CTAB as dispersant (NPs=0.5 gm, CTAB=0.25 gm).

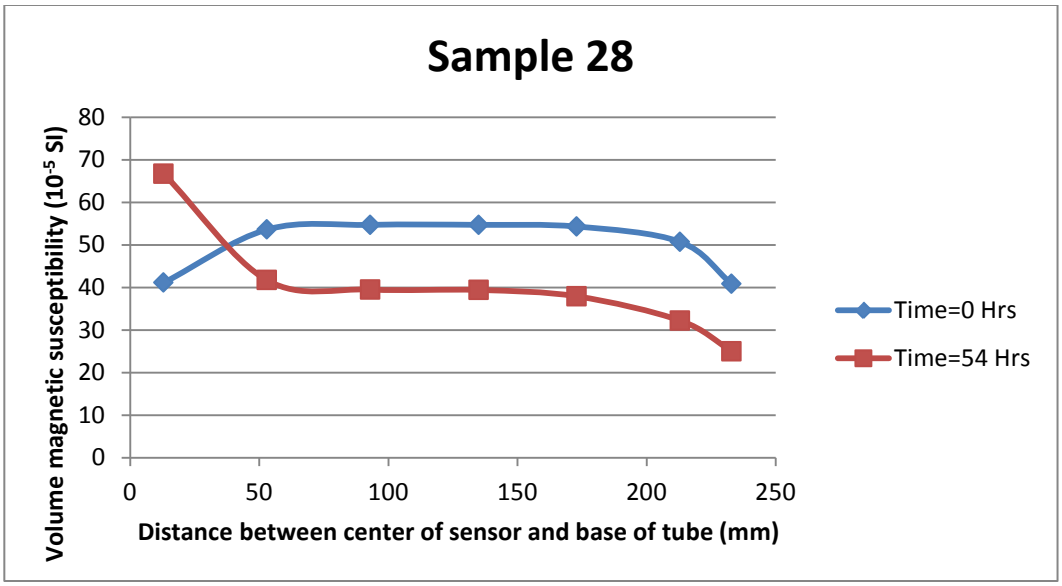

Figure 4-36: Susceptibility response of nanoparticle suspensions with CTAB as dispersant (NPs=0.5 gm, CTAB=1.0 gm).

Based on the above observation it may be concluded that optimum concentration requirement of surfactant does not change with the variation in concentration of nanoparticles. Shown below are the plots of initial volume magnetic susceptibilities of two different concentrations of Maghemite NP suspensions with different concentrations of CTAB surfactant as dispersant.

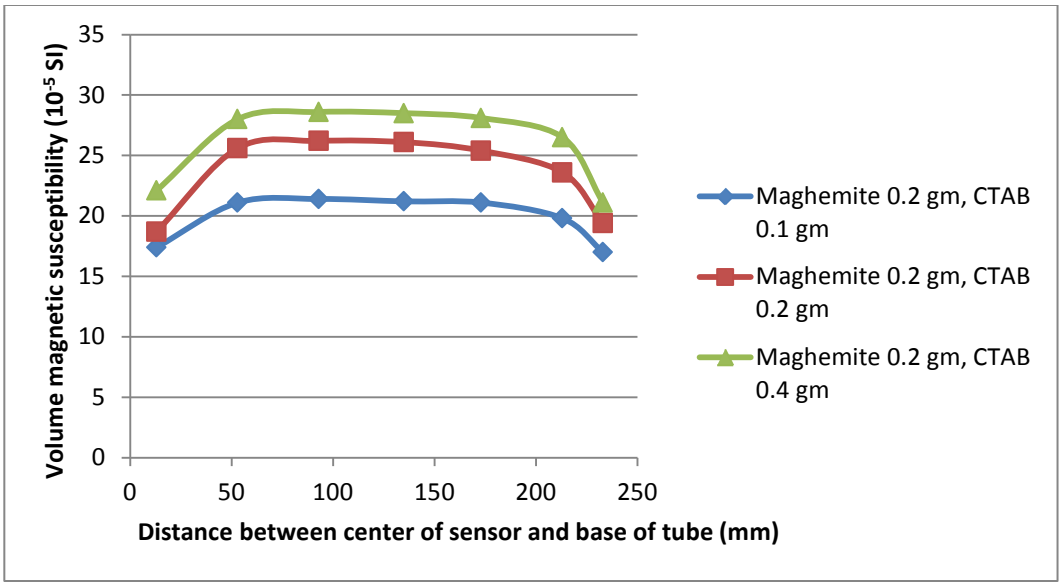

Figure 4-37: Effect of changing CTAB concentration on nanoparticle suspensions (Maghemite= 0.2 gm, sonication 70 watts for 30 mins).

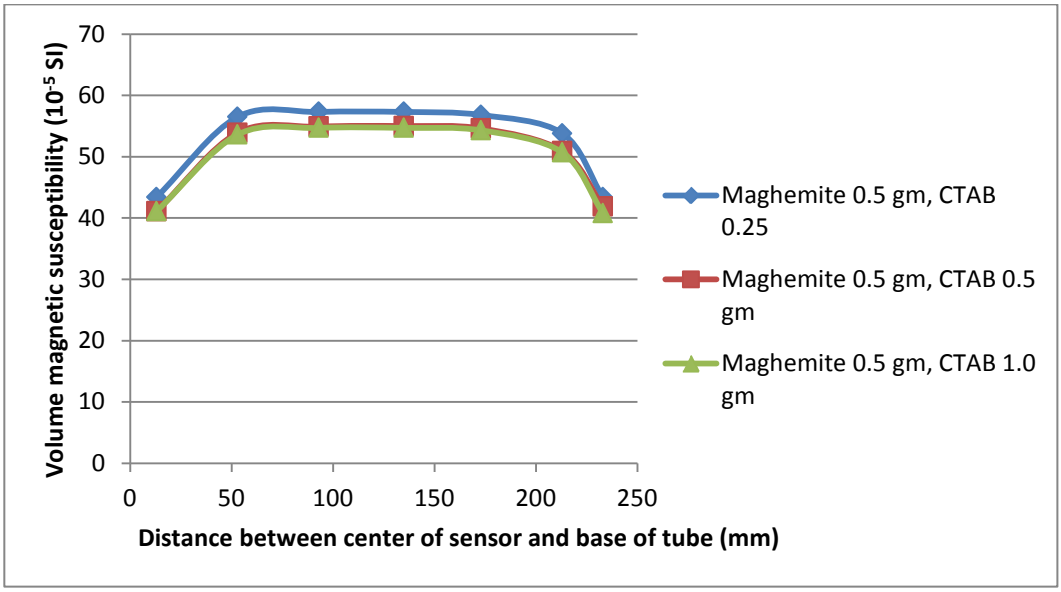

Figure 4-38: Effect of changing CTAB concentration on nanoparticle suspensions (Maghemite= 0.5 gm, sonication 70 watts for 30 mins).

There is an obvious increase in initial susceptibility response with increase of CTAB concentration in nanoparticle suspensions containing 0.2 gm Maghemite (figure 4-37). Similar NPs to CTAB ratio was maintained in nanoparticle suspensions containing 0.5 gm Maghemite NPs but similar differences were not

obtained (figure 4-38) and the initial as well as final susceptibility responses were almost same regardless of any increase in volume magnetic susceptibility. As said earlier, the possible reason for such behaviour could be that optimum concentration of CTAB is not a function of quantity of nanoparticles in suspensions, thus, any further increase beyond that optimum concentration of CTAB does not bring any noticeable improvement in suspension stability.

A plot between concentration of surfactant used in preparation of suspensions (while all other parameters were kept the same) and the initial susceptibility value at the center of graduated tube is shown in figure 4-39. Plots like this could be helpful in finding an optimum concentration of dispersant/ surfactant for preparation of nanoparticle suspensions.

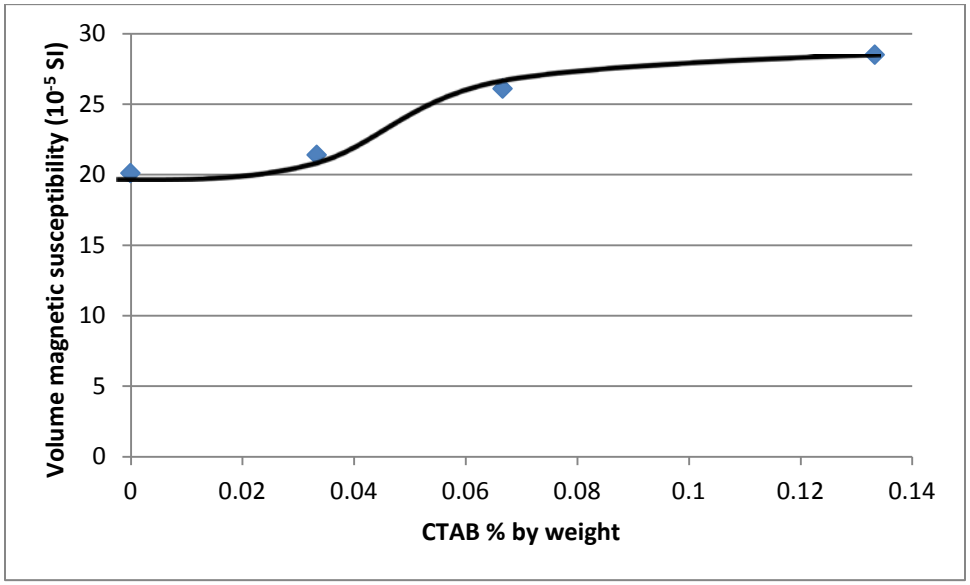

Figure 4-39: Initial susceptibility responses of nanoparticle suspensions with different concentration of CTAB surfactant in 300 ml water.

Above plot is generated from the suspensions prepared with 0.2 gm of Maghemite nanoparticles which shows that CTAB concentration of approximately 0.1% by weight will be sufficient to obtain good suspension. The optimum concentration requirement for other nanoparticles (having different chemistry and surface

charge) and different nanoparticle concentration may vary and should be found accordingly.

4.8 Method of Sample Preparation: (Samples 11, 17, 21, 29)

It has been described in earlier section (section 4.4) that dispersion followed by sonication (sample 17) give better response in terms of initial susceptibility and suspension stability as compared to process of sonication followed by dispersion (Samples 11). This fact was established while using CTAB as dispersant. The effect of changing sonication/ dispersion pattern was re-examined for samples with XG dispersant. Figure 4-40 is a plot of initial susceptibilities of same suspension recipe (with XG dispersant) except that in one sample sonication is performed prior to dispersion and vice versa in other.

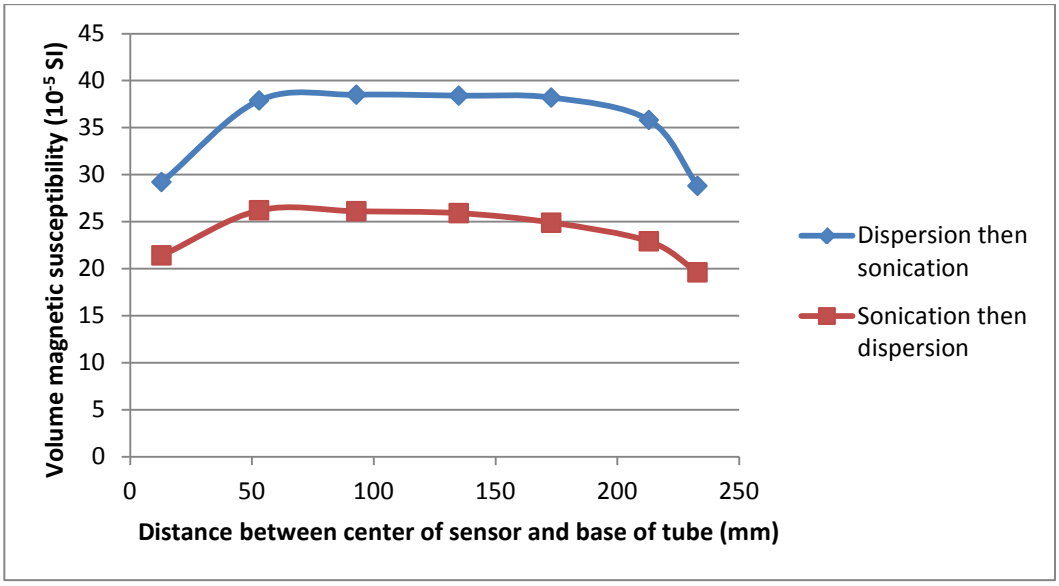

Figure 4-40: Effect of changing method of preparing nanoparticle suspensions with XG.

Initial susceptibility of the sample wherein dispersion was performed before sonication, gave much higher initial susceptibility values, which is a behaviour concurrent with earlier observations about suitable method for stable suspension preparation (section 4.3). The initial susceptibility response was although quite

high but it was less than that seen with suspension having CTAB dispersant instead.

Figure 4-41 presents the initial/ final susceptibility trends which are not as close as seen in sample 17, where suspension was prepared first by adding CTAB surfactant/ dispersant and then sonication. Hence, CTAB surfactant offered higher initial susceptibility and better stability than XG polymer. Furthermore, unlike XG, addition of surfactant does not drastically change the rheological properties. Therefore, it may be considered a better choice for flow through porous media as least obstruction/ resistance will be faced with the use of surfactants.

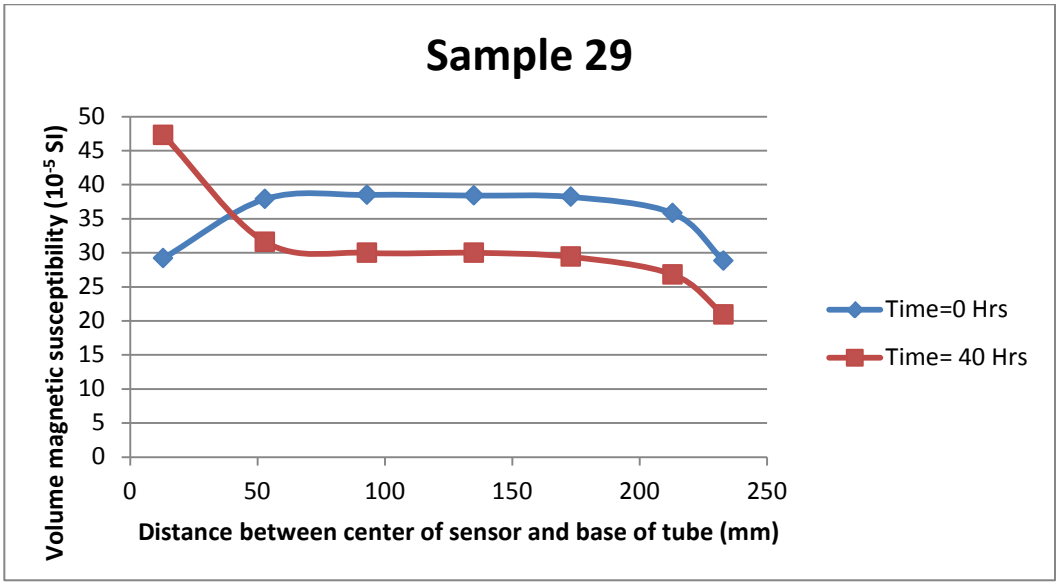

Figure 4-41: Susceptibility response of Maghemite nanoparticle suspensions with XG (Dispersion then sonication).

4.9 Applied Magnetic Field: (Samples 11, 30)

Two similar samples were tested to observe any change in stability of nanoparticle suspensions with the exposure duration of applied magnetic field. One sample was subjected to weak applied magnetic field of sensor for less than 30 minutes (sample 11) and the other was subjected for 6 hours (sample 30). Sample 30, which is exposed to magnetic field for longer period of time has

shown relatively less suspension stability. Reason for decrease in suspension stability would be the additional attractive force due to magnetization of nanoparticles, favouring formation of nanoparticle agglomerates.

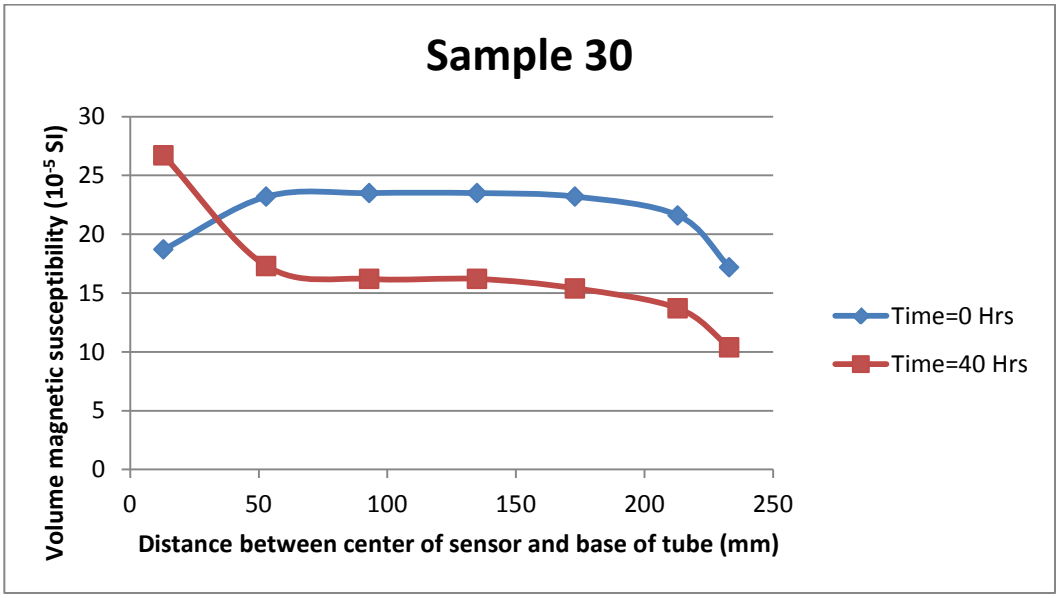

Figure 4-42: Susceptibility response of Maghemite nanoparticle suspension (6 hours exposure to applied magnetic field).

4.10 Second Set of Suspensions Stability Experiments

After the initial investigation on various factors affecting stability of the nanoparticle suspensions it was planned to conduct some more stability experiments using the "dispersion followed by sonication" approach. Table 3-11 presents different suspension recipes prepared by using the above mentioned technique, to observe:

a) NPs concentration versus susceptibility response
b) Effect of cationic, anionic, non-ionic surfactants with and without XG

4.10.1 **Nanoparticle Concentration Versus Susceptibility**

The initial susceptibility response of samples 31 through sample 34 is shown in figure 4-43.

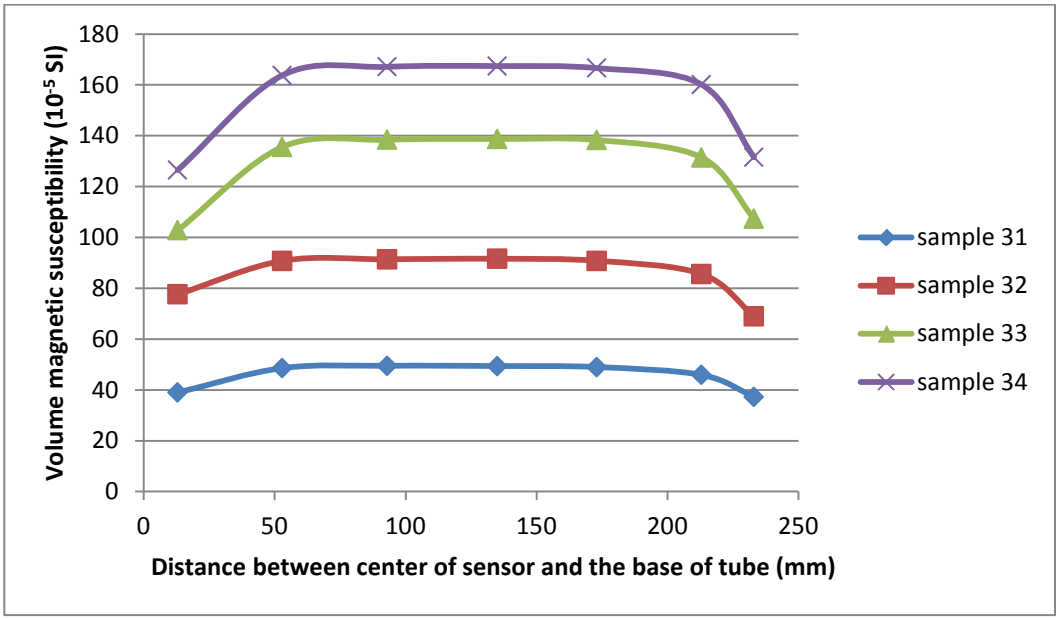

Figure 4-43: Susceptibility response of Maghemite nanoparticle suspensions (Sample 31-34).

In above figure, different initial susceptibility trends for sample 31 to 33 are mainly due to different concentrations of nanoparticles in suspensions. However, sample 33 and 34 have same nanoparticle concentration, but relatively higher sonication energy was used for sample 34. The need for increasing sonication energy is explained in below discussion.

Plotting concentration of NPs versus susceptibility readings at the center of tube for samples 31-33 gave a linear trend with a regression coefficient of less than 0.9 (figure 4-44).

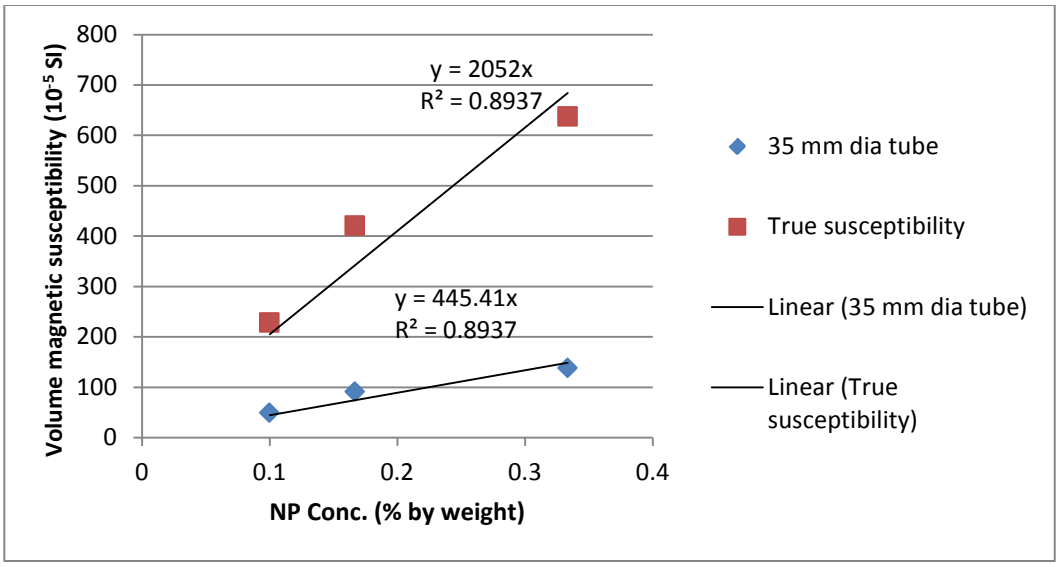

Figure 4-44: Maghemite conc. versus susceptibility plot (Sample 31-33).

The regression coefficient (>0.99) was improved when sample 34 was used instead of sample 33 (figure 4-45). It was thought that may be the sonication energy (70 watts for 30 minutes) used for disintegration of higher quantity of NPs might be insufficient to achieve same level of dispersion as was achieved for less concentrated nanoparticle suspensions.

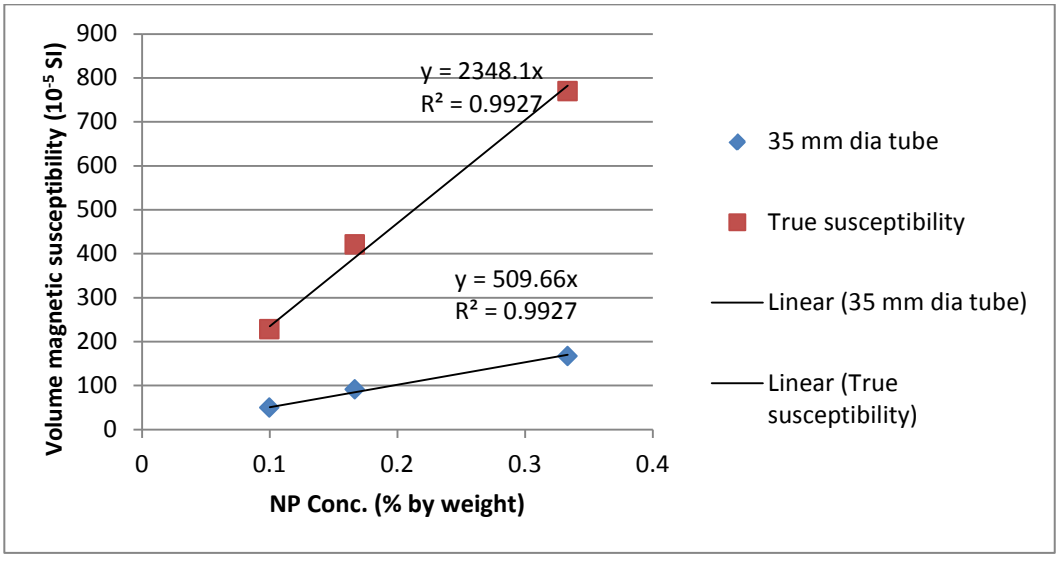

Figure 4-45: Maghemite conc. versus susceptibility plot (Sample 31-32, 34).

Previously, it was shown that increasing the sonication energy (sonication time and/ or sonication power) increases the initial susceptibility response and thus stability of nanoparticle suspensions but up to a certain limit beyond which increasing sonication energy does not aid any further. The significant difference between the susceptibility value of sample 33 and 34 may be explained by considering the above conclusion valid for the same concentration of nanoparticles. Based on above observation, sonication energy is found to be a function of NPs concentration in nanoparticle suspension.

4.10.2 Effect of Ionic and Non-ionic Surfactants with and without XG (Sample 36-42)

Anionic and non-ionic surfactants are also tried with γ-Fe_2O_3 NPs to see what effect do these bring to the stability and susceptibility response of nanoparticle suspensions. Figures 4-46 and 4-48 are plots of initial volume magnetic susceptibility response of nanoparticle suspensions with different concentrations of anionic surfactant, DDBS and non-ionic surfactant, TGT respectively.

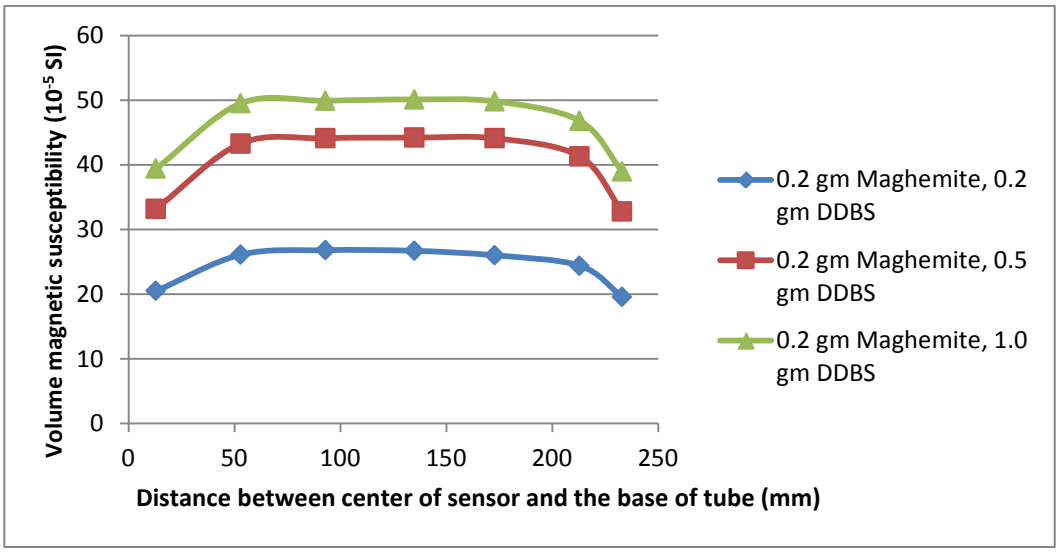

Figure 4-46: Initial susceptibility responses of nanoparticle suspensions with different concentration of DDBS surfactant.

Increased susceptibility response with increase in DDBS concentration is consistent with similar finding with CTAB concentration. However, the increase in susceptibility is not linear with increase in concentration and that increase in susceptibility decreases with increase in concentration of surfactant. Optimum concentration of surfactant from this data can be estimated by plotting susceptibility versus concentration (or quantity) of surfactant.

Figure 4-47 shows susceptibility response against weight percentage of DDBS surfactant in 300 ml water.

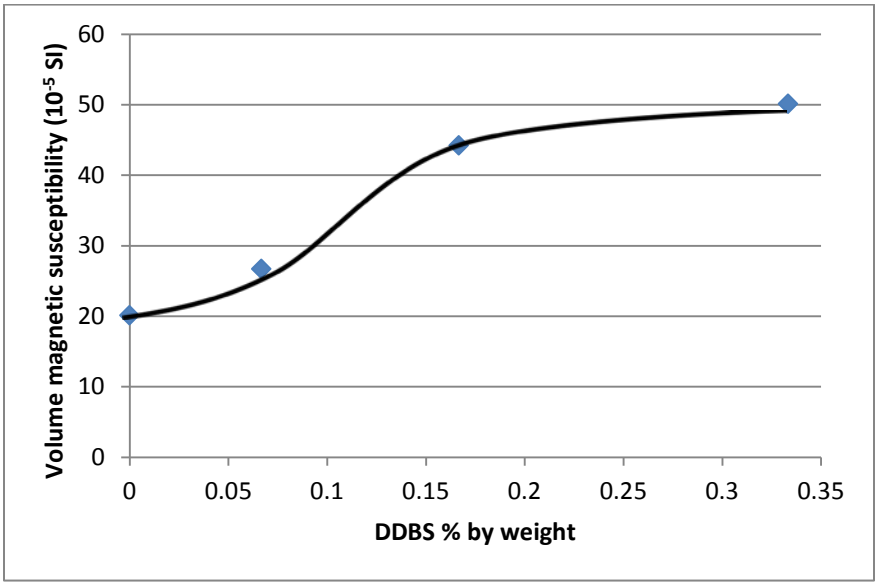

Figure 4-47: Initial susceptibility responses of nanoparticle suspensions with different concentration of DDBS surfactant in 300 ml water.

From the above plot, it may be inferred that 0.3 to 0.35 % by weight of surfactant would be enough for preparing stable Maghemite nanoparticle suspension.

The initial susceptibility response with different concentrations of Tergitol is presented in figure 4-48.

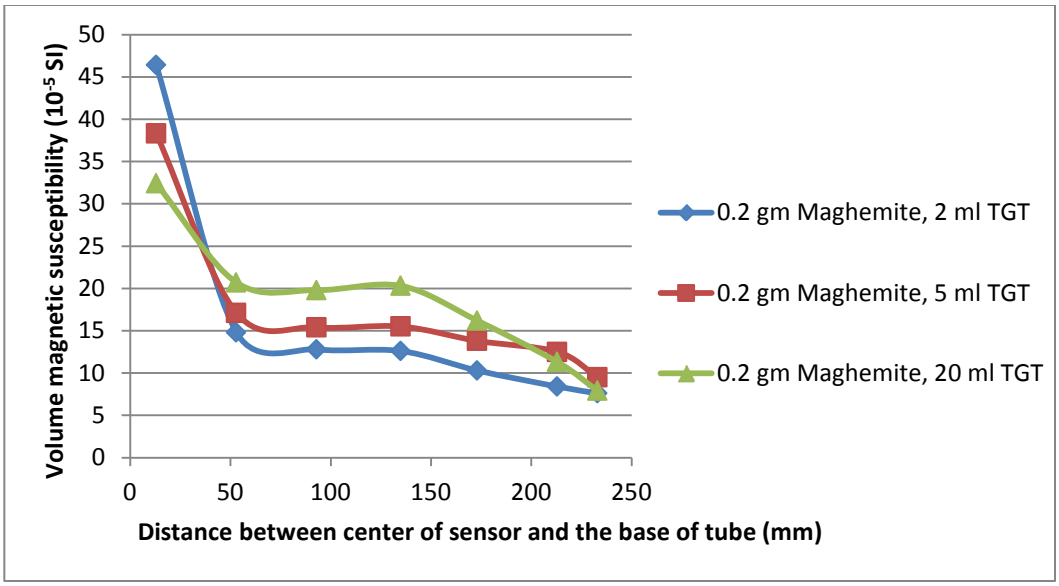

Figure 4-48: Initial susceptibility responses of nanoparticle suspensions with different concentration of TGT surfactant.

It is obvious from these responses that TGT which is a non-ionic surfactant did not work well at all in terms of stability of nanoparticle suspensions. The initial susceptibility values near the base of the tube are considerably higher than rest of the values, which is due to that fact that these suspensions are highly unstable and particle settlement has already started taking place.

The initial susceptibility and stability responses of the nanoparticle suspensions having DDBS and CTAB surfactants as dispersants were better and resembled each other. It was therefore decided to use both surfactants (separately) in fluid flow experiments through porous medium.

The susceptibility and stability response of DDBS based nanoparticle suspensions (sample 38) is presented below in figure 4-49 which is close to the susceptibility response of CTAB based nanoparticle suspensions (sample 17).

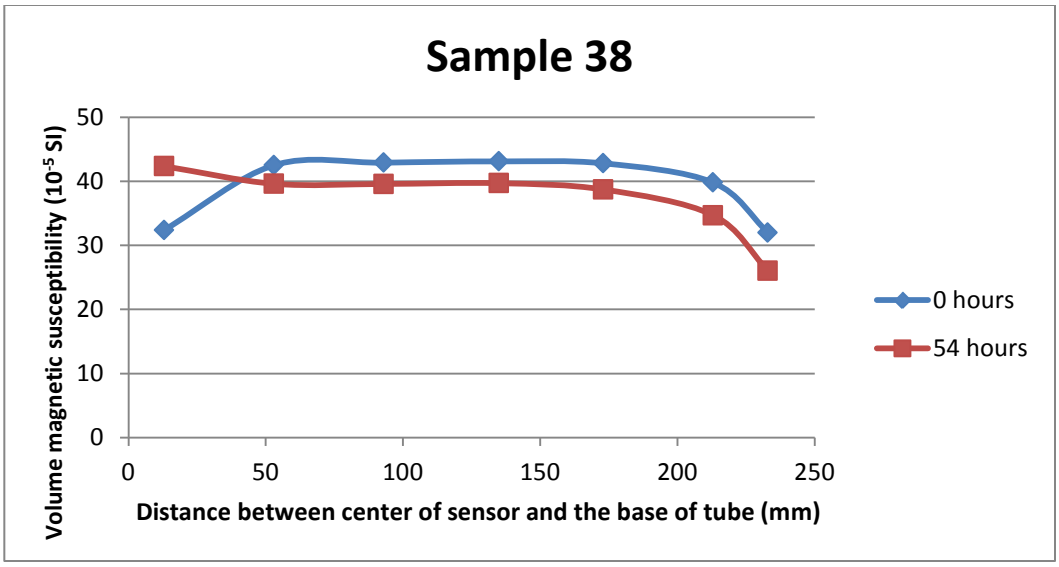

Figure 4-49: Susceptibility response of 0.2 gm Maghemite NPs with water and 1.0 gm DDBS (dispersed then sonicated).

A combination of surfactant and polymer (CTAB+XG) was also tested in nanoparticle suspensions with intend that CTAB will act as a dispersant and XG would change the rheological characteristics of suspension, thus, improving the time based particle suspension. However, the suspension showed a totally unstable response (figure 4-50).

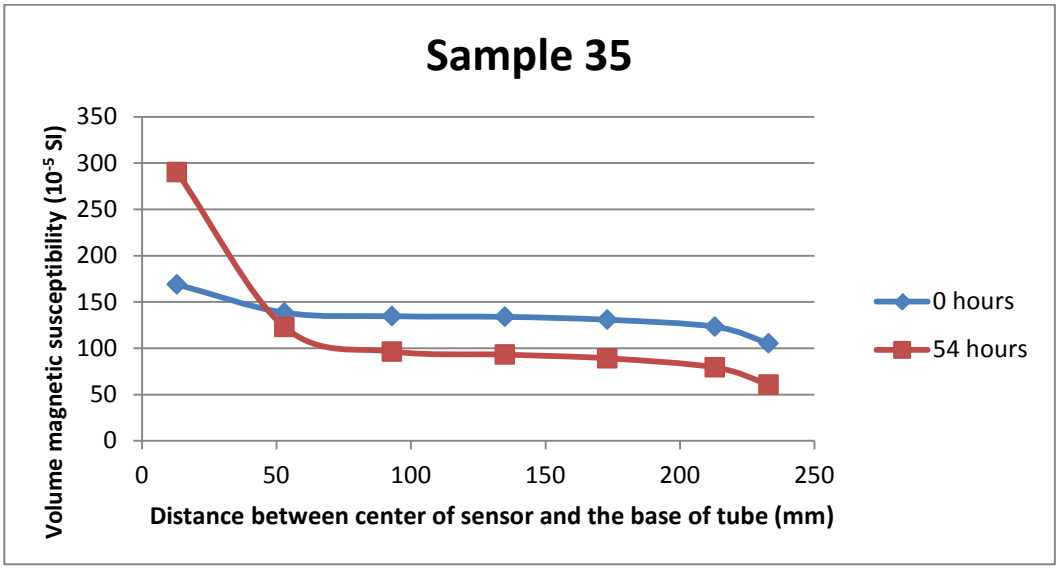

Figure 4-50: Susceptibility response of 1.0 gm Maghemite NPs with water, 1.0 gm CTAB and 0.5 gm XG.

In contrast, suspensions with DDBS and XG as dispersant performed way better (figure 4-51) and exhibited initial susceptibility response similar to sample 34 which contained same amount of DDBS concentration.

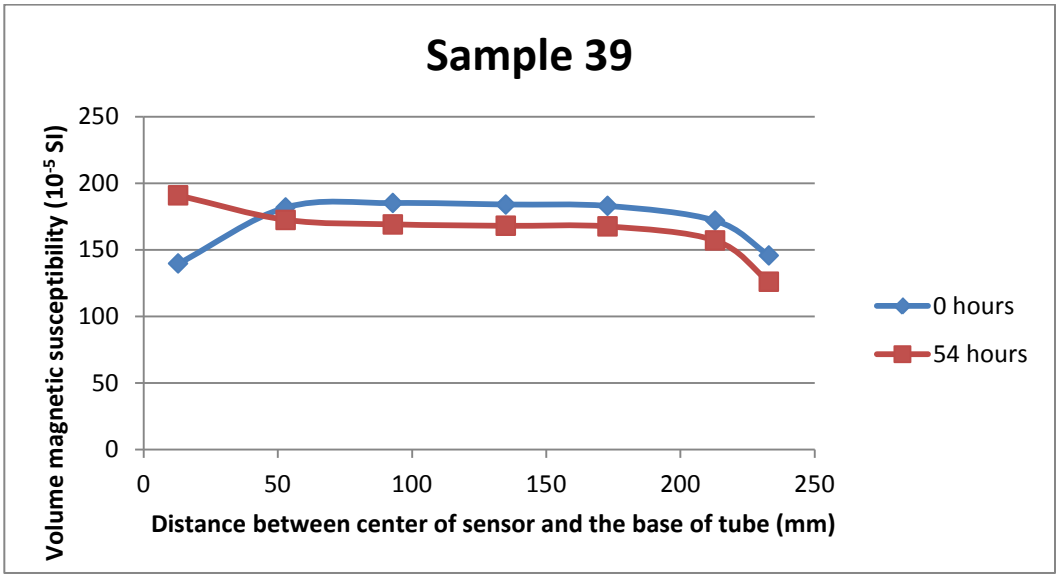

Figure 4-51: Susceptibility response of 1.0 gm Maghemite NPs with water, 1.0 gm DDBS and 0.5 gm XG.

5 DYNAMIC (FLUID FLOW) EXPERIMENTS

The dynamic experiments were mainly aimed at finding the effect of adhesion/ sorption to the material of porous media (walls of pores) or in other words the transport efficacy of nanoparticle suspensions through porous media. Formation of agglomerates due to nanoparticles interaction with each other is also likely to contribute in the transport characteristics of nanoparticle suspensions but the main phenomena for retention of nanoparticles in porous media is adhesion of nanoparticles.

In these fluid flow experiments multiple pore volumes of nanoparticle suspensions are injected in glass beads/ sand pack followed by flushing with de-ionized water and susceptibility measurements at various points along the length of the glass beads/sand pack are taken after different pore volume injections of nanoparticle suspensions/ water. Particle sticking/ adhesion or in broader term transport efficacy of nanoparticle suspensions was observed by changing the recipe of nanoparticle suspensions, fluid flow parameters and material type/ size used for porous flow media. Effects of these parameters on transport behaviour/ adhesion of nanoparticles and their aggregates are briefly discussed below:

5.1 Effect of Recipe Preparation Method

In static experiments mainly two types of suspension recipe preparation methods were used, one in which sonication was performed after addition of dispersant and the other wherein dispersion followed the sonication of the suspensions. Former method showed much better suspension stability than later.

Flow experiments were performed with both types of recipes. Figures 5-1 shows the susceptibility measurements of an experiment wherein injected Maghemite nanoparticle suspensions were prepared following sonication then dispersion procedure, whereas figure 5-2 shows the results of the experiment in which nanoparticle suspensions were prepared by dispersion and then sonication. Basic

information about the recipe used for preparation of nanoparticle suspensions, core material (i.e. glass beads/ sand), measured porosity and permeability of core and injection rates used are tabulated along with relevant plots.

Recipe	3.0 gm ɣ -Fe_2O_3 + 600 ml water + 1 gm CTAB (sonicated then dispersed)		
Injection Rate	20 cc/min	Core Material	Glass beads: 170-325 mesh (44-88 μm)
Measured Porosity	0.33	Measured Permeability	2.2 Darcy
Sonication Power	120 watts	Sonication Time	40 minutes

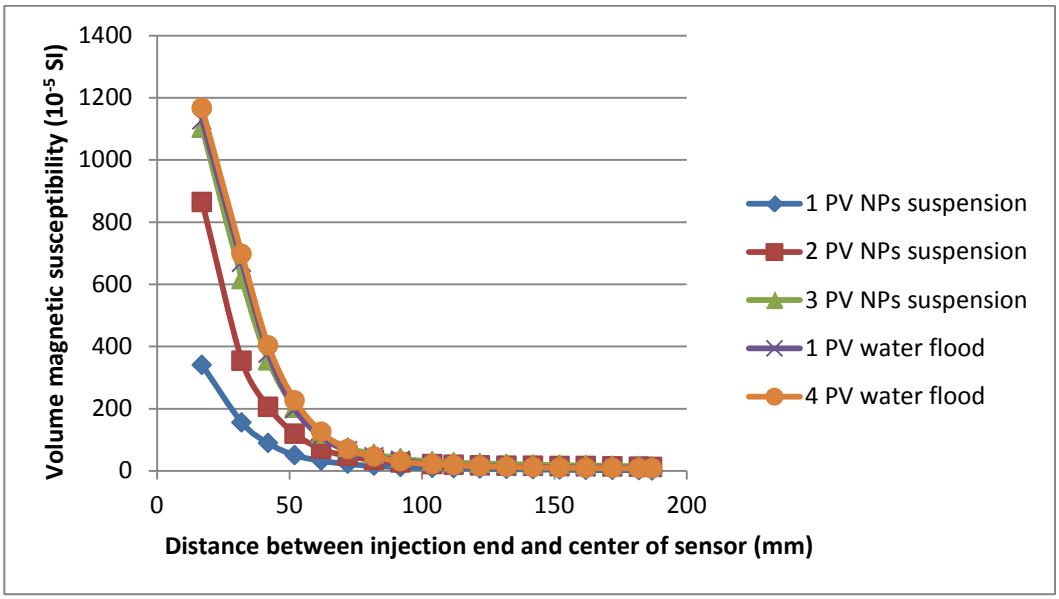

Figure 5-1: Susceptibility response after different pore volumes injections of Maghemite nanoparticle suspension and water in 170-325 mesh glass beads pack (Suspensions sonicated then dispersed).

The susceptibility response is a direct function of concentration of nanoparticles. Therefore, the high susceptibility response at the inlet of glass beads filled flow cell indicate large amount of NPs settlement/ deposition. Even with number of pore volume injections of nanoparticle suspensions, the susceptibility value are changing only within a short distance near inlet/ injection end. The susceptibility response shows that this recipe for nanoparticle transport is totally inefficient resulting in entire nanoparticle deposition/ adhesion at or near the injection point.

Post flushing of nanoparticle suspensions with number of PVs of de-ionized water also did not help mobilizing even a small fraction of deposited nanoparticles. The susceptibility trends stays almost same for 3 PV injection of nanoparticle suspensions, 1 PV flooding and 4 PV flooding with de-ionized water.

The nanoparticles accumulation/ adhesion was considerably reduced when same recipe ingredients were used but dispersants were added prior to sonication. Comparison of figures 5-1 and 5-2 shows that considerable improvement is observed in terms of NPs transport in porous media. However, a large amount of NPs was still left as shown by susceptibility trends in figure 5-2.

Recipe	3.0 gm γ -Fe_2O_3 + 600 ml water + 1 gm CTAB (dispersed then sonicated)		
Injection Rate	20 cc/min	Core Material	Glass beads: 170-325 mesh (44-88 μm)
Measured Porosity	0.33	Measured Permeability	2.2 Darcy
Sonication Power	120 watts	Sonication Time	40 minutes

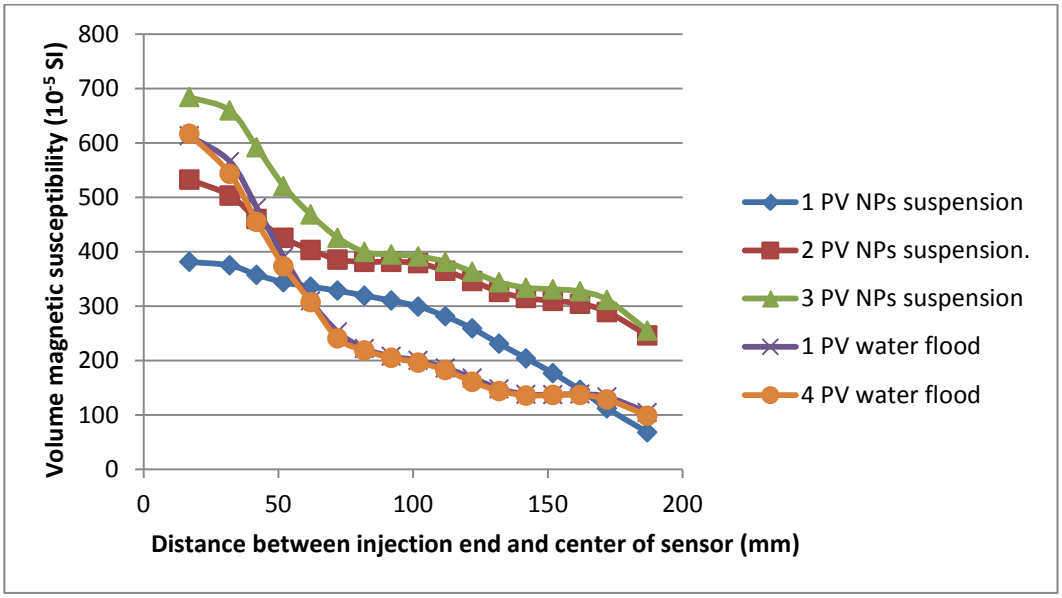

Figure 5-2: Susceptibility response after different pore volumes injection of Maghemite nanoparticle suspension and water (Suspensions dispersed then sonicated).

Unlike figure 5-1, where susceptibility values were changing only in fraction of flow cell length, the susceptibility values are increasing along the entire length of the flow cell in figure 5-2. This implies that this suspension recipe is better than that tried in earlier experiment (figure 5-1). However, particle deposition is seen to be higher near the injection point. It could also be interpreted from figure 5-1 that fraction of the nanoparticles present in flow cell are recovered by water flush and majority of these mobile nanoparticles are recovered from 1 PV injection of de-ionized water. Further injection of de-ionized water did not bring any noticeable change in susceptibility curve, which means no further movement/ removal of nanoparticle left in the flow cell.

5.2 Effect of Dispersant Type

Introducing new recipe with DDBS surfactant replacing CTAB brought most of the change in terms of recovery of NPs from porous media and adhesion of NPs. It can be seen from the comparison of figures 5-2 and 5-3 that the transport of nanoparticle suspensions was enhanced many folds when anionic DDBS surfactant was used (figure 5-3) in nanoparticle suspensions instead of cationic CTAB (figure 5-2). It can be inferred from these different responses that anionic nature of surfactant might have increased the electrostatic repulsive forces between glass beads and nanoparticles resulting in a less adhesion. On the other hand, CTAB although showed suspension stability response similar to suspensions having DDBS as surfactant but failed to keep the repulsive electrostatic forces sufficient enough to prevent adhesion of Maghemite nanoparticles with glass beads having different surface charge.

Recipe	3.0 gm γ -Fe_2O_3 + 600 ml water + 2 gm DDBS (dispersed then sonicated)		
Injection Rate	20 cc/min	Core Material	Glass beads: 170-325 mesh (44-88 μm)
Measured Porosity	0.339	Measured Permeability	2.3 Darcy
Sonication Power	120 watts	Sonication Time	40 minutes

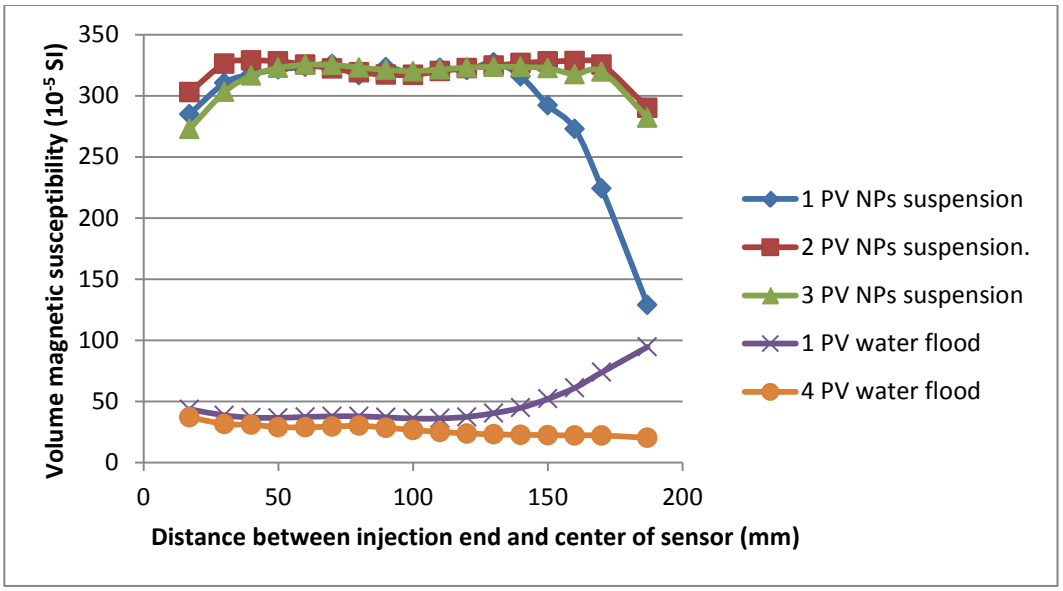

Figure 5-3: Susceptibility response after different pore volumes injection of Maghemite nanoparticle suspensions and water (DDBS used as dispersant).

From figure 5-3, it can be inferred that there is no or negligible nanoparticle adhesion or accumulation taking place as the susceptibility trends are almost overlapping each other for different pore volume injections of nanoparticle suspensions. The decline in 1 PV NPs suspension injection trend near the end of the flow cell is due to suspension breakthrough and sweep efficiency effects, thus not entirely displacing the earlier fluid present therein. Nearly 90% of nanoparticle suspensions were removed after flooding the glass beads packed flow cell with de-ionized water. Such a high recovery of nanoparticles and excellent stability of suspensions prepared with this method makes these a suitable option for use in porous media applications.

Due to better transport behaviour of nanoparticles through porous media with DDBS as surfactant in nanoparticle suspensions and dispersion followed by sonication as a better method of suspension recipe preparation, these were used in subsequent flow experiments to investigate the effect of other parameters.

5.3 Effect of concentration of NPs

To see the effect of concentration of NPs used in flow studies two more suspensions using different concentrations of NPs (1 gm and 0.4 gm) were prepared and flowed through similar porous media. The results of their flow behaviour are plotted in figures 5-4 and 5-5 and are compared with figure 5-3 (NPs = 3 gm). Figures 5-4 and 5-5 show the susceptibility responses of suspensions transport having 1 gm and 0.4 gm of Maghemite respectively.

Recipe	1.0 gm γ -Fe_2O_3 + 600 ml water + 2 gm DDBS (dispersed then sonicated)		
Injection Rate	20 cc/min	Core Material	Glass beads:170-325 mesh (44-88 μm)
Measured Porosity	0.34	Measured Permeability	2.25 Darcy
Sonication Power	120 watts	Sonication Time	40 minutes

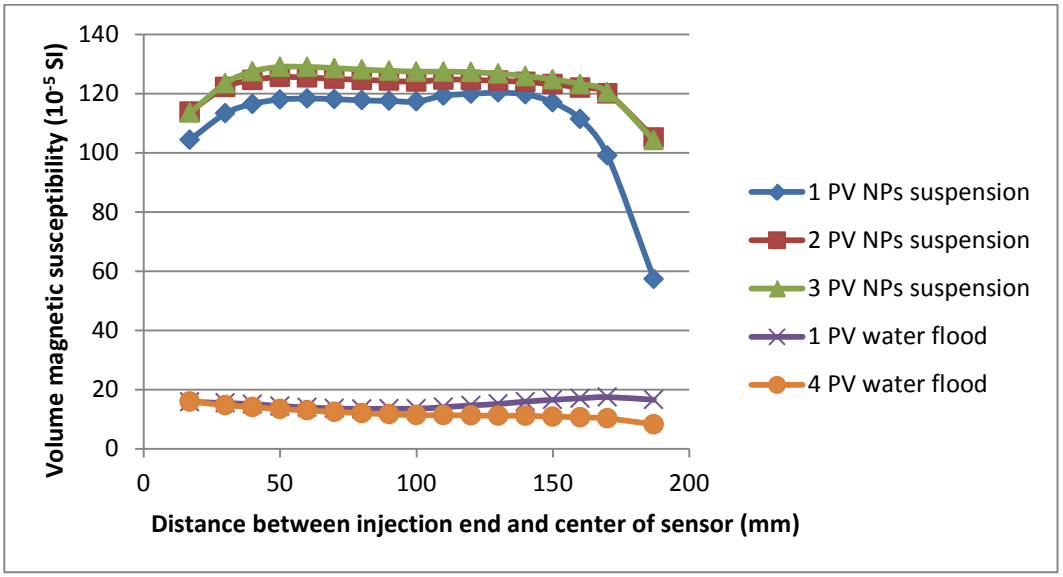

Figure 5-4: Susceptibility Response after different pore volumes injection of Maghemite nanoparticle suspensions and water (Maghemite = 1.0 gm).

Recipe	0.4 gm γ -Fe_2O_3 + 600 ml water + 2 gm DDBS (dispersed then sonicated)		
Injection Rate	20 cc/min	Core Material	Glass beads:170-325 mesh (44-88 μm)
Measured Porosity	0.352	Measured Permeability	2.4 Darcy
Sonication Power	120 watts	Sonication Time	40 minutes

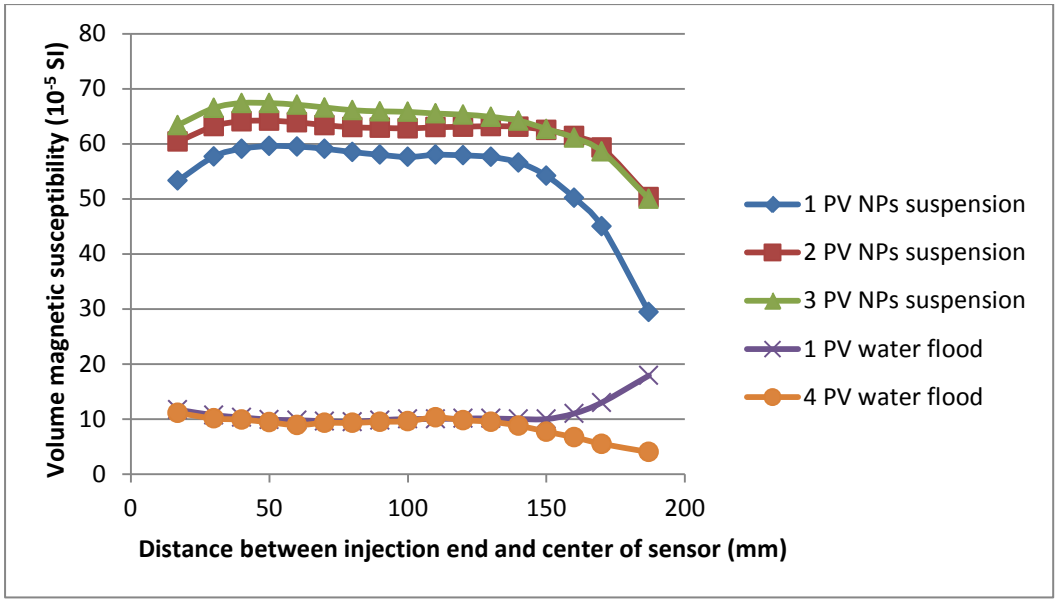

Figure 5-5: Susceptibility Response after different pore volumes injection of Maghemite nanoparticle suspensions and water (Maghemite = 0.4 gm).

In general, figures 5-3, 5-4 and 5-5 all have similar kind of trends wherein almost 85-90% of the susceptibility response is reduced after 4 pore volumes of water flooding. The final susceptibility response after water flooding could be either due to the immobile water that contained NPs which could not be displaced with water flooding or it could be due to particle sticking/ adhesion with the walls of pores.

A common feature in all these plots is the magnetic susceptibility near the end of the flow cell after the water flush. This low susceptibility value may be explained by poor sweeping of the fluid with nanoparticle suspensions, due to geometry of the flow cell and position and size of the exit port.

The difference between these three plots is the separation between susceptibility trends of different PVs injections of nanoparticle suspensions. With increase in nanoparticle concentration the separation is decreased. Higher concentration nanoparticle suspension would enhance the nanoparticle diffusion which might be a reason for close separation between the trends. Furthermore, adding nanoparticles will change the rheology of suspensions too which would lead to better sweep efficiency of the NP suspensions.

5.4 Effect of Injection Rate

Decreasing the injection rate (figures 5-6 to 5-8) showed an increase in the final susceptibility response after water flooding. Variation in the final susceptibility response could be the result of low sweeping efficiency due to low viscous pressure losses.

Recipe	0.4 gm ɣ -Fe_2O_3 + 600 ml water + 2 gm DDBS (dispersed then sonicated)		
Injection Rate	60 cc/min	Core Material	Glass beads:170-325 mesh (44-88 μm)
Measured Porosity	0.352	Measured Perm.	2.25 Darcy
Sonication Power	120 watts	Sonication Time	40 minutes

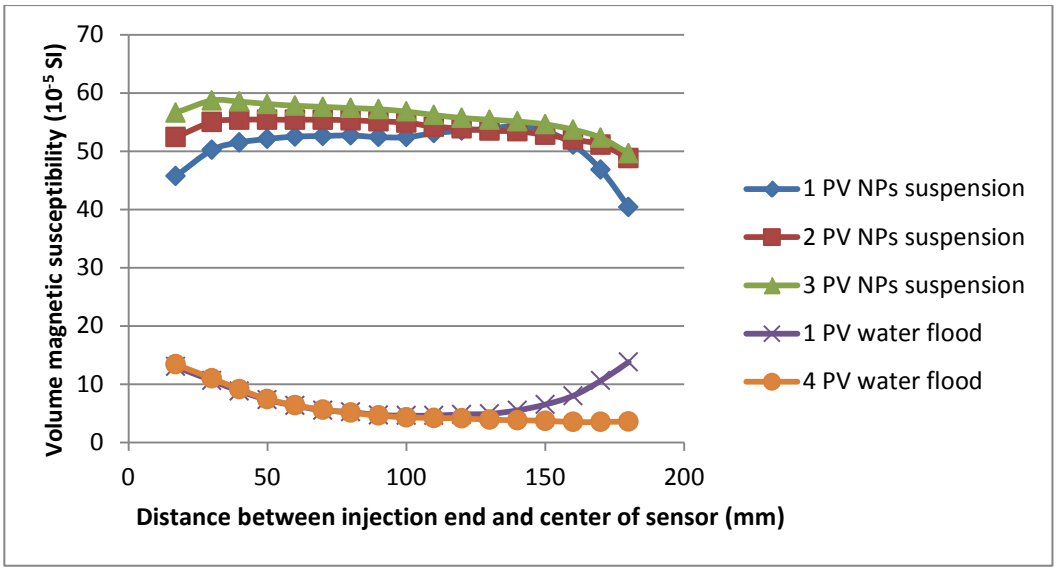

Figure 5-6: Susceptibility Response after different pore volumes injection of Maghemite nanoparticle suspensions and water (Injection rate = 60 cc/min).

In above figure, the susceptibility trends are rising near the injection point after each PV injection of nanoparticle suspension. Reason for that increase is probably the high injection velocity near the injection point due to small area available (1/4" injection port) for fluid flow. The high injection velocity jet effect would provide additional force for collision of dispersed nanoparticles to get in contact with each other and the walls of porous media, thus increasing the chances of nanoparticles adhesion/ retention. The high nanoparticle adhesion near the injection end is also evident from the post flush susceptibility trend, which is higher than in most of the section away from the injection end.

Recipe	0.4 gm γ -Fe_2O_3 + 600 ml water + 2 gm DDBS (dispersed then sonicated)		
Injection Rate	20 cc/min	Core Material	Glass beads: 170-325 mesh (44-88 μm)
Measured Porosity	0.346	Measured Permeability	2.4 Darcy
Sonication Power	120 watts	Sonication Time	40 minutes

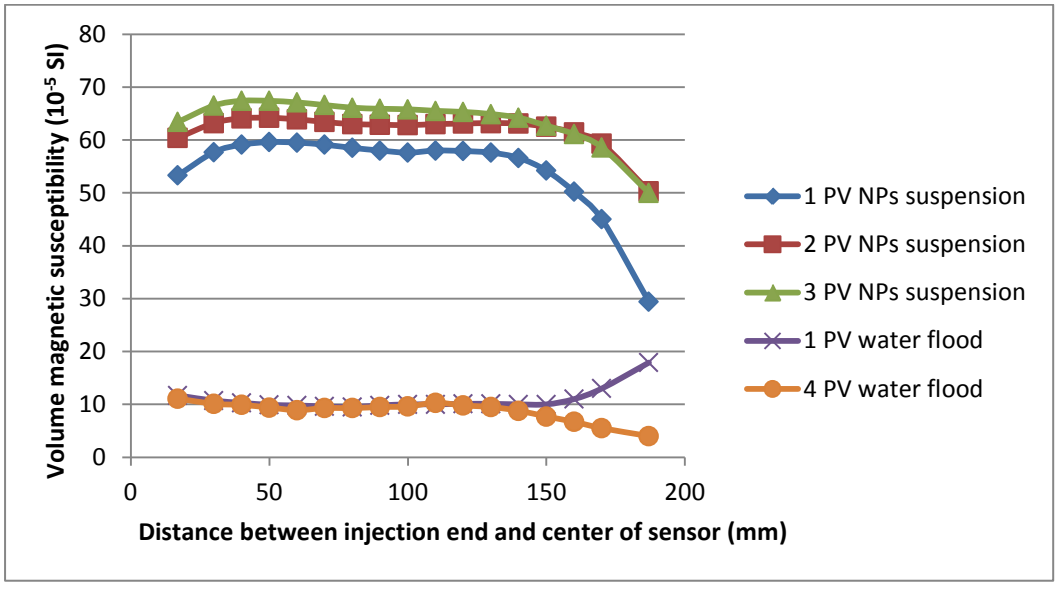

Figure 5-7: Susceptibility Response after different pore volumes injection of Maghemite nanoparticle suspensions and water (Injection rate = 20 cc/min).

In figure 5-7, relative rise near the injection end is less. In fact, an overall rise in susceptibility is a sign of low sweeping efficiency due to relatively lower viscous force. Overall, Post flushing susceptibility response in this case is also lower than seen in higher flow rate injection case (figure 5-6), justifying the lower sweeping phenomena.

Recipe	0.4 gm ɣ -Fe_2O_3 + 600 ml water + 2 gm DDBS (dispersed then sonicated)		
Injection Rate	5 cc/min	Core Material	Glass beads: 170-325 mesh (44-88 μm)
Measured Porosity	0.35	Measured Permeability	2.3 Darcy
Sonication Power	120 watts	Sonication Time	40 minutes

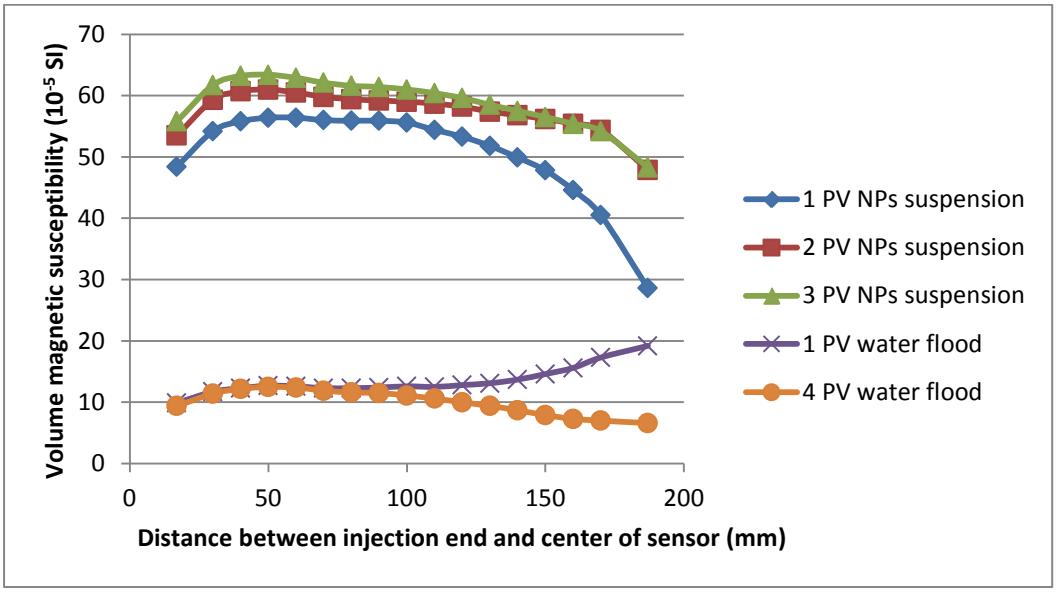

Figure 5-8: Susceptibility response after different pore volumes injection of Maghemite nanoparticle suspensions and water (Injection rate = 5 cc/min).

In above plot, the steeper NP PV injection trends could again be explained with poor sweeping of nanoparticle suspensions at lower rate. The saturation of NP suspensions is higher near the injection end that decreases with distance due to channelling/ breakthrough of these nanoparticle suspensions (i.e. less change in saturation/ susceptibility with distance). The final susceptibility trend is similar to

seen in figure 5-7 except a bump where susceptibility value is higher due corresponding higher saturation of suspension present there. Another reason for higher particle retention could be the longer exposure time of nanoparticle suspensions that might result in increased particle adhesion.

5.5 Effect of Permeability

Increase in permeability resulted in a decrease in final susceptibility response post water flood. A possible cause of lower final suspension stability could be lower specific surface area of high permeability glass beads pack and lower immobile water saturation. Figures 5-9 to 5-11 shows the susceptibility response of lower to higher permeability glass beads packs.

Recipe	0.4 gm γ -Fe_2O_3 + 600 ml water + 2 gm DDBS (dispersed then sonicated)		
Injection Rate	60 cc/min	Core Material	Glass beads:170-325 mesh (44-88 μm)
Measured Porosity	0.34	Measured Permeability	2.25 Darcy
Sonication Power	120 watts	Sonication Time	40 minutes

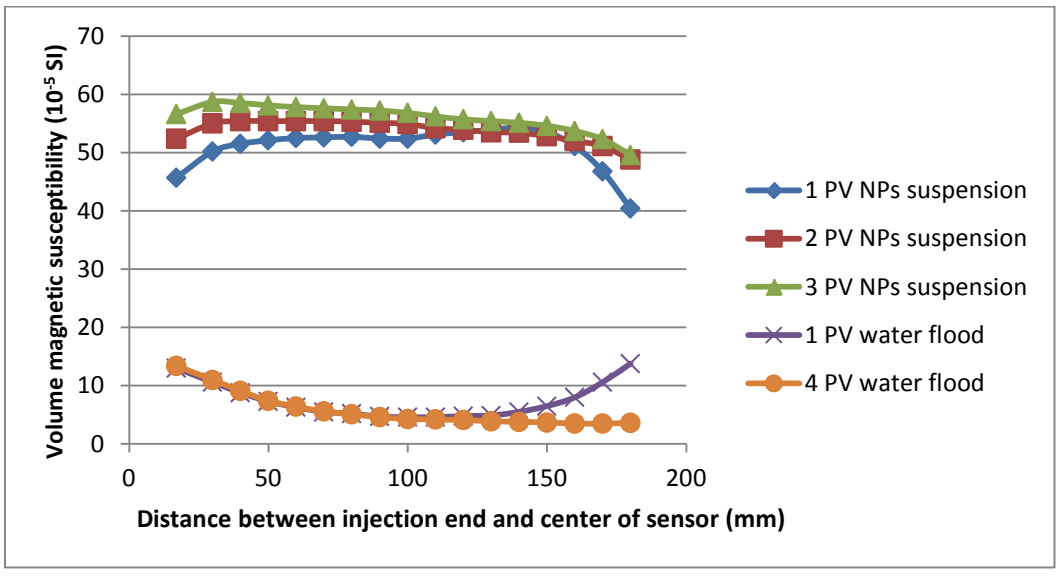

Figure 5-9: Susceptibility response after different pore volumes injection of Maghemite nanoparticle suspensions and water (170-325 mesh glass beads).

Recipe	0.4 gm ɣ -Fe_2O_3 + 600 ml water + 2 gm DDBS (dispersed then sonicated)		
Injection Rate	60 cc/min	Core Material	Glass beads: 100-170 mesh (88-149 μm)
Measured Porosity	0.37	Measured Permeability	6.35 Darcy
Sonication Power	120 watts	Sonication Time	40 minutes

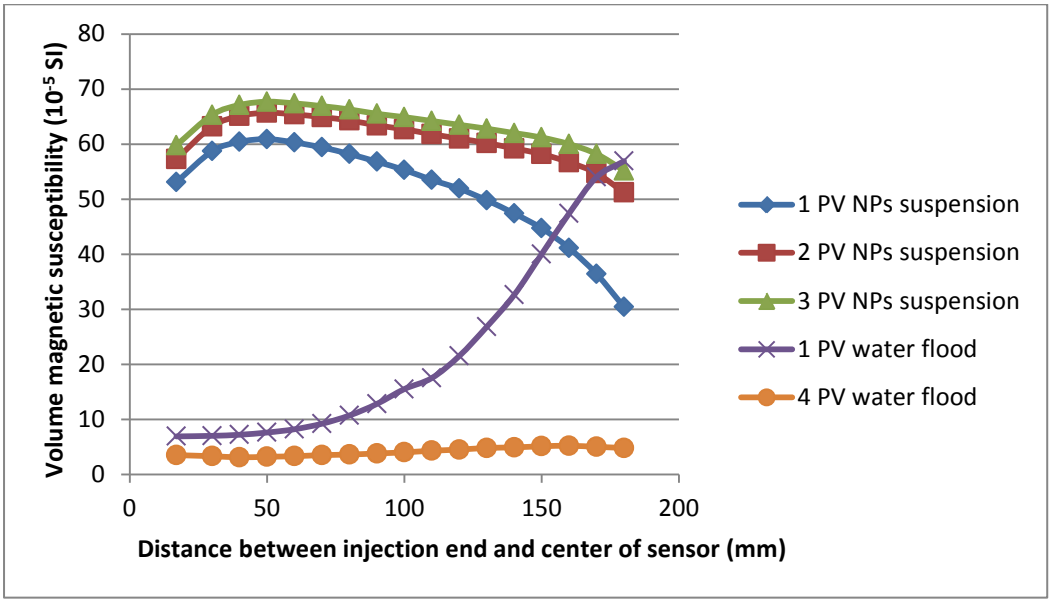

Figure 5-10: Susceptibility response after different pore volumes injection of Maghemite nanoparticle suspensions and water (100-170 mesh glass beads).

Figure 5-10 is showing transport/ retention behaviour of nanoparticles quite different in number of ways from figure 5-9. First of all the final susceptibility trend is almost a straight line with lower susceptibility value, which is due to lower surface area available for nanoparticle adhesion and/ or lower immobile water saturation (because of larger pore sizes and less capillary effects). Secondly, the sweeping effect is less due to lower viscous pressure losses in high permeability/ porosity formation. The poor sweeping effect is evident from the lower susceptibility values after 1 PV injection of nanoparticle suspensions and high susceptibility values after 1 PV injection of de-ionized water, detected near the withdrawal/ production end of the flow cell.

Recipe	0.4 gm ɣ -Fe_2O_3 + 600 ml water + 2 gm DDBS (dispersed then sonicated)		
Injection Rate	60 cc/min	Core Material	Glass beads:40-70 mesh (210-400 μm)
Measured Porosity	0.368	Measured Permeability	22.8 Darcy
Sonication Power	120 watts	Sonication Time	40 minutes

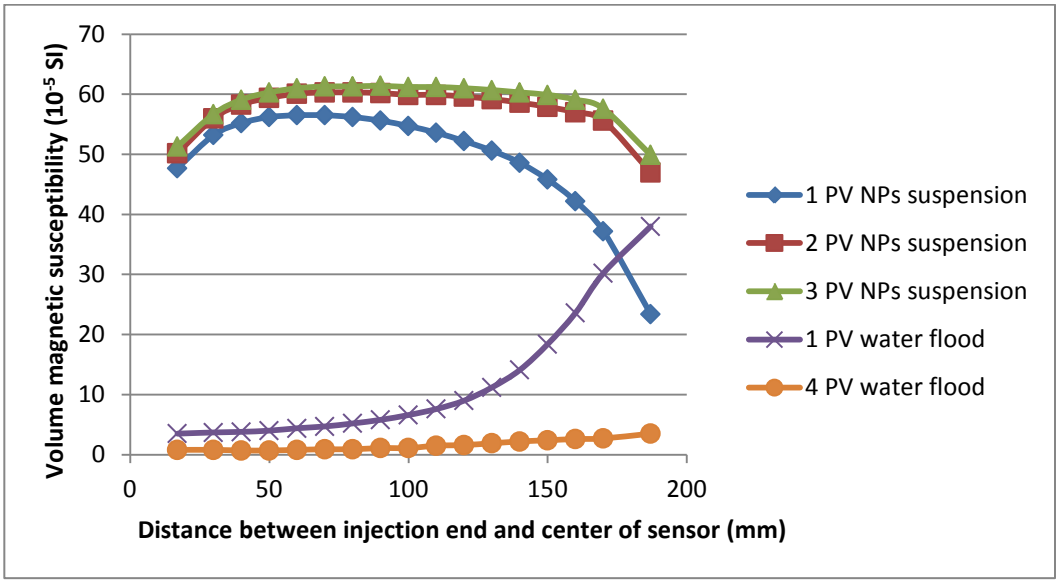

Figure 5-11: Susceptibility response after different pore volumes injection of Maghemite nanoparticle suspensions and water (40-70 mesh glass beads).

Again, the results of this experiment of nanoparticle suspension transport from highest permeability sample compliment the earlier findings of lower retention of nanoparticles after water flood in high permeability porous media. The sweeping efficiency is though decreased due to lower viscous effects at higher injection rates. The particle adsorption effect near inlet end of the flow cell (seen earlier in low permeability, high flow rate case) is not observed in high permeability samples.

Earlier, figure 5-1 showed a severe particle deposition with CTAB containing suspension recipe flow through 170-325 mesh glass beads. Similar suspension

recipe was also flowed through higher permeability glass beads pack to examine whether same level of adhesion is observed or it improved the nanoparticle transport. Figure 5-12 shows that nanoparticles were mobile in higher permeability samples and part of these travelled all the way to the withdrawal/ production end.

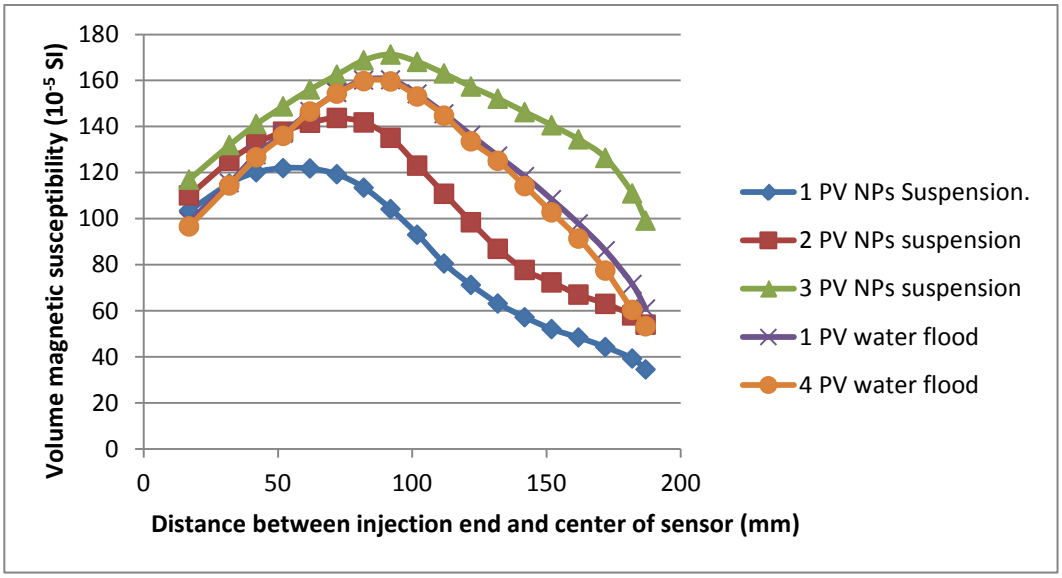

Figure 5-12: Susceptibility response after different pore volumes injection of Maghemite nanoparticle suspensions and water, suspensions sonicated then dispersed (40-70 mesh glass beads).

5.6 Effect of Matrix Type (Sand/ glass beads)

Figures 5-13 & 5-14 show that similar permeability samples exhibited more or less same susceptibility response regardless of any change in matrix type (i.e. sand or glass beads). This may however not be true for all materials because the charge on matrix plays a very important role in adhesion of nanoparticles. Glass beads and sands are both negatively charged and the difference between their surface charges might not be significant to bring any noteworthy affect on the adsorption of nanoparticles.

Recipe	0.4 gm γ -Fe_2O_3 + 600 ml water + 2 gm DDBS (dispersed then sonicated)		
Injection Rate	60 cc/min	Core Material	SIL-4 sand: (250-595 μm)
Measured Porosity	0.367	Measured Permeability	20 Darcy
Sonication Power	120 watts	Sonication Time	40 minutes

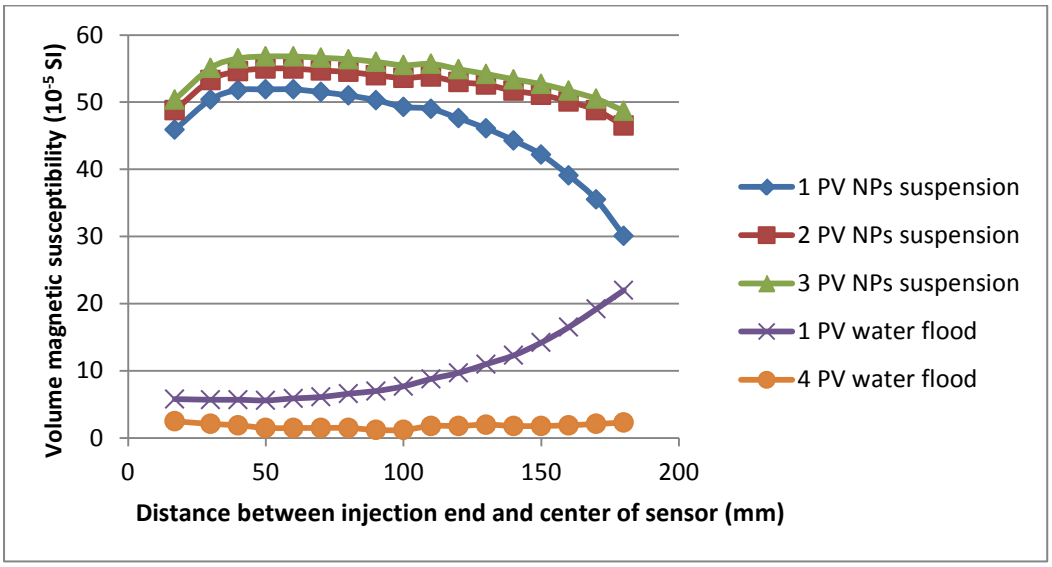

Figure 5-13: Susceptibility response after different pore volumes injection of Maghemite nanoparticle suspensions and water (High permeability sand pack).

Recipe	0.4 gm γ -Fe_2O_3 + 600 ml water + 2 gm DDBS (dispersed then sonicated)		
Injection Rate	60 cc/min	Core Material	Glass beads: 40-70 mesh (210-400 μm)
Measured Porosity	0.368	Measured Permeability	22.8 Darcy
Sonication Power	120 watts	Sonication Time	40 minutes

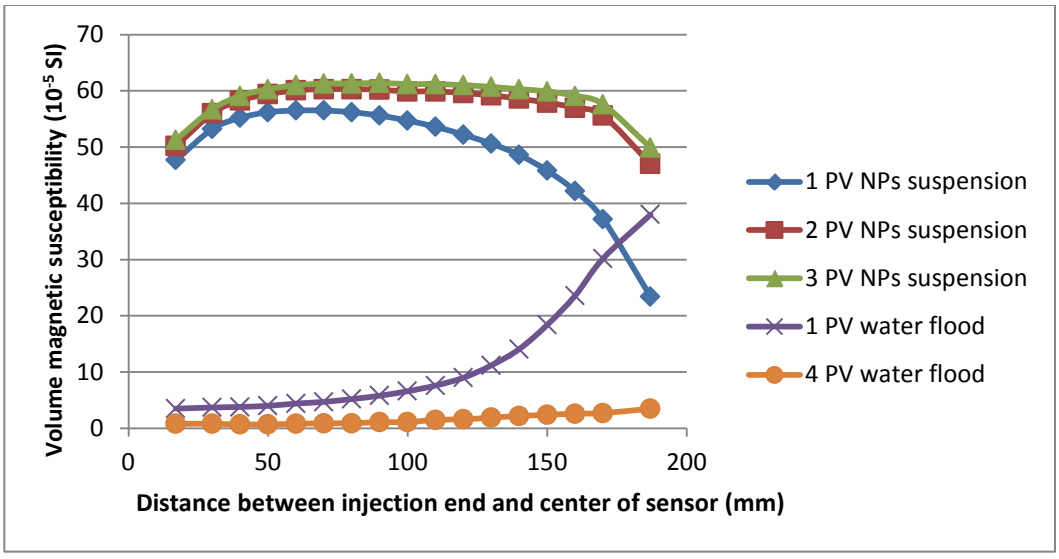

Figure 5-14: Susceptibility response after different pore volumes injection of Maghemite nanoparticle suspensions and water (High permeability glass beads pack).

5.7 Effect of Type of NPs

Figures 5-15 through 5-18 show the susceptibility trends produced from dynamic experiments wherein ɣ -Fe_2O_3, Fe_3O_4, $NiFe_2O_4$ and $CoFe_2O_4$ nanoparticles were used respectively in nanoparticle suspensions. Just like all other experiments, in this set of experiments all parameters/ properties were kept same except one (i.e. type of nanoparticle) was changed. Here figure 5-9 is reproduced as figure 5-15 for comparison purposes with the susceptibility trends of other nanoparticle suspensions.

Recipe	0.4 gm ɣ -Fe_2O_3 + 600 ml water + 2 gm DDBS (dispersed then sonicated)		
Injection Rate	60 cc/min	Core Material	Glass beads: 170-325 mesh (44-88 μm)
Measured Porosity	0.352	Measured Permeability	2.25 Darcy
Sonication Power	120 watts	Sonication Time	40 minutes

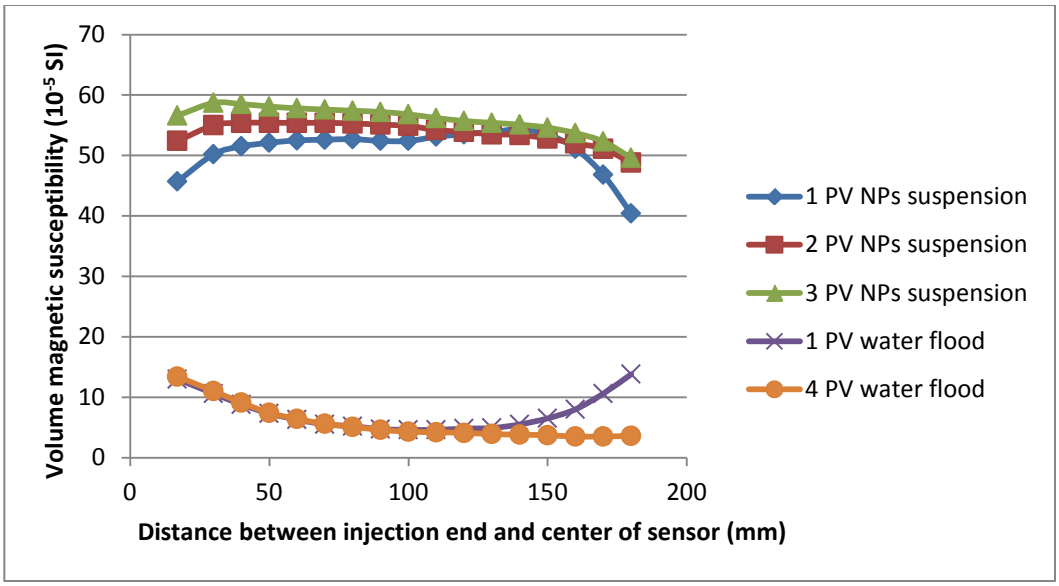

Figure 5-15: Susceptibility response after different pore volumes injection of Maghemite (ɣ -Fe_2O_3) nanoparticle suspensions and water.

ɣ -Fe_2O_3 (Maghemite) happened to exhibit better result than any other nanoparticle suspension recipe in terms of drop in susceptibility response after water flooding, which is quite understandable because most of the suspension stability experiments were performed using ɣ -Fe_2O_3 NPs and the recipe has been customized to give better results for those particular NPs. Detailed suspension stability studies on other NPs might give a recipe which produces even better results than ɣ -Fe_2O_3 based nanoparticle suspensions.

Recipe	0.4 gm Fe_3O_4 + 600 ml water + 2 gm DDBS (dispersed then sonicated)		
Injection Rate	60 cc/min	Core Material	Glass beads: 170-325 mesh (44-88 μm)
Measured Porosity	0.352	Measured Permeability	2.5 Darcy
Sonication Power	120 watts	Sonication Time	40 minutes

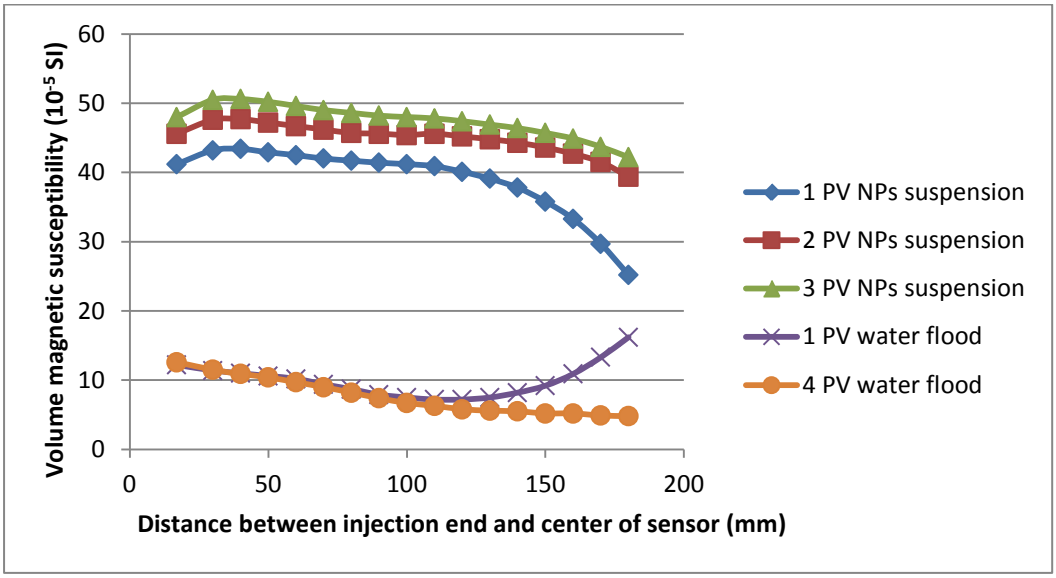

Figure 5-16: Susceptibility response after different pore volumes injection of Magnetite (Fe_3O_4) nanoparticle suspensions and water.

The slopping trend of figure 5-16 is due to higher retention/ deposition of nanoparticles near injection end. Also the overall particle retention after water flooding is slightly higher than observed in figure 5-15, even though the Maghemite posses higher magnetic susceptibility.

Recipe	0.4 gm $NiFe_2O_4$ + 600 ml water + 2 gm DDBS (dispersed then sonicated)		
Injection Rate	60 cc/min	Core Material	Glass beads: 170-325 mesh (44-88 μm)
Measured Porosity	0.35	Measured Permeability	2.43 Darcy
Sonication Power	120 watts	Sonication Time	40 minutes

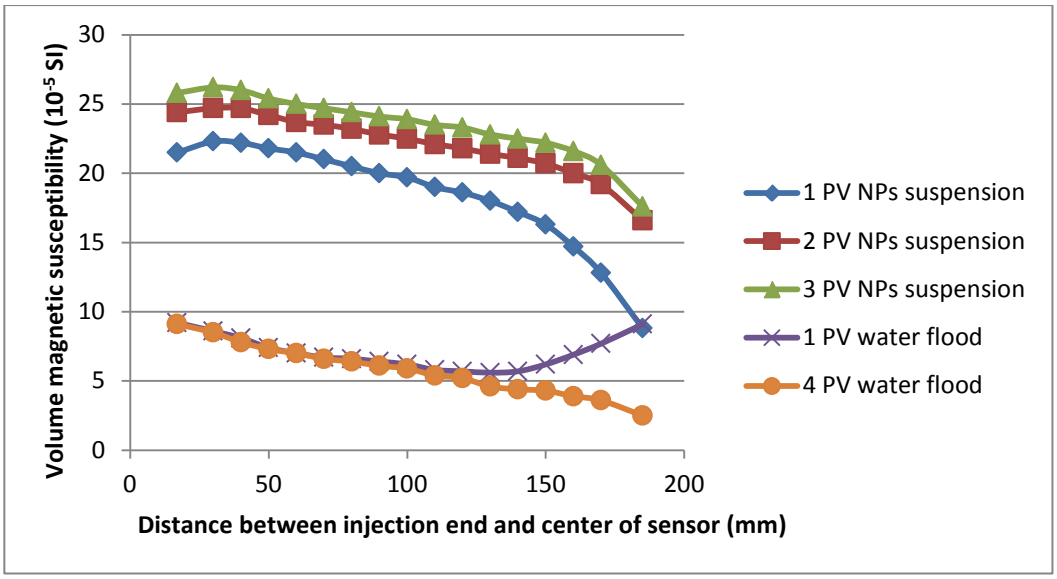

Figure 5-17: Susceptibility response after different pore volumes injection of Nickel Iron Oxide ($NiFe_2O_4$) nanoparticle suspensions and water.

The nanoparticle sticking/ adhesion seem to be highest in $NiFe_2O_4$ suspensions than in any other sample. Possible reasons for high sticking/ retention would be poor inter-particle repulsion, which results in particle aggregation, adhesion and settlement.

Recipe	0.4 gm $CoFe_2O_4$ + 600 ml water + 2 gm DDBS (dispersed then sonicated)		
Injection Rate	60 cc/min	Core Material	Glass beads: 170-325 mesh (44-88 μm)
Measured Porosity	0.35	Measured Permeability	2.48 Darcy
Sonication Power	120 watts	Sonication Time	40 minutes

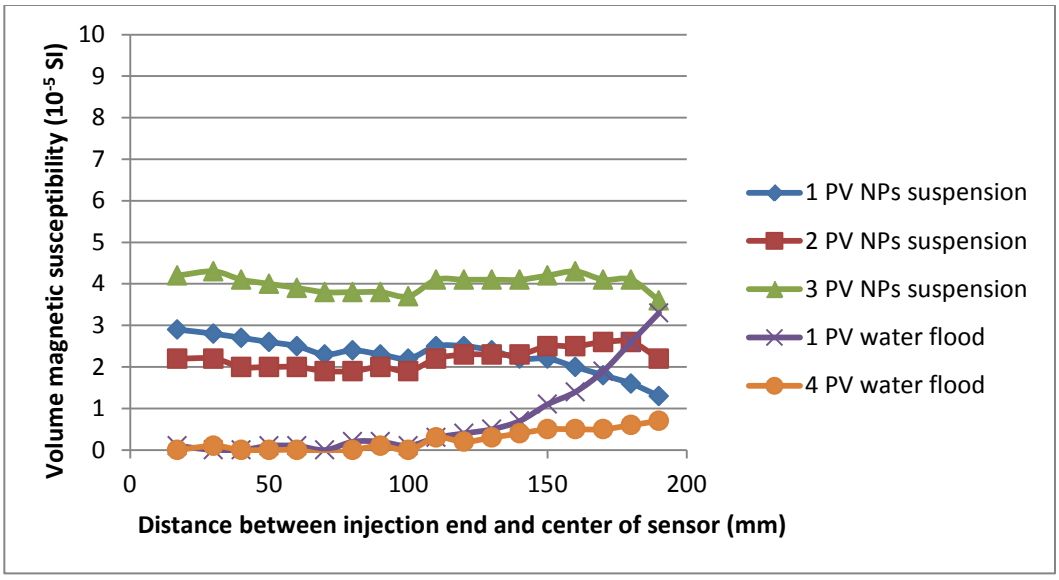

Figure 5-18: Susceptibility response after different pore volumes injection of Cobalt Iron Oxide ($CoFe_2O_4$) nanoparticle suspensions and water.

The cobalt iron oxide nanoparticles did not provide stable suspensions when CTAB was used as dispersant (mentioned in previous chapter), but these exhibited better suspension when DDBS surfactant was tried as dispersant. However, due to very poor magnetic susceptibility response cobalt iron oxide nanoparticles may not be suitable for use in static and dynamic experiments due to their poor susceptibility response.

5.8 Effect of Ionic Strength

One experiment using tap water with 0.3% by weight of CTAB was used in transport experiment to see the effect of CTAB based water and higher ionic strength. The ultimate particle retention was still lower and in fact relatively less than seen in de-ionized based water flood experiments. Lower ultimate retention could be due to relatively higher permeability of glass bead pack. Only obvious difference between ionized water based experiment (Figure 5-19) and de-ionized based experiments (Figure 5-3) is the lower susceptibility response. This means high ionic concentration results in bigger agglomerate size and contributes towards reduction of stability of suspensions. Further experiments with different

ionic strengths of ionized water need to be done for detailed investigation of dependence of optimum dispersant concentration and sonication requirement on ionic strength of the ionized water.

Recipe	3.0 gm ɣ -Fe_2O_3 + 600 ml water + 2 gm DDBS (dispersed then sonicated)		
Injection Rate	20 cc/min	Core Material	Glass beads: 170-325 mesh (44-88 μm)
Measured Porosity	0.342	Measured Permeability	2.48 Darcy
Sonication Power	120 watts	Sonication Time	40 minutes

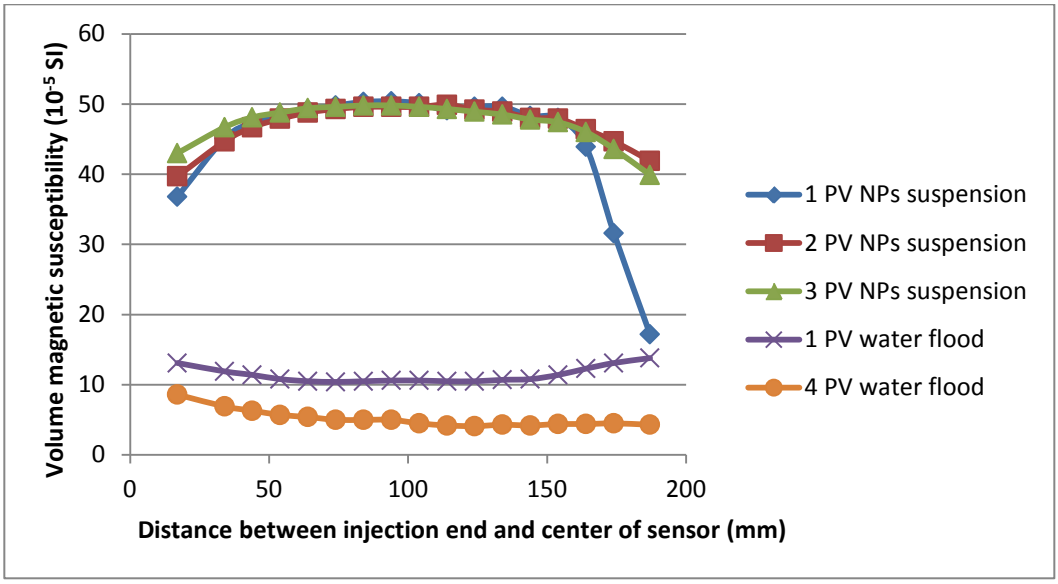

Figure 5-19: Susceptibility response after different pore volumes injection of Maghemite nanoparticle suspensions and CTAB based ionized water.

6 THEORETICAL DISCUSSION ON APPLICATION OF MAGNETIC TECHNIQUE IN FRACTURE DIAGNOSTICS AND DOWNHOLE MONITORING OF TRANSPORT OF NANOPARTICLES

Due to unavailability of high pressure experimental set up for fracturing and tool unavailability to measure susceptibility response at the face of core sample, simulating bore hole conditions for hydraulic fracturing or fluid invasion study were not possible. Therefore, in this section only theoretical discussion on how susceptibility response can be used to monitor the downhole transport of nanoparticles, interpret the fracture dimensions/ orientation and its potential use in other applications is described. Expected response behaviour is presented with different set of assumptions considered.

Susceptibility response during hydraulic fracturing with high susceptibility proppants is analogous to nanoparticle traced fluid invasion within the volume of investigation of susceptibility tool. The only difference would be that in hydraulic fracturing, fracture porosity will be a function of susceptibility response as against effective porosity during fluid invasion.

6.1 Applications of Magnetic Susceptibility Technique

Magnetic susceptibility technique has been used in identification/ detection of minerals, well to well and within well depth correlations apart from many other medical applications. Whalen (1954) used magnetic susceptibility technique in determination of fluid saturation during steady state relative permeability experiments. He used high concentration of paramagnetic salt to increase the susceptibility contrast between the two fluids used in the experiments.

Broding et. al (1952) used induction based well logging tool with an electric bridge to measure the insitu downhole magnetic susceptibility and related it with measured permeability. Broding et. al (1952) also showed that the susceptibility response is more affected by the material close to sensor. They (Broding et. al,

1952) also demonstrated that the depth of investigation of magnetic susceptibility sensing tool is directly related to length of the sensor. 90% of the maximum susceptibility reading was achieved for depth of investigation of 1 solenoid length.

It was discussed in chapter 4 that MS2C sensor response is also a function of distribution of magnetic material. The magnetic susceptibility response is more affected by the material close to the sensor. If the tool response function is established, the susceptibility response could be interpreted to estimate the content of known high susceptibility material. This relationship of high susceptibility material and measured susceptibility response may be used;

a) To estimate the fracture geometry (fracture height, width & azimuth) when ferromagnetic/ super paramagnetic particles are used in proppants.
b) To estimate permeability anisotropy around and along the length of the borehole.
c) To estimate porosity, if no particle accumulation is taking place due to adhesion or bridging and when the injected fluid has completely displaced the formation fluid.
d) To monitor the downhole transport of fluids and solids (e.g. particle bridging/ sticking etc.) through various formations.

6.1.1 **Estimating Fracture Height and Width**

The nanoparticle coated proppants can be sensed with change in downhole magnetic susceptibility. The response (change in susceptibility) shall be a function of the nanoparticle characteristics, the concentration of nanoparticles, the fracture dimensions, lateral distribution of proppants, proppants inside the borehole, the volume of investigation of susceptibility tool and up to some extent by the fracturing fluid and the formation characteristics. If the volume of investigation, the magnetic characteristics of injection fluid and the calibration chart for conversion of uniformly distributed concentration of nano materials is known,

fracture dimension estimates can be made. With an assumption that proppants are uniformly distributed inside the fracture volume, the susceptibility variation shall provide the fracture height and fracture width estimates. Figure 6-1 is a schematic of tools sensing and the expected theoretical response of high susceptibility nanoparticle coated proppants in a fracture.

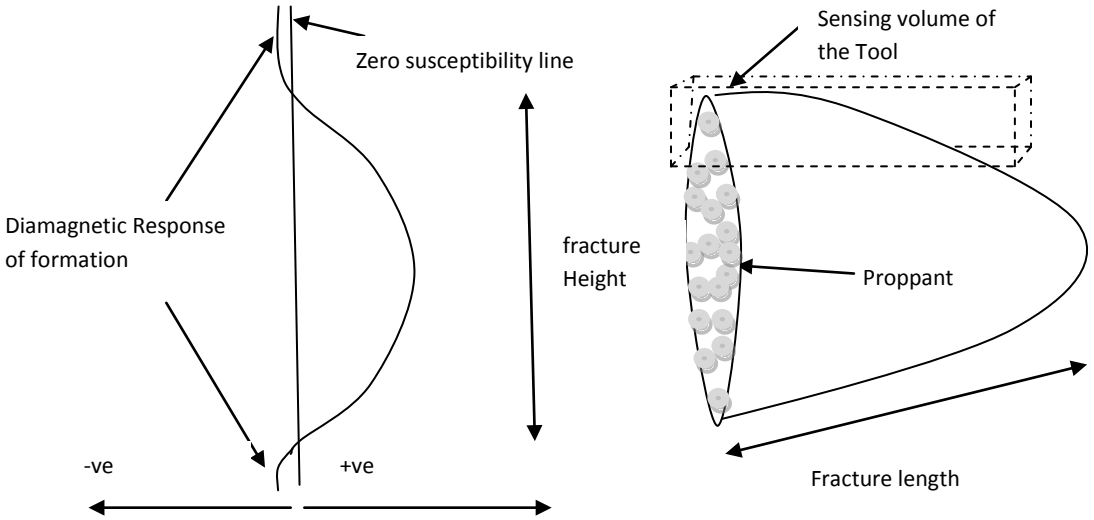

Figure 6-1: Schematic of magnetic sensing in fracture diagnostic.

The rock matrix in the above case is assumed to be diamagnetic in nature, however it can be slightly paramagnetic too, but the overall susceptibility response, in the absence of ferromagnetic/ super paramagnetic particles, shall remain close to the zero susceptibility line. The moment fracture volume (containing ferromagnetic/ paramagnetic material coated proppants) comes into range of ”volume of investigation” of the susceptibility measuring tool, a sudden increase in susceptibility response should be observed. The response shall depend on the volume of fracture within the “volume of investigation” of the tool. This information can be further interpreted to make an estimate of fracture width. Furthermore, if the tool is capable of sensing considerably deep into the formation, an estimate of fracture dip can also be made.

6.1.2 **Determining the Fracture Azimuth**

Fracture azimuth may also be estimated, if the tool is capable of seeing only in a particular direction (as shown by Figure 6-2). By rotating the sensor (360^{o}) within the borehole, direction of fracture (fracture azimuth) and type of fracture (Horizontal/ Vertical) may be established.

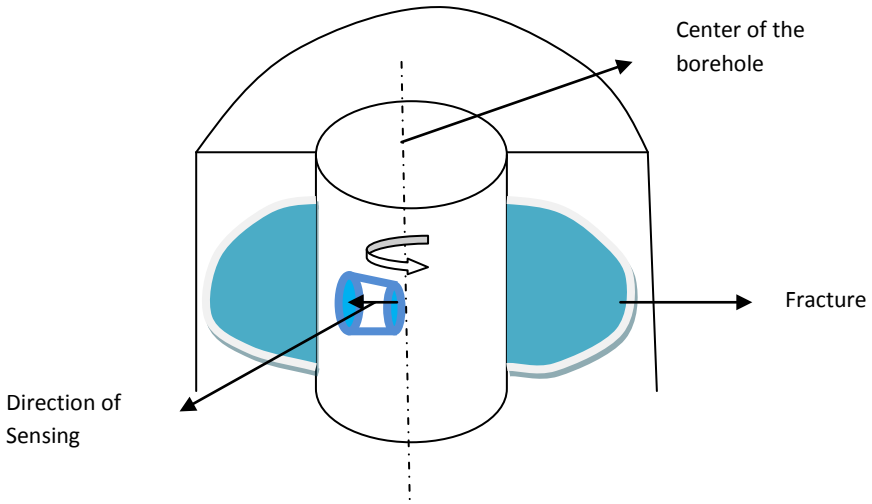

Figure 6-2: Schematic of downhole measurement of the fracture azimuth.

The expected response of 1 dimensional susceptibility measuring tool is presented in figure 6-3.

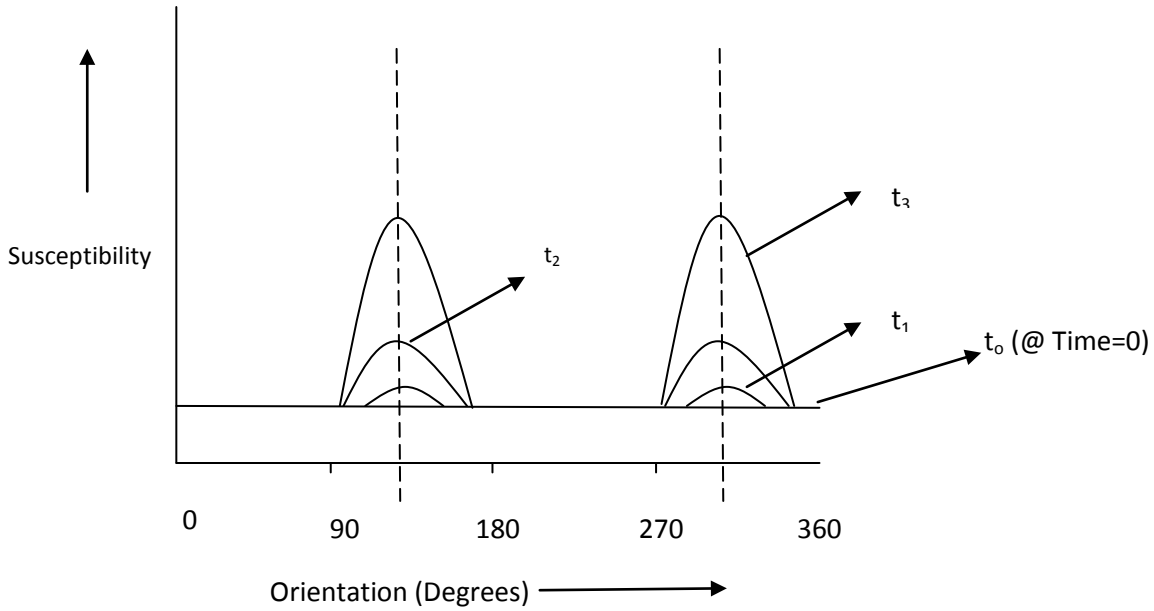

Figure 6-3: Schematic of expected susceptibility response around the bore hole during fracturing with 1D measurement.

The apex in the Figure 6-3 shows the susceptibility response at different angles around the borehole and thus provide fracture azimuth. As time passes, volume of fracture inside the volume of investigation of the susceptibility measuring tool increases. t_o represents time before the initiation of fracture. The susceptibility response at that point will be more or less the same around the borehole (assuming homogeneous matrix composition). However, in real case scenario fluctuations may be observed due to porosity/permeability variations. Here $t_3>t_2>t_1>t_o$.

If the tool is not designed to see in a particular direction and covers whole 360^o for a single measurement, azimuth of the fracture may be assessed by offsetting the sensor from center of the borehole and taking measurements by rotating it inside the borehole. Offsetting the tool from center shall generate similar response to figure 6-3, except that the magnitude of susceptibilities around the borehole will be different and that large susceptibility contrasts may not be observed. Schematic for such a case is presented in figure 6-4.

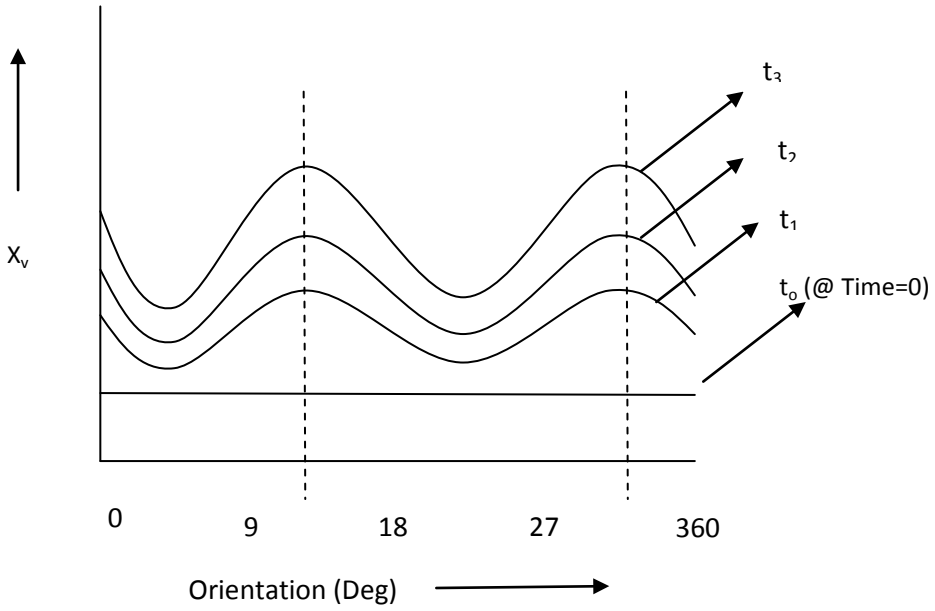

Figure 6-4: Expected susceptibility response during fracturing with 360^o scanning tool.

Again the apex of the curves gives us an indication of fracture azimuth. Angles/ Orientation is assigned arbitrarily and can be set with respect to magnetic or true north.

6.1.3 Comparison of Magnetic Susceptibility Technique with Radioactive Tracer Technique

The radioactive tracer technique has been widely used as a near well bore fracture diagnostic technique to estimate fracture height, fracture width and in some cases fracture azimuth. The main advantage of using this technique is that it can estimate the fracture width behind the casing. Limitation of this technique is that it gives the lower bound of fracture height when the fracture is not perfectly aligned to the borehole wall. The radioactive tracer technique can only see 1 to 2 feet into the formation and thus does not identify the fracture near the end when fracture is making some angle with the borehole wall.

The radioactive tracer technique involves safety risk due to handling of radioactive material which can be avoided if magnetic susceptibility technique is proved as a suitable near well fracture diagnostic technique. Furthermore, by

increasing the depth of investigation of susceptibility tool better estimates of fracture height and fracture dip may be made. A unique advantage of this technique would be that fracture diagnostic could be performed any time during the life of the well to monitor any changes in the direction and dimensions of the fracture. Main limitation of this technique is that it would not be useful for fracture diagnostics in a cased hole environment, since the casing material in most cases is ferromagnetic and therefore the susceptibility contrast before and after fracturing operation may not be observed.

6.1.4 **Measuring Permeability Anisotropy**

Formations may have permeability anisotropy due to different in situ horizontal stresses. This permeability anisotropy may be determined from nanoparticle injection into the formation. This technique would not only help in determining the severity of permeability anisotropy but may also used in establishing the direction of major and minor horizontal stresses. Lower permeability formations will have higher nanoparticle retention and therefore would show higher magnetic susceptibility response. Thus susceptibility contrast around and along the length of bore hole may give an idea about permeability variation in three dimensions.

6.1.5 **Porosity Estimation and Porosity Profile Determination**

Complete invasion of traced fluid into a formation, where no particle accumulation is taking place due to adhesion or bridging and no other phenomena are affecting the susceptibility response, can provide us porosity estimate of that formation. This porosity estimate can be slightly lower than actual effective porosity due to presence of residual fluid saturation. However, it still can be useful in providing lower bound for effective porosity or porosity for mobile fluids. In laboratory studies, 100% saturating the core sample with traced fluid can give the average total porosity estimate. If measurements are taken along the length of core sample, porosity profiles are generated that can tell about the homogeneity of core.

6.2 Numerical Simulation for Expected Susceptibility Response

Numerical simulation is performed with different set of assumptions. These assumptions may not all be true, therefore predicted susceptibility response could be different than measured. Some of the plots (i.e. results of numerical simulation) are constructed with an assumption of uniform applied magnetic field within the volume of investigation of the tool. In other words, in these plots tool response function is not considered and it is assumed that the response of the magnetic susceptibility measuring tool would be unaffected by the distance of the material from sensor. The plots from numerical simulation are presented for the purpose of understanding the effect of different parameters and properties, so that when actual response is measured it could be easily interpreted.

6.2.1 **Factors Affecting Magnetic Susceptibility Response**

Following information is essentially needed before for proper interpretation of susceptibility response before performing experiments.

- Volume of investigation of susceptibility tool
- Correction factors due to surrounding environment
- Susceptibility characteristics of injection fluid, formation fluid and nanoparticles
- Effect of lateral distribution of the nanoparticles on susceptibility response
- Injection rates
- Nanoparticle adhesion/ sticking rate in formation/rock matrix
- Diffusion rate of nanoparticles

6.2.2 **Common Assumptions and Data**

Common assumptions used in developing all the susceptibility plots are:

- Injected fluid completely displaces the formation fluid (i.e. 100% sweep efficiency).
- No or negligible diffusion of solid particles into the displaced fluid.

The data used for constructing these various plots is shown in Table 6-1.

Table 6-1: Data used for constructing theoretical model response

Mineral/Fluid	**Volume Magnetic Susceptibility x 10^{-08} SI Units**
Quartz	-1,636
Calcite	-1,311
Dolomite	-1,369
Illite	41,250
Kaolinite	-1,683
Magnetite (Fe_3O_4)	258,500,000
Iron Oxide (Fe_2O_3)	23,613,015
Formation Fluid (water)	-900
Injected Fluid (water)	-900

The volume magnetic susceptibility values in of quartz, calcilte, dolomite, illite, kaolinite and water are calculated from mass magnetic susceptibility data presented by Ivakhnenko and Potter (2004), by multiplying with corresponding density. Magnetite volume magnetic susceptibility is calculated by taking an arbitrary value from the reported range of mass magnetic susceptibility (Ivakhnenko and Potter, 2004). Whereas, the magnetic susceptibility value of Fe_2O_3 is taken from "Reade Advanced materials" material specification data.

6.2.3 **Effect of Porosity Change**

Increase in sample's total volume susceptibility with increase in pore volume injected and increase in porosity is observed in Figure 6-5. "Tools Response Function" is not considered in Figures 6-5 through 6-8. Total volume susceptibility response is obtained using following relationship.

$$X_{VT} = \sum_{i=1}^{n} X_{vi} f_i \qquad (6\text{-}1)$$

Where,

X_{VT} = Total volume susceptibility within volume of investigation of tool

X_{vi} = Volume susceptibility of i component

f_i = Volume fraction of i component

The typical response of “no bridging/ sticking” would be trends going flat, after all the formation fluid are displaced by injected fluid. In such case, any sensor looking just at any slice of the formation/ core will show same susceptibility value.

Other Considerations & Parameters:

- No particle adhesion/ bridging
- Magnetite concentration, 2% by volume in injected fluid
- Rock matrix: 100% Quartz.

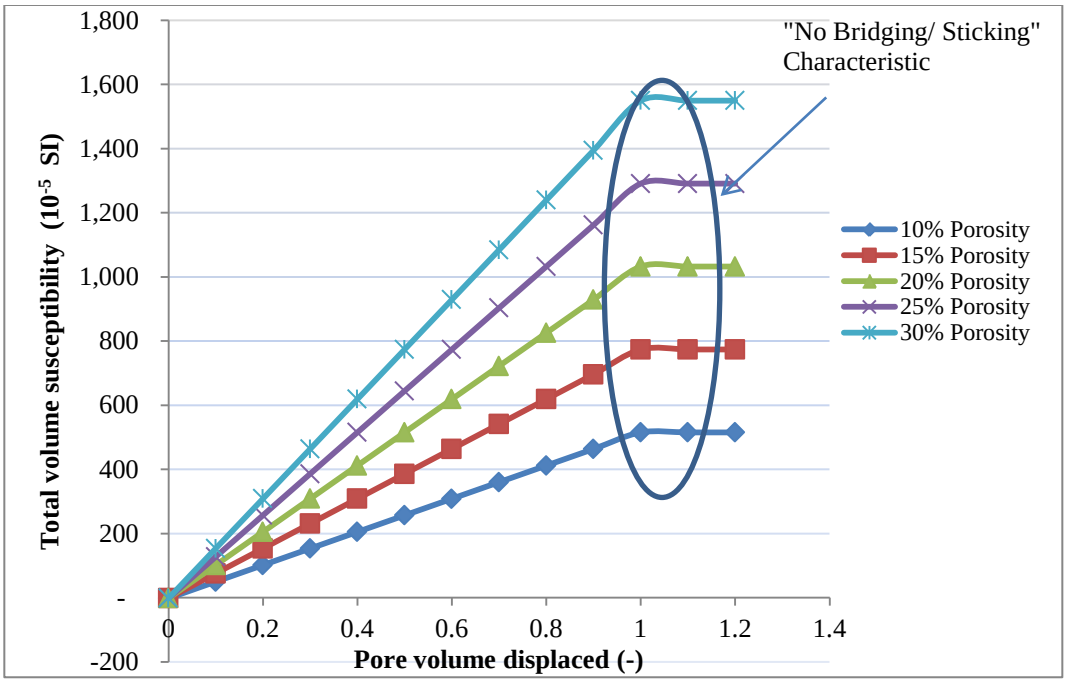

Figure 6-5: Volume magnetic susceptibility response for different formation porosities.

As the porosity increases, the magnetic susceptibility measurements also increase. The susceptibility trends keep on rising till all the formation fluid is completely displaced by high susceptibility injection fluid. Once all the formation fluid is displaced, the susceptibility trend goes flat provided no particle accumulation (due to bridging or adhesion) is taking place.

6.2.4 Effect of Change in Matrix Composition

Figure 6-6 shows that change in rock matrix does not affect much on the total magnetic susceptibility response. The data points are almost overlapping each other. This is mainly due to very high susceptibility contrast between nanoparticles and rock matrix. However, if very low concentration of solid ferromagnetic particles or relatively low susceptibility solid particles is used then the matrix composition can have a profound effect.

Other Considerations & Parameters:

- No particle adhesion/ bridging
- Magnetite concentration, 2% by volume in injected fluid
- Porosity: 15%

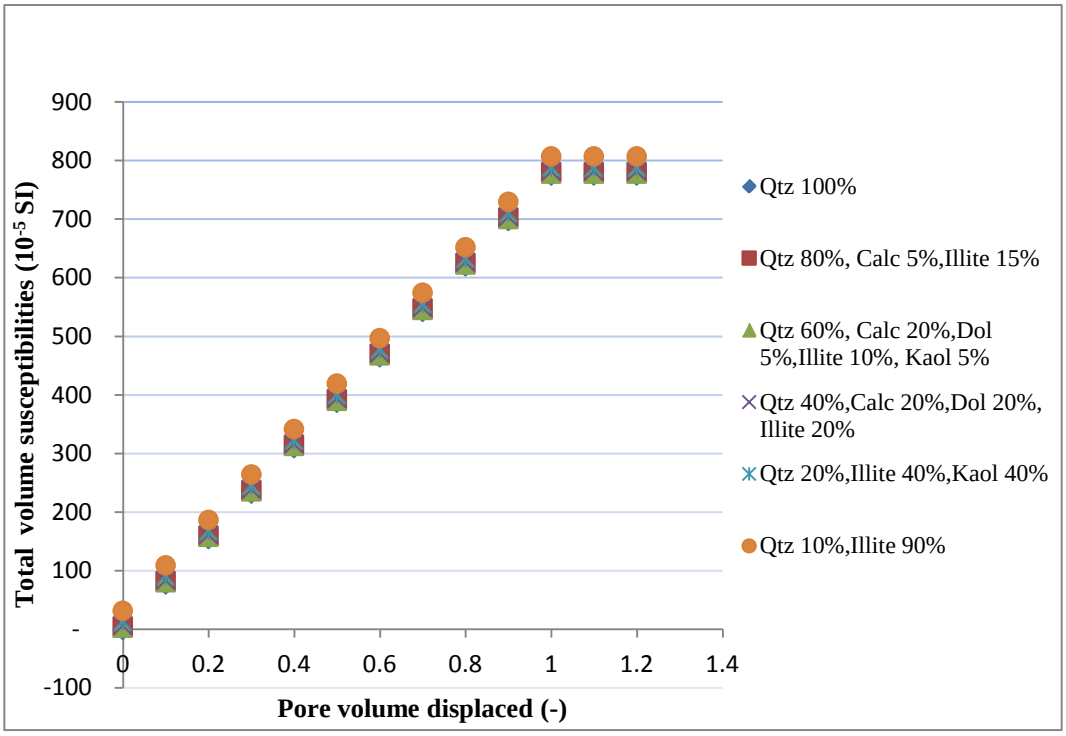

Figure 6-6: Volume magnetic susceptibility response with different formation composition.

6.2.5 Effect of Concentration and Type of Nanoparticles

Figures 6-7 and 6-8 show volume magnetic susceptibility responses of different volumes of nanoparticle suspensions having different type and concentration of nanoparticles in it. High susceptibility ferromagnetic or super paramagnetic nanoparticles require less concentration by volume in injected fluid to achieve a good susceptibility response. It can be seen that 1% magnetite is giving higher response than 10% ferrite (Fe_2O_3). In chapter 4, it was shown that less concentration of ferromagnetic particles demonstrate less aggregation and higher stability. A compromise should be made between the concentration and type of

ferromagnetic particle based on the objectivity of particle injection. For example, in case, where it is intended to form bridging, relatively higher concentration of ferromagnetic particles may be desired.

Other Considerations & Parameters:

- No particle adhesion/ bridging
- Porosity: 15%
- Rock matrix: 100% Quartz

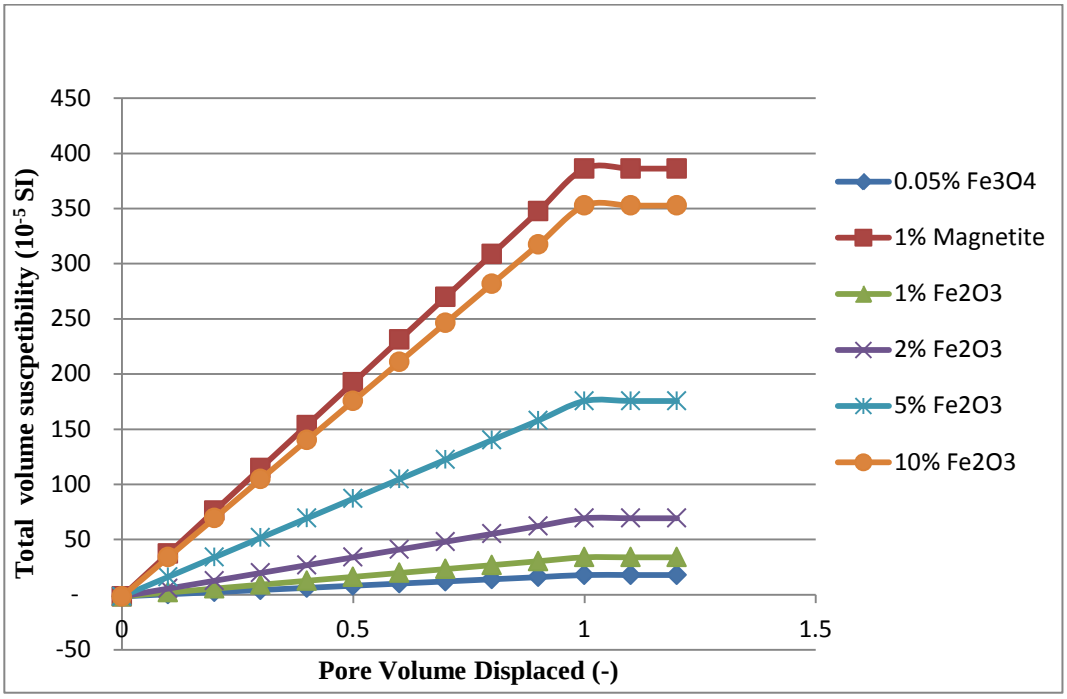

Figure 6-7: Volume magnetic susceptibility response with various type and concentrations of ferromagnetic nanoparticles.

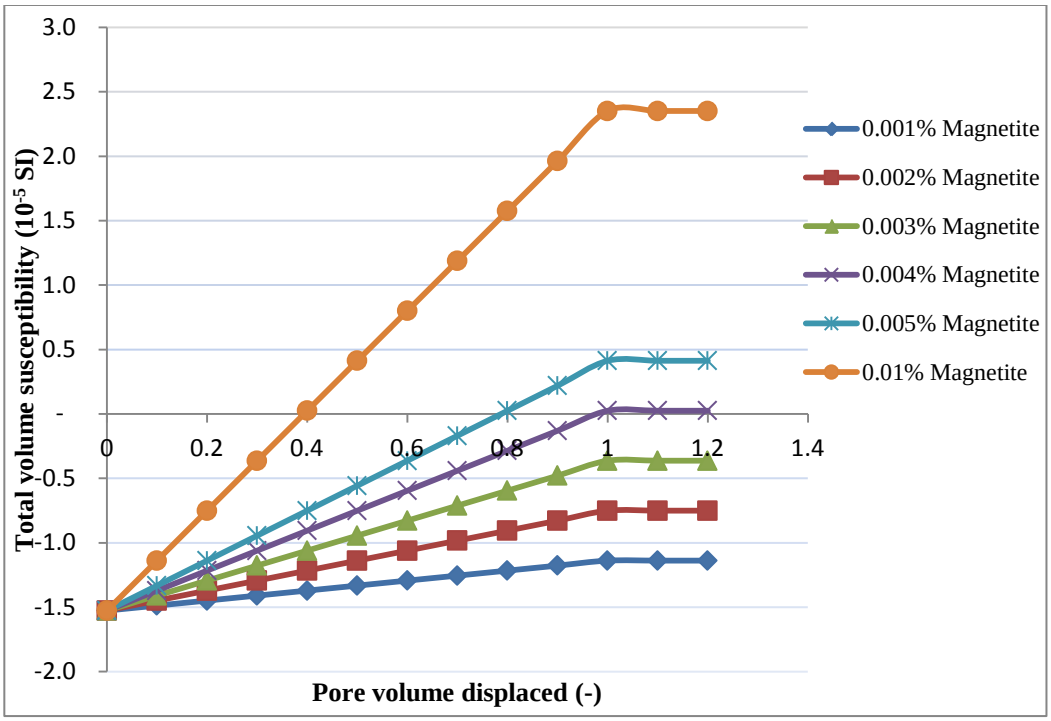

Figure 6-8: Volume magnetic susceptibility response with different concentrations of Magnetite nanoparticles.

As discussed earlier, the material closer to the downhole induction based tool (sensing element) has a larger contribution to the total susceptibility response. This implies that the nonlinear susceptibility response with the depth of investigation would be one of the concerns that need to be addressed in order to get a good estimate the ferromagnetic content from magnetic susceptibility readings. All above plots are generated by ignoring this factor and it was assumed that the material away from the susceptibility measuring tool will have the same affect on susceptibility response as the material close to the sensor.

Figure 6-9 is developed by considering a tool response function of $2R-R^2$, R (R=x/depth of Investigation of tool) being the distance fraction of depth of investigation. Shape of the curve depends and will vary based on the experimentally determined tool response function.

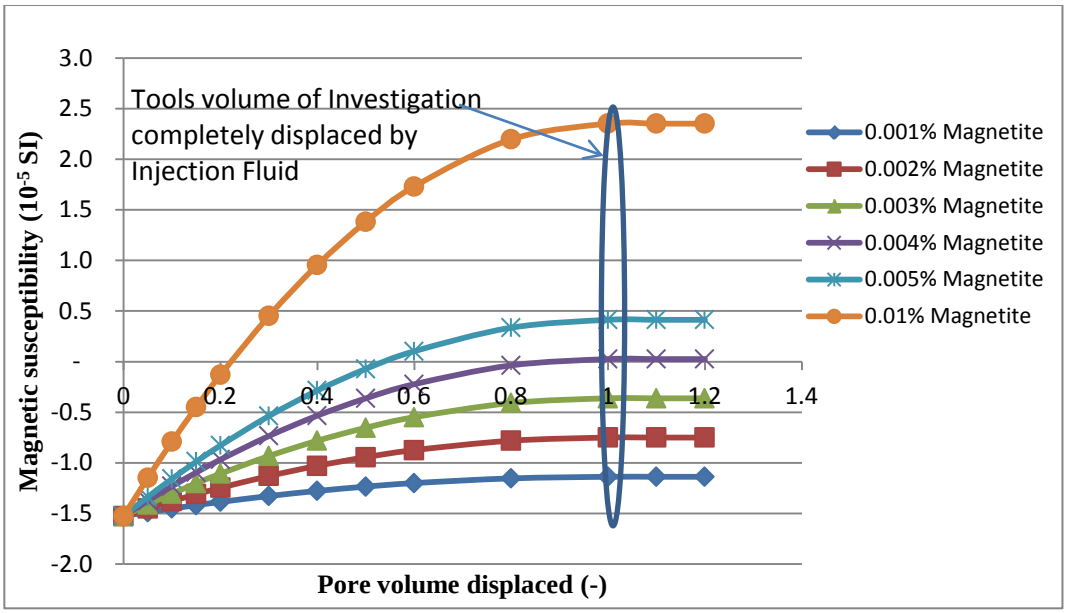

Figure 6-9: Volume susceptibility response measured at the face of core plug holder with different solid particle concentration.

Figure 6-9 has curved trends unlike linear trends seen in figure 6-8. Concaving down trends depicts that material/ fluid close to sensor is affecting more on susceptibility response. However, in the absence of adhesion or bridging, ultimately these trends go horizontally flat after all the formation fluid is displaced by injected fluid.

6.2.6 **Effect of Particle Sticking**

In figure 6-9, change in one rising trend to another indicate the particle accumulation due to sticking or bridging phenomena, in contrast to the horizontal trend of "no bridging/ sticking". Higher slopes of curves are indicative of higher particle sticking rate. Particle sticking and agglomeration can be avoided by treating the nanoparticles with appropriate method of suspension preparation such as sonication, dispersion etc.

Other Considerations & Parameters:

- Nanoparticle sticking but no bridging
- Porosity: 15%
- Rock matrix: 100% Quartz

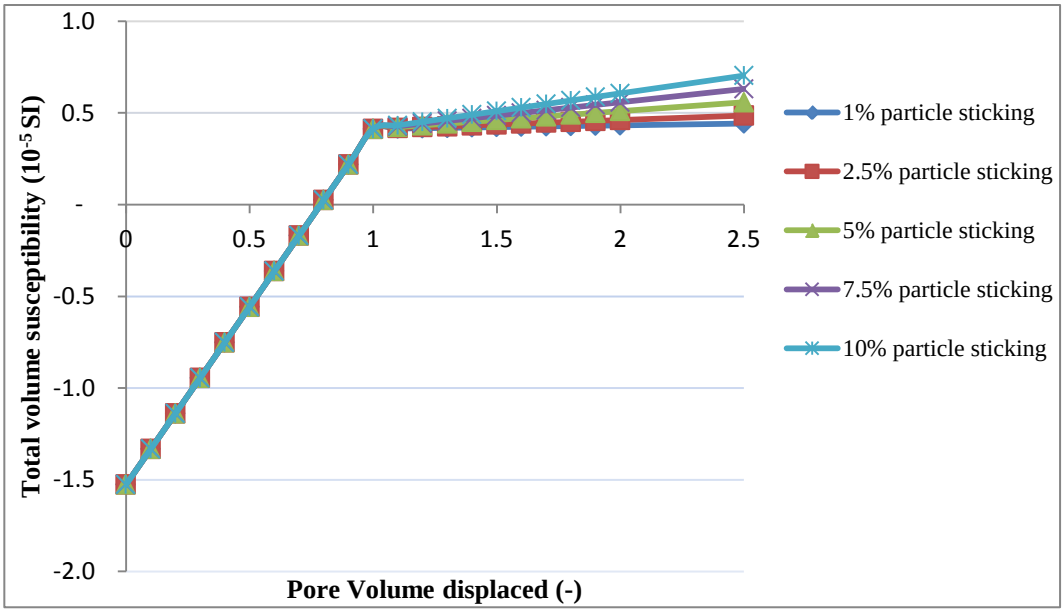

Figure 6-10: Total Volume Magnetic Susceptibility with different sticking coefficients.

6.2.7 Nanoparticle Concentration at Various Lengths after different Pore Volume (PV) Injections

Suri and Sharma (2004) mentioned one dimensional solution to the concentration distribution of bridging particles as a function of time and space and is given below in the form of Eq. (6-2).

$$C_i(x,t) = C_{i(in)}\exp(-\lambda_i x) \qquad (6\text{-}2)$$

Where,

(t= □x/u)

$C_i(x,t)$ = Particle concentration in fluid, % (vol/vol)

$C_{i(in)}$ = Injected particle concentration, % (vol/vol)

λ = Filtration coefficient, 1/m , determined empirically

x = distance (one Dimensional Coordinate), m

Based on the exponentially declining particle concentration, following expression is suggested and used for nanoparticle distribution away from the injection point.

$$C_x = C_o Exp(-P * D_i) \quad (6\text{-}3)$$

Where,

C_x = Concentration of solid particles at any point before the drainage front, %

D_i = L_x/L_{core} (L_x is length from injection point till the point of interest), m/m

C_o = Concentration of particles at the start of core plug, % (vol/vol)

P = Particles distribution factor, dimensionless (empirically determined)

Figure 6-11 shows particle distribution with particle distribution coefficient of 0.9 whereas a particle distribution coefficient of 1.1 is used in figure 6-12. It can be observed that higher particle distribution coefficient would result in higher concentration near the injection point and less concentration away from the injection end when compared with other system having smaller distribution coefficient.

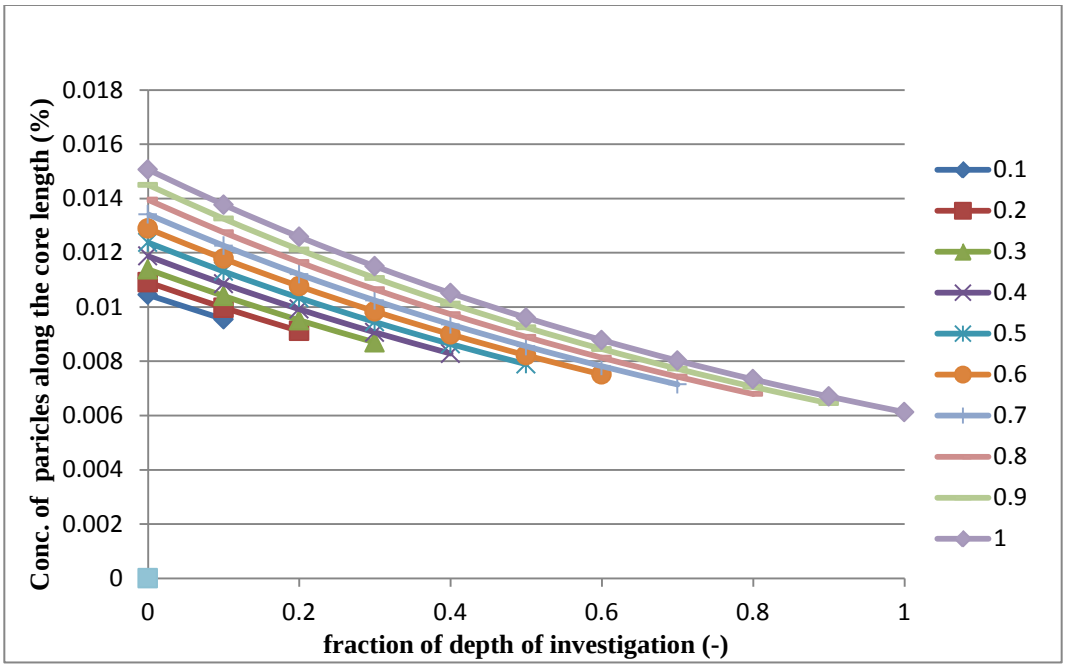

Figure 6-11: Nanoparticle distribution with different pore volumes injections (solid distribution coefficient = 0.9)

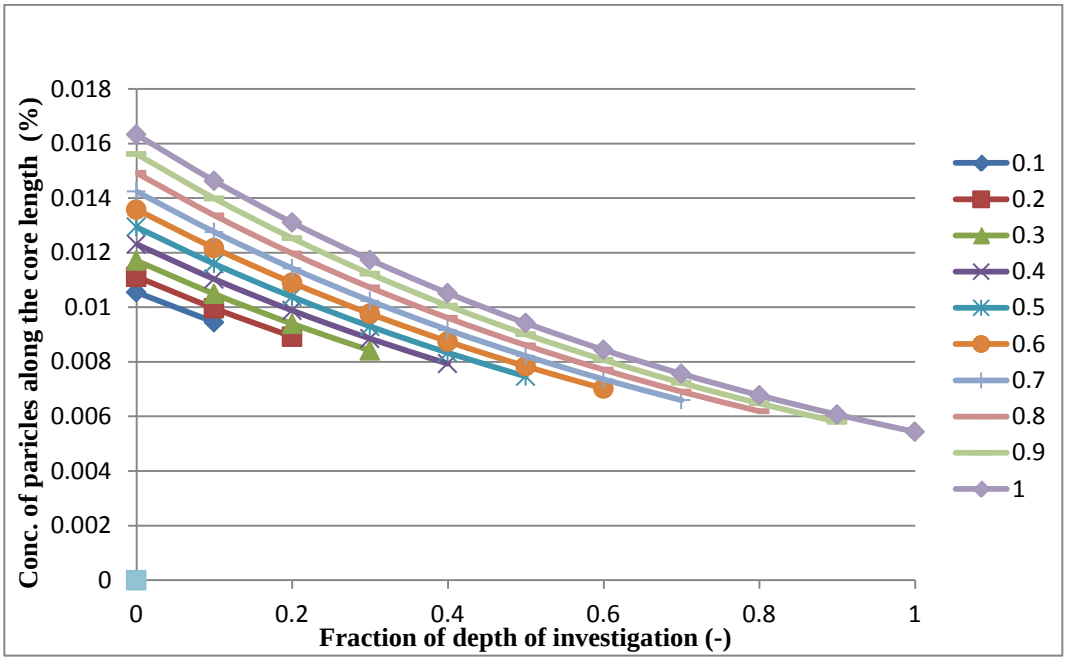

Figure 6-12: Nanoparticle distribution with different pore volumes injections (solid distribution coefficient = 1.1)

Figure 6-13 shows that for same amount of pore volume injected, magnetic susceptibility response will be higher with bridging. Magnetite concentration of 0.01% by volume in injection fluid is used in developing this plot.

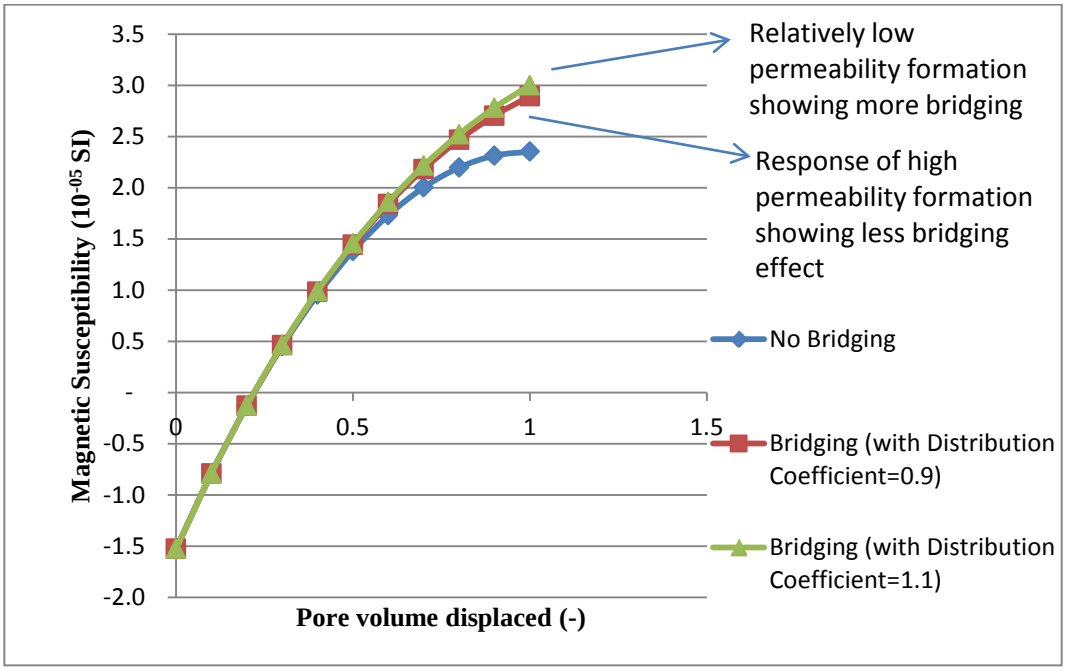

Figure 6-13: Magnetic susceptibility response measurements with tools response function and different distribution coefficient

7 CONCLUSIONS AND RECOMMENDATIONS

7.1 Conclusions

1. Magnetic susceptibility measurement is a rapid and non destructive mean of estimating the concentration of high susceptibility (paramagnetic/ ferromagnetic) materials.

2. Due to the different phenomena described in this report such as particle adhesion/ sticking, particle agglomeration, dependence of sensor response on axial and radial fluid distributions it is not possible to precisely estimate/ predict the concentration of NPs at any point along the length of flow cell/ core holder. Although magnetic susceptibility response is affected by abovementioned factors, the magnetic susceptibility measurements in static and dynamic experiments can give a semi quantitative estimate of concentration of nanoparticles. The magnetic susceptibility change in susceptibility response can be used to determine the stability of nanoparticle suspensions and adhesion/ sticking of nanoparticles or their agglomerates during static and dynamic experiments respectively.

3. The stability of nanoparticle suspensions is found to be poorest with mixing only. The particle suspension characteristics are improved by sonication and addition of surfactants however particle settlement was not avoided completely.

4. Mixing of nanoparticles in de-ionized water followed by dispersion and sonication respectively is found to be the best among all other methods tried in this study for preparation of stable nanoparticle suspensions.

5. Increasing the concentration of surfactants improves the initial susceptibility response and stability of nanoparticle suspensions but that

increase in susceptibility response is not a linear function of surfactant concentration. The increase in susceptibility response decreases with increase in concentration of surfactants. A surfactant concentration versus susceptibility plot can be used to find out an optimum concentration of surfactant.

6. Optimum concentration of surfactants is found out to be independent of nanoparticle concentrations (for the range of nanoparticle concentrations studied) in suspensions stability experiments.

7. The stability of nanoparticle suspensions also depends on sonication energy which is multiplication of sonication time and sonication power. High sonication energy is needed to disintegrate the large concentration of nanoparticles in suspensions. The optimum sonication energy would be a function of volume of nanoparticle suspensions and concentration of nanoparticles in suspensions.

8. The Maghemite nanoparticle suspensions prepared using optimum concentration of CTAB, the cationic surfactant and DDBS, the anionic surfactant exhibits similar susceptibility responses in suspension stability experiments. However, TGT, the non-ionic surfactant does not work well at all for effective dispersion of these nanoparticle suspensions.

9. Comparison of stability responses using surfactants and polymer as dispersant shows that same level of stability is achieved with considerably less concentration of surfactant and without bringing any drastic change in rheology of suspensions. However, when Xanthan Gum polymer is used significant change in the low shear rate viscosity (LSRV) is observed.

10. Addition of XG polymer in CTAB dispersant based suspensions distorts the stability of Maghemite nanoparticle suspensions that can be seen from the initial susceptibility of suspensions. However, addition of XG in

DDBS dispersant based nanoparticle suspensions does not disturb the initial susceptibility response. Since addition of XG polymer increases the LSRV, the particle settlement due to gravitational effects is reduced.

11. The duration of exposure of nanoparticle suspensions to low applied magnetic field by MS2C sensor may bring down the stability of nanoparticle suspensions.

12. Different types of nanoparticles possess different surface charge and may require different amount of sonication energy and different type(s) and concentration of dispersants (surfactant/ polymer).

13. "In-line" monitoring of transport of nanoparticle suspensions provides semi quantitative estimation of concentration of nanoparticles. The magnetic susceptibility trends which are indicative of concentration of nanoparticles are helpful in understanding the mechanisms responsible for change in concentration at different points along the length of the well.

14. The optimum Maghemite nanoparticle suspension recipe, prepared after investigating the effects of various parameters, works reasonably well for other nanoparticles ($NiFe_2O_4$, $CoFe_2O_4$, Fe_3O_4) during dynamic experiments. However, due to different chemical composition and hence different surface charge, the optimum suspension recipes for each nanoparticle may require further study using both static and dynamic experiments.

15. Use of CTAB surfactant as dispersant in Maghemite nanoparticle suspensions results in a high level of particle adhesion/ sticking with the glass beads pack during dynamic flow experiments.

16. DDBS surfactant performs very well in dynamic flow experiments when Maghemite or other metallic Nanoparticle suspensions are flowed through

glass beads/ sand packs, leaving less than 15% of nanoparticle after glass beads/sand pack flooding with de-ionized water.

17. Particle accumulation in glass beads could be due to particle sticking/ adhesion, presence of nanoparticles in immobile water layer or composite effect of both.

18. Increase in permeability of porous media has shown better transport of nanoparticle suspensions. This increase gets very significant for suspension recipes exhibiting high nanoparticle adhesion/ sticking.

19. High flow rates bring down the final concentration of retained nanoparticles in porous media after water flooding.

7.2 Recommendations

1. Based on the experimental findings, following empirical method may be used for determination of suitable recipes for improved suspension stability and low or high level of adhesion/ sticking with the matrix of porous media.

    a) Prepare nanoparticle suspensions using at least two types of dispersants (surfactants and/or polymers) and following below mentioned two procedures.

        - Mix nanoparticles at any fixed rpm in base fluid, sonicate and add dispersant.

        - Mix nanoparticles at same rpm in base fluid, add dispersant and sonicate.

    Use same sonication energy in both procedures.

b) Place the suspensions in graduated non-metallic tube having length more than the double of susceptibility sensor's diameter and take the susceptibility measurements at different points along the height of cylindrical tube. Take these measurements, soon after the preparation of suspensions and after any particular period of time.

c) Follow the procedure which gives better initial susceptibility and less change in susceptibility profile with time (i.e. high stability suspension) for rest of the steps/ experiments.

d) Select at least three quantities of nanoparticles for a specific volume of base fluid and use the highest of these three selected quantities; prepare at least three samples of nanoparticle suspensions by using different quantities of dispersant. Plot these quantities as a function of initial susceptibility reading taken at the center of tube and determine the optimum concentration of dispersant. There is also a likelihood that more than three suspension samples be needed in order to figure out optimum concentration of surfactant.

e) Follow step d) for any other type(s) of dispersant(s) which may be of interest to be studied.

f) Again, take the highest concentration of nanoparticles, prepare suspensions using the optimum concentration of dispersant (found by following step d)) and better method of sample preparation, established from step c). Use different sonication energies to find out optimum sonication energy.

g) The same value of sonication energy may be used for less concentrated nanoparticle suspensions or sonication energies for different concentration nanoparticle suspensions may be determined separately (which shall be less than that found for high concentration sample).

h) Using the optimum suspension recipe, prepare suspensions with three different nanoparticle concentrations and construct a calibration plot of true volume susceptibility of nanoparticle suspension versus concentration of nanoparticles in suspension. The susceptibility values used in constructing such a plot would be those measured at the center of graduated tube, soon after the preparation of suspensions and corrected for the size of the tube used in the experiments. These concentrations versus susceptibility plots h can be used for an estimate of nanoparticle concentration retained/ left in core holder during dynamic (fluid flow) experiments.

i) Use the nanoparticle suspensions with different dispersants (e.g. anionic, cationic, non-ionic surfactants, polymers etc.) using optimum concentration and sonication power and observe the particle retention and transport behaviour.

j) Depending upon the nature of application of nanoparticle suspensions, level of adhesion/ retention may be varied by introducing different types of recipes having different adhesion/ sticking characteristics.

2. Ionic strength and pH of suspensions have been reported by many researchers to be of key importance in suspension stability and transport of these suspensions. These parameters may have significant influence on the type, optimum concentration of dispersant and optimum sonication energy. Therefore, in future studies, type of dispersant, change in optimum concentration of dispersant, change in optimum sonication energy etc. with change in PH, nanoparticle type and ionic strength could be of interest.

8 REFERENCES

Alivisatos, P. (1996): Semiconductor Clusters, Nano-crystals, and Quantum Dots, Science, 271, 933-937.

Barron, A.R., Tour, J.M., Busnaina, A.A., Jung, Y.J., Somu, S., Kanj, M.Y., Potter, D.K., Resasco, D., and Ullo, J., (2010) Big Things in Small Packages. Oilfield Review, December 2010, 38-49.

Bensasson, R.V., Bienvenue, E., Dellinger, M., Leach, S., Seta, P. (1994) C60 in Model Biological Systems. A Visible UV Absorption Study of Solvent-dependent Parameters and Solute Aggregation. J. Phys. Chem., 98, 3492-3500.

Bhattacharjee, S.; Elimelech, M. (1997) Surface Element Integration: A Novel Technique for Evaluation of DLVO Interaction between a Particle and a Flat Plate. J. Colloid Interface Sci., 193, 273 285.

Brant, J.A., Labille, J., Bottero, J.Y., Wiesner, M.R. (2006) Characterizing the Impact of Preparation Method on Fullerene Cluster Structure and Chemistry. Langmuir, 22, 3878–3885.

Broding, R.A., Zimmerman C.W., Somers, E.V., Wilhelm E.S. and Stripling, A.A. (1952) Magnetic Well Logging, Geophysics, XVII (I).

Brønsted, J.N. (1922) Physik. Z. Chem. 102, 169-207.

Cameselle, C., Darko-Kagya, K., Khodadoust, A., and Reddy, K.R. (2008) Influence of Type and Concentration of Dispersants on the Zeta Potential of Reactive Nanoiron Particles, Proc. International Environmental Nanotechnology Conference, USEPA, Chicago.

Chopkar, M., Das, P.K., Manna, I. (2006) Synthesis and Characterization of Nanofluid for Advanced Heat Transfer Applications, Scripta Materialia 55, 549-552.

Clark, P. D., Clarke, R. A., Hyne, J.B. and Lesage, K.L. (1990) Studies on the Effect of Metal Species on Oil Sands Undergoing Steam Treatments. AOSTRA J Res 6 (1): 53-64

Darko-Kagya, K. and Reddy, K.R. (2010) Monitoring Nanoiron Transport in Porous Media using Magnetic Susceptibility Sensor, 6th International Congress on Environmental Geotechnics, New Delhi, India.

Deguchi, S.; Rossitza, G. A.; Tsujii, K. (2001) Stable Dispersions of Fullerenes, C60 and C70 in Water. Preparation and Characterization. Langmuir, 17, 6013-6017.

Derjaguin, B.V. and Landau, L. (1941) Acta Physiochim, URSS, 14, 633.

Ding, Y. and Wen D. (2005) Particle Migration in a Flow of Nanoparticle Suspensions, Powder Technol., 149, 84-92.

Eastman, J.A., Choi, S.U.S., Li, S., Yu, W., and Thompson, L.J. (2001) Anomalously Increased Effective Thermal Conductivity of Ethylene Glycol-based Nanofluids Containing Copper Nanoparticles, Applied Physics Letters 78, 718–720.

Espinasse, B., Hotze, E. M. and Wiesner, M. R. (2007) Transport and Retention of Colloidal Aggregates of C60 in Porous Media: Effects of Organic Macromolecules, Ionic Composition and Preparation Method, Environ. Sci. Technol., 41: 7396-7402

Guzman, K.A.D., Finnegan, M.P. and Banfield, J.F. (2006) Influence of Surface Potential on Aggregation and Transport of Titania Nanoparticles. Environ.Sci.Technol. 40, 7688-7693.

Hong, T.K., Yang, H.S., Choi, C.J. (1999) J. Appl. Phys. 97, 280.

Iijima, M. and Kamiya, H., (2009) Surface Modification for Improving the Stability of Nanoparticles in Liquid Media, KONA Powder and Particle J. 27, 119-129.

Ivakhnenko, O.P. and Potter, D.K., (2004) Magnetic Susceptibility of Petroleum Reservoir Fluids. Physics and Chemistry of the Earth, 29, 899-907.

Jun, Y.–W., Huh, Y.–M., Choi, J.–S., Lee, J.–H., Song, H-T., Kim, S., Yoon, S., Kim, K.–S., Shin, J.–S. and Cheon, J. (2005) Nanoscale Size Effect of Magnetic Nanocrystals and Their Utilization for Cancer Diagnosis via Magnetic Resonance Imaging, J. Am. Chem. Soc., 127, 5732-5733.

Kallay, N. and Zalac S. (2002) Stability of Nanodispersions: A Model for Kinetics of Aggregation of Nanoparticles. J. Colloid Interface Sci., 298, 50-58.

Kawashima, Y., Okumura, M. and Takenaka, H. (1984) The Effects of Temperature on the Spherical Crystallization of Salicylic Acid, Powder Technology, 39 (1), 41-47.

Keblinski, P., Phillpot, S.R., Choi, S.U.S., Eastman J.A. (2002) Mechanism of Heat Flow in Suspensions of Nanosized Particles (Nanofluids), International Journal of Heat and Mass Transfer 45, 855–863.

Kobayashi, M., Juillerat F., Galletto P., Bowen, P. and Borkovec, M. (2005) Aggregation and Charging of colloidal Silica Particles: Effect of Particle Size. Langmuir, 21, 5761-5769.

Lee, S., Choi, S.U.S., Li, S., and Eastman, J.A. (1999) Measuring Thermal Conductivity of Fluids Containing Oxide Nanoparticles, ASME Journal of Heat Transfer 121, 280.

Li, W., Wang, Y., Pennell, K.D. and Abriola, L.M. (2008) Investigation of the Transport and Deposition of Fullerene (C60) Nanoparticles in Quartz Sands under Varying Flow Conditions, Environ. Sci. Technol., 42, 7174-7180.

Malvern Instruments, User Manual Bohlin CVOR.

Manual, Sonicator® Misonix model 3000 ultrasonic liquid processor.

Masuda, H., Ebata, A., Teramae, K., Hishinuma, N. (1993) Alteration of Thermal Conductivity and Viscosity of Liquid by Dispersing Ultra-fine Particles (Dispersion of g-Al2O3, SiO2 and TiO2 Ultra-fine Particles), Netsu Bussei 4, 227– 233.

MS2 manual, Bartington® Instruments.

Nettleton, H.R. and Sugden, S. (1939) The Magnetic Susceptibility of Nickel Chloride, Proceedings of the Royal Society of London. Series A, Mathematical and Physical Sciences, 173, 313-323.

Nsib, F., Ayed, N. and Chevalier, Y. (2006) Dispersion of Hematite Suspensions with Sodium Polymethacrylate Dispersants in Alkaline Medium, Colloids and Surf. A, 286, 17-26.

Ozin, G.A. (1992) Nanochemistry: Synthesis in Diminishing Dimensions, Adv. Mater., 4, 612-649.

Polytron User Manual for PT 6100.

Reed J. S. (1995) Principles of Ceramic Processing, John wiley and sons, 2nd edition, 1995.

Rodriguez, E., Roberts, M. R., Yu, H., Huh, C. and Bryant, S. L. (2009) Enhanced Migration of Surface-treated Nanoparticles in Sedimentary Rocks. SPE 124418. Presented at Annual Technical Conference, New Orleans, Louisiana, Oct. 4-7.

Ryoo, S., Rahmani, A.R., Yoon, K.Y., Prodanovic, M., Kotsmar, C., Milner, T.E., Johnston, K.P., Bryant, S.L. and Huh, C. (2010) Theoretical and Experimental Investigation of the Motion of Multiphase Fluids Containing Paramagnetic Nanoparticles in Porous Media, SPE 134879, Presented at Annual Technical Conference, Florence, Italy, Sep. 19-22.

Saleh, N., Kim, H. Y., Phenrat, T., Matyjaszewski, K., Tilton, R. D. and Lowry, G.V. (2008) Ionic Strength and Composition Affect the Mobility of Surface-modified Fe0 Nanoparticles in Water-saturated Sand Columns, Environ. Sci. Technol., 42: 3349-3355.

Samal S. (2009), Production and Dispersion Stability of Ultrafine Al, Cu and Al-Cu Particles in Base Fluid for Heat Transfer Applications, Masters of Technology Thesis, National Institute of Technology, Rourkela, India.

Suri, A., and Sharma M.M. (2004) Strategies for sizing particles in Drilling and Completion Fluids, SPE 87676, SPE Journal, 9 (1), 13-23.

Shah, R.D. (2009) Application of Nanoparticle Saturated Injectant Gases for EOR of Heavy Oils. SPE 129539- STU, presented at SPE Annual Technical Conference, New Orleans, Louisiana, Oct. 4-7.

Shen, D., Zhang, P., Kan, A.T., Fu, G., Farrell, J. and Tomson, M.B. (2008) Control Placement of Scale Inhibitors in the Formation with Stable Ca-DTPMP

Nanoparticle Suspensions and its Transport in Porous Media, SPE 114063, Presented at International Oilfield Scale Conference, Aberdeen, May 28-29, 2008.

Shokrlu, Y.H. and Babadagli, T. (2010) Effect of Nano sized Metals on Viscosity Reduction of Heavy Oil/ Bitumen during Thermal Applications. CSUG/SPE 137540, presentation at CSUG/SPE conference, Calgary, Alberta, Oct 19-21.

Thapa, D., Palkar, V.R., Kurup, M.B. and Malik, S.K. (2004) Properties of Magnetite Nanoparticles Synthesized Through a Novel Chemical Route, Mater. Lett., 58, 2692-2694.

Tseng, W.J. and Wu, C.H. (2002) Aggregation, Rheology and Electrophoretic Packing Structure of Aqueous Al_2O_3 Nanoparticle Suspensions, Acta Mater., 50, 3878-3887.

Verway, E.J.W. and Overbeek, J.Th.G. (1948) Theory of the Stability of Lyophobic Colloids, Elsevier, Amsterdam.

Wang, Y., Li, Y., Fortner, J. D., Huges, J.B., Abriola, L.M. and Pennell, K.D. (2008) Transport and Retention of Nanoscale C60 Aggregates in Water-saturated Porous Media. Environ. Sci. Technol., 42, 3588-3594.

Reade Advanced Materials , (2006) Magnetic Properties & Susceptibilities Chart [Online] (Updated 11 January, 2006) Available at: http://www.reade.com/Particle_Briefings/magnetic_susceptibilities.html [Accessed 20 January 2011].

Whalen, J.W. (1954) A Magnetic Susceptibility Method for the Determination of Liquid Saturation in Porous Materials, SPE 347-G, JPT, 6 (9), 111-116.

Zhang, T., Espinosa, D.A., Yoon, K.Y., Rahmani, R.A., Yu, H., Caldelas, F.M., Ryoo, S., Roberts, M.R., Prodanovic, M., Johnston, K.P., Milner, T.E., Bryant, S.L., and Huh, C. (2011) Engineered Nanoparticles as Harsh-Condition Emulsion

and Foam Stabilizers and as Novel Sensors, Paper presented at Offshore Technology Conference in Houston, Texas.